D2 receptor plasticity and effector coupling

By

Alec Condon

A DISSERTATION

Presented to the Neuroscience Graduate Program,

Vollum Institute,

Oregon Health and Science University,

And School of Medicine

In partial fulfillment of the degree requirements for the degree of

Doctor of Philosophy

January 2022

School of Medicine

Oregon Health & Science University

CERTIFICATE OF APPROVAL

This is to certify that the Ph.D. dissertation of

Alec F Condon

has been approved

Advisor, John T Williams, Ph.D.

Committee Chair, Laurence O Trussell, Ph.D.

Member, Kim A Neve, Ph.D.

Member, David L Farrens, Ph.D.

Member, Christopher P Ford, Ph.D

TABLE OF CONTENTS

List of Figures

List of Tables

List of Abbreviations

AAV	Adeno-associated virus	HEK	Human embryonic kidney
AMPA	α-amino-3-hydroxyl-5-methyl-4-isoxazolepropionic acid	IPSC	Inhibitory postsynaptic current
BAPTA	1,2-Bis(2-aminophenoxy) ethane-N,N,N',N',-tetraacetic acid	KCTD	Potassium channel tetramerization domain
BRET	Bioluminescence resonance energy transfer	KO	Genetic knock out
Cmpd101	GRK2/3 inhibitor Compound 101	LED	Light-emitting diode
CNS	Central nervous system	LTD	Long-term depression
CyHQ	8-cyano-7-hydroxyquinolinyl	MD	Molecular dynamics
D2L	D2 receptor long isoform	mRNA	Messenger ribonucleic acid
D2S	D2 receptor short isoform	NMDA	N-methyl-D-aspartate
DA	Dopamine	pA	Picoamp
DIO	Double-floxed inverted open readying frame	pF	Picofarad
EGFP	Enhanced green fluorescent protein	PI(4,5)P2	phosphatidylinositol 4,5-bisphosphate
EGTA	ethylene glycol tetraacetic acid	PLC	phospholipase C
FCS	Fetal Clone| Serum	RGS	Regulator of G protein signaling
FSK	forskolin	RIM	RAB3A-interacting molecule
GABA	Gamma-aminobuteric acid	RLuc	Renilla luciferase
GDP	guanosine diphosphate	RM ANOVA	Repeated measures analysis of variants
GFP	Green fluorescent protein	SD	Standard deviation
GIRK	G protein-coupled inwardly rectifying potassium channel	SEM	Standard error of the mean
GPCR	G protein-coupled receptor	SNc	Substantia nigra pars compacta
GRK	G protein-coupled receptor kinase	TM	Transmembrane domain
GTP	guanosine 5'-triphosphate	WT	Wild type

Acknowledgements

There are numerous people to thank for helping me through this process. Starting with John, his mentorship is legendary. I can't thank him enough for his guidance, his willingness to let me follow my interests, and giving me enough freedom to fail and learn from those failures. I have to thank the Williams lab as a whole; I have learned something from every single member that I overlapped with over the years. In (approximate) order of their departures, thank you to Erika, Paul, Danny, Will, Brooks, Emily, Jim, Sweta, and the current members in Seksiri, Joe, Omar, and second Emily. A special second thanks to Brooks for agreeing to teach me how to patch, bringing me up to speed on team dopamine, and being the person I would hound with a million dumb questions that I couldn't (and likely shouldn't) bring myself to bug John with. Thank you to the extended Williams community including former members who been an invaluable resource in interactions, specific requests for help, and unexpected insights with a special shoutout to Team Dopamine.

Thank you to the members of the OHSU and the Vollum. Starting as a technician off in the BRB, I was quickly made to feel welcome at OHSU which has been my place of work for over 8 years. Students, employees and faculty in my first position in the Jungers Center, interacting with folks on the 2nd floor, folks at Thursday lectures (back in those halcyon days of in person events), in the physiology journal club, or during Friday ~~happy~~ discussion hour. Thank you to my fellow students with a special emphasis on my matriculating class. Those times meeting up for beers and complaining about failed experiments and the state of academia were invaluable outlets for the stress and frustration intrinsic to pushing new areas of research and learning.

Thank you to the intro lecturers for the NGP classes. It was wild to receive lessons from folks like Craig, Larry, Dave, and Gary who talked about these amazing discoveries only to look down at the citation at the bottom of the screen and see it was these same folks who had made the

discoveries. Those intro courses had a large impact on my research direction as I was both blown away by neuronal physiology and instantly fascinated by GPCR and G protein signaling.

Thank you to my committee, it has been great to have a captive audience with whom to discuss my research and of course many of the discussions in those sessions were critical in the course of my work. Beyond those sessions, I have repeatedly turned to these folks for advice, interacted with them in courses, or forged ahead with collaborations. Thank you to Tim Dore who I happened to run in to at a conference which blossomed into a long collaboration providing me with valuable caged-reagents and opening up new avenues of research.

Thank you to all the mentors, scientific or no, I have had over the years. Thank you to Fred for taking a chance on me for my first job in the Jungers Center out of college and to all the folks of the Jungers who welcomed me. Thank you to Danielle, Annie, and Anna for being a part of that lab and guiding me through me through my entry into graduate school. Thank you to my undergraduate thesis advisor Janis and to all the fantastic biology/science teachers in my high school who solidified a lifelong love of molecular biology. And shoutout to Perry and Johnson for being amazing and helping me through tough times.

Thank you to my friends. Over the years, really couldn't have done it without y'all.

Finally, thank you to my family. Steph has been my partner for over 10 years and I really don't know who I would be without her. She has supported me and made me a better person (with the occasional bit of making me a worse person). Thank you for putting up with and sorry for when we are sitting out on a deck looking at an amazing view or having a nice romantic dinner together, when she asks what I am thinking about, the number one answer being "oops, I was thinking about science." Thank you to my two pets Grim the monster cat and Sandwich the angelic tortoise who have both brought me a lot of comfort, but also the occasional non-sciencey crisis when they have health emergencies—that's a good thing to force me to focus on other things right? Thank you to my

sister Julia for growing up together and never being able to identify with stories about horrible fights with siblings (you know, among other things too). Thank you to my parents for… well literally everything. Everything I am today in some way goes back to their efforts. It has taken a lifetime to truly appreciate everything they did for me, the support they gave, and the privileges in life that gave me the constant leg up. And of course, thank you to the newer family additions in Bob and Julie. Y'all may not have been there for the first half to two thirds, but it has been great having y'all around what has effectively been my whole adult life.

Abstract

Dopamine transmission is critical for a variety of functions in the brain including reward processing and movement while its pharmacological regulation is used to treat dysregulation states like depression and psychosis. Despite its importance, relatively little is known about the mechanisms regulating dopamine receptor sensitivity and signal transduction in large part due to the complex nature of the pathway. Dopamine is sensed by a family of receptors called G protein-coupled receptors (GPCRs) which is a large family that senses a wide variety of neurotransmitters such as endogenous opioids, serotonin, acetylcholine, glutamate, adrenaline, adenosine, and signaling lipids. Understanding the regulation and signal transduction pathways of dopamine signaling is therefore important both for understanding the roles of dopamine in the brain and for broader insights into G protein signaling.

Dopamine is produced by midbrain dopamine neurons which send projections and release dopamine throughout the brain, but also release dopamine from dendrites as a form of regulation between dopamine neurons. These neurons express inhibitory D2 receptors which couple to G protein-coupled inwardly rectifying potassium (GIRK) channels that reduce dopamine neuron excitability. Dendritic dopamine release and the resulting D2 dependent inhibitory post-synaptic current (IPSC) depends on molecular machinery common to other forms of neurotransmission and similarly exhibits pre-synaptic plasticity, but the post-synaptic regulation of cellular response has received less description.

The bulk of this dissertation focuses on D2 receptor-GIRK channel coupling. Chapter topics include how structural variants of the D2 receptor modulate G protein engagement, measurements of the time course of dopamine-D2 receptor functional interactions in the IPSC, and characterization of post-synaptic interactions between $GABA_B$ and D2 receptor signaling.

Following a chapter focusing on tool development (Chapter 3), the first experimental chapter (Chapter 4) consists of a study using genetically modified mice that express only the long or short isoform of the D2 receptor. These experiments followed from results of a previous study using virally expressed receptors which found a major difference between the long and short splice variants was differential sensitivity to calcium. However, results from these new strains of genetically modified animals showed a calcium sensitivity for both receptor subtypes. This difference highlights the distortions associated with protein over expression. Despite this difference from previous results, data did confirm differential response to cocaine pre-treatment suggesting the two splice variants may indeed play a role in longer-term responses to drug-induced plasticity.

Next, this dissertation presents the results of studying a constitutively active mutant D2 receptor (D2-I212F) discovered by studying the pathology of a human family. Experiments with virally transduced dopamine neurons clarified a dual role of constitutive activity and slowed kinetics in signal termination, consistent with molecular dynamic models of modified receptor movements. These results highlight the role of agonist unbinding for the decay of the endogenous D2 receptor IPSC by dramatically increasing the duration of responses, associated both with increased receptor affinity and deficiencies in returning the intracellular face to its off state. These results complement data from Chapters 3 and 6 showing how high agonist-receptor affinities slow the kinetics of response such that agonist unbinding may be a substantial determinant of the time course of signaling.

Chapter 6 explores the functional kinetics of agonist-receptor interactions and subsequent GIRK currents using a photosensitive chemically caged D2 receptor antagonist. Blocking the D2 receptor at different time points following electrical stimulation of dopamine release showed 100 ms of functional agonist-receptor interaction produces the peak of the IPSC.

Finally, use of rapidly applied agonist to probe post-synaptic plasticity shows functional crosstalk between D2 receptor signaling and other GPCRs coupled to a shared pool of GIRK channels with robust heterologous desensitization. These results also highlight the non-linear GIRK concentration response curve as co-activation of multiple receptor subtypes show facilitating interactions which are parsimoniously explained by models of the GIRK channel concentration-response curve.

In conclusion, the results of this dissertation shed additional light on mechanisms of signal transduction for D2 receptor signaling and acute plasticity of dopamine signaling which can support a growing knowledge base of GPCR signaling.

Chapter 1 – Introduction

Basics of (dopamine) neuron function

The primary function of a neuron is to receive, process, and transmit information between neurons, most commonly by neurotransmitter release. The information that is received can be sensory such as with mechanosensitive cells like somatosensory systems sensing things like touch (Handler and Ginty, 2021) or auditory hair cells sensing vibrations (Gillespie and Walker, 2001), or information can be received from other neurons. But a common feature of all neurons is the use of electrochemical ion gradients to set up a voltage gradient across neuronal membranes and use of active and passive ion channels to allow for ion currents to control and respond to voltage (Hille, 2001).

Neurotransmitter release is sensed through membrane neurotransmitter receptors that directly or indirectly open ion channels to affect membrane voltage (Dale, 1914; Loewi, 1921). Neurotransmitters like glutamate can directly excite neurons by opening sodium conductance to depolarize membranes. Depolarized membranes activate voltage-sensing ion channels to further depolarize the neuron's membrane voltage (Fonnum, 1984). Other voltage-sensitive ion channels then respond to depolarized voltages and open inhibitory potassium ion conductance to hyperpolarize the membrane with the complete cycle of rapid depolarization to hyperpolarization known as an action potential (Hodgkin and Huxley, 1952).

Neurons are polarized cells which receive information in their dendrites, an often-complex branching structure that can receive many summating inputs to control somatic voltages. This information is then transmitted down the axon via self-propagating action potentials to open calcium channels at axon terminals. The digital action potential is converted to chemical by calcium

dependent fusion of synaptic vesicles to release neurotransmitter (Katz and Miledi, 1967). However, dopamine neurons, the subject of this dissertation, deviate from this directionality of information flow as rather than simply receiving information in their dendrites, they exhibit somatodendritic release as a form of lateral inhibition onto neighboring dopamine neurons (Björklund and Lindvall, 1975; Wilson et al., 1977; Beckstead et al., 2004).

Ligand-gated ion channels like glutamate-sensitive AMPA and NMDA receptors can directly affect voltage by the presence of ion channels in these same protein structures that bind neurotransmitter, but other classes of neurotransmitter sensitive receptors also exist that often have more subtle effects on neuronal function. G protein-coupled receptors (GPCRs) represent a large class or receptors that do not directly gate ion channels but work through second messenger systems to modulate neuronal activity via functions like inhibition of voltage-sensitive channels (Loewi, 1921; Lefkowitz, 2013). Dysregulation of GPCR signaling can often lead to disease states due to this indirect modulation, rather than the seizures and death that might follow from dysregulation of ligand-gated ion channels. The modulatory nature of GPCR signaling has also been leveraged by pharmaceutical sciences for therapeutic medication, to the point that 30-60% of medications target GPCRs (Schöneberg et al., 2004; Hauser et al., 2017). Disease states such as depression, psychosis, and movement disorders are thought to be due to dysregulation in neurotransmitter systems sensed by GPCRs such as serotonin, dopamine, adrenaline/epinephrine (Wong et al., 2000). Most recreationally used drugs also act through GPCRs with examples such as cannabis (Howlett et al., 2010), opioids (Brownstein, 1993), amphetamines, cocaine (Hyman et al., 2006), MDMA (Kalant, 2001), LSD (Liechti, 2017), mescaline, psilocybin (Aghajanian and Marek, 1999), and salvia (Coffeen and Pellicer, 2019) all work through systems of GPCRs, with mechanisms acting either directly on GPCRs or by modulating the agonists that activate these receptors.

The subject of this dissertation is dopamine transmission between dopamine neurons whose axonal dopamine release is important in reward-processing and movement (Schultz, 2007). Two classes of GPCR primarily sense dopamine: excitatory D1-like receptors (Kebabian, 1978) and inhibitory D2-like receptors (Seeman et al., 1976) meaning dopamine can have differential effects on neurons in the same brain region based on the receptors expressed. Midbrain dopamine neurons are the primary source of neuronal dopamine, and these neurons send long axons with highly arborized projections throughout the brain (Matsuda et al., 2009). One notable feature of dopamine neurons is their ability to release dopamine not just from axon terminals, but from their dendrites (Björklund and Lindvall, 1975; Wilson et al., 1977; Beckstead et al., 2004). Inhibitory D2 receptors expressed on dopamine neurons couple to GIRK channels (Pucak and Grace, 1994, Beckstead et al., 2004) such that dopamine release results in lateral inhibition to coordinate the actions of connected dopamine neurons (Figure 1.1). This D2-mediated inhibitory post-synaptic current (D2 IPSC) is an atypical form of neurotransmission that both modulates critical functions of cognitive functioning. Furthermore, that D2 receptors couple to GIRK channels provides a window into often opaque dynamics of G protein signaling.

Synaptic plasticity

The brain is plastic; it can change and grow. Connections between individual neurons are also plastic (Hebb, 1949). The number of synaptic connections can increase or decrease, as can the strength of those connections both in pre-synaptic release probability and number of receptors sensing that release (Citri and Malenka, 2008). These changes can be long lasting or as short as milliseconds with an array of mechanisms and functions for every synapse. The ability for change is critical for making new associations and learning new concepts— with synaptic plasticity often being

referred to as the cellular correlate of learning (Hawkins et al., 1983)— but also for maintaining homeostasis and avoiding overexcited circuitry causing seizure (Bridi et al., 2018).

The D2 receptor IPSC exhibits synaptic plasticity like any other neuronal connection with many molecular mechanisms shared with other forms of neurotransmission (Beckstead et al., 2004; Fortin et al., 2006; Mendez et al., 2011; Gantz et al., 2013; Robinson et al., 2019). However, compared to systems sensed by ligand-gated ion channels, many basics of dopamine transmission are still poorly described. Fundamentals such whether there are true synaptic connections with directly opposed release sites and receptors are still contested (Cragg and Rice 2004; Wiencke et al., 2020). Recently developed optical sensors of dopamine concentration have promise for sophisticated experiments to strengthen our current understanding of pre-synaptic control and release of dopamine (Patriarchi et al., 2018, Sun et al., 2018), but relatively little is known about post-synaptic plasticity to quantitatively translate (Ford et al., 2009) extracellular concentrations into post-synaptic effects.

D2 receptor signaling is known to desensitize (Beckstead and Willams, 2007), measured in dopamine neurons as decline or "sag" in peak current response in the continued presence of agonist (Figure 1.2). The relevance of this desensitization to normal biology of dopamine neurons is unclear. With ligand-gated ionotropic signaling, receptors are known to rapidly desensitize, even shaping the response to single vesicle release events (Otis et al., 1996). But the repertoire of D2 receptor plasticity has not been described except in the context of non-physiological application of sustained high concentration of agonists (Beckstead and Willams, 2007; Perra et al., 2011; Gantz et al., 2015; Robinson et al., 2017). It is unclear if physiological desensitization would happen rapidly enough to affect short-term integration of signals and if yes, whether recovery would be sufficiently rapid to reset dopamine systems to new input. Characterizing these properties of plasticity is one of the

major goals of this dissertation (Chapter 7) as well as how variations in the intracellular region of the D2 receptor contribute to acute and long-term plasticity (Chapter 4).

Fundamentals of GPCR biology

The GPCR signaling cascade is a subject that has required decades of experimentation with new fundamental jumps in understanding continuing to this day (Kühn H, 1974; Touhara and MacKinnon, 2018). As the name would imply, G protein-coupled receptors couple to heterotrimeric G αβγ proteins (note: there are other types of G proteins than heterotrimeric G proteins, but for the purposes of this dissertation, "G proteins" refers exclusively to G αβγ), known as G proteins for their interactions with guanosine triphosphate (GTP) and guanosine diphosphate (GDP) which act as molecular on and off switches (Sternweis et al., 1981; Gilman, 1984; Gierschik et al., 1985). Agonists binding to receptors causes structural changes that are transduced to the receptor's intracellular face (Figure 1.3A; Dunham and Farrens, 1999; Rasmussen et al., 2011). Inactive GDP-bound G proteins interact with the activated receptor and the G α subunit opens to allow for the higher concentrations of intracellular GTP to displace the GDP (Figure 1.3B). In turn, GTP-bound G α assumes a different conformation which lowers its affinity for G βγ and the heterotrimer splits into GTP-bound G α and free G βγ (Figure 1.3C). Both halves of the now split G protein diffuse and participate in cellular signaling functions. The active GPCR continues to catalyze GTP exchange for other GDP-bound inactive G αβγs in a process of signal amplification. After a time, either through the innate GTPase activity of G α or by interaction with RGS proteins which accelerate this GTPase activity, the terminal phosphate of GTP is cleaved, leaving GDP bound to the G α subunit (guanosine triphosphate to diphosphate Figure 1.3D). With the return of the initial GDP-G α conformation with high affinity for G βγ, the two halves of the heterotrimer rebind, returning to the start of the G protein cycle (Figure 1.3E) (see Birnbaumer, 1990 for a contemporary review of G protein signaling).

Both GTP-G α and free G βγ act as second messengers for GPCRs (Figure 1.3C) and serve in an array of cellular functions depending on the G protein subtype and presence of effector systems expressed in the cellular context. That second messenger systems involve many steps translates to slower signaling rates than "primary messages" that directly affect cell systems such as ligand gated ion channels where ion flux serves as the primary output (Hille, Chp7, 2001). For instance, ionotropic signaling peaks in milliseconds after neurotransmitter release vs taking hundreds of milliseconds for the peak of GCPR dependent GIRK currents (Beckstead et al., 2004). None-the-less, GPCR signaling can still be rapid in the context of behavior. For instance, the retina senses light through rhodopsin, one of the first characterized GPCRs (Deupi, 2013).

There are many related systems of G proteins with each serving different cellular function and with each GPCR having different affinities for G protein subtypes. But for the purposes of this dissertation, two main classes are considered: excitatory G α_s and inhibitory G $\alpha_{i/o}$. An interesting quirk of G protein signaling is that G α signaling was initially considered the "important" one in G protein signaling. Almost all the effects of G_s-coupled are dependent on interactions with the G α_s subunit without much acute contribution of G βγ (Birnbaumer, 1990). In contrast, though G $\alpha_{i/o}$ also performs cellular functions, much of $G_{i/o}$-coupled GPCR activity such as GIRK channel gating acts through G βγ. Yet, the βγ in G $\alpha_s\beta\gamma$ heterotrimer is not much different from G $\alpha_{i/o}\beta\gamma$, so how does βγ produced by G_s-coupled GPCRs not activate effector pathways such as GIRK channels? This question has only recently been addressed. A first hint comes from affinity measurements of G βγ for GIRK channels in isolated systems showing that their affinity is actually quite low (K_d of hundreds of micromolar) (Wang et al., 2014; Wang et al., 2016). GIRK channels also have four G βγ binding sites, all of which must be occupied for efficient gating. Therefore, GIRK channels require a high concentration of G βγ to open (Wang et al., 2016). Following from this observation, it was demonstrated that $G_{i/o}$-coupled GPCRs have a much higher catalytic rate for producing active G

proteins as compared to other GPCRs. G_s-coupled GPCRs simply do not produce enough free G βγ to activate GIRK channels or other G βγ effector systems (Touhara and MacKinnon, 2018).

Combined with data suggestion G proteins are quite mobile (Sungkaworn et al., 2017), these observations lead to the conclusion that inhibitory G protein signaling through βγ is a fundamentally graded response rather than the sum of a large number of high affinity interactions each contributing a small portion of maximal response; active receptors contribute to a shared pool of active G proteins to interact with effectors with low affinity (Touhara and MacKinnon, 2018). In other words, effectors like GIRK channels become sensors of G βγ concentration rather than acting through rarer but higher affinity triggered responses.

D2 receptors in dopamine neurons are found in clusters (Robinson et al., 2017) which has been suggested as an efficient means of boosting local G protein concentrations to overcome steep concentration requirements (Touhara and MacKinnon, 2018). The predictions of this model are concentration gradients of higher concentration proximal to clusters of receptors but with G βγ concentrations being raised across the membrane due to the mobility of G proteins. Efficient coupling to GPCRs can be achieved by proximity to receptors or clusters of receptors. This view of GPCR signaling has several implications discussed in Chapter 7 regarding how different types of receptors coupled into this same G protein system interact.

The combination of unknown rates between agonist receptor interactions, receptor-G protein interactions, G protein diffusion and lifetime dynamics, and time course of dopamine release make understanding the D2 IPSC from a reductionist standpoint difficult. Chapter 6 describes work uncovering the functional time course of dopamine-receptor interactions in the IPSC by rapidly antagonizing receptors with light-activated antagonist. Combined with Chapter 5, which consists of work describing a novel mutation in the D2 receptor that modifies how the receptor couples to G

proteins, this dissertation contributes to a progressive demystification of the GPCR-G protein signaling system.

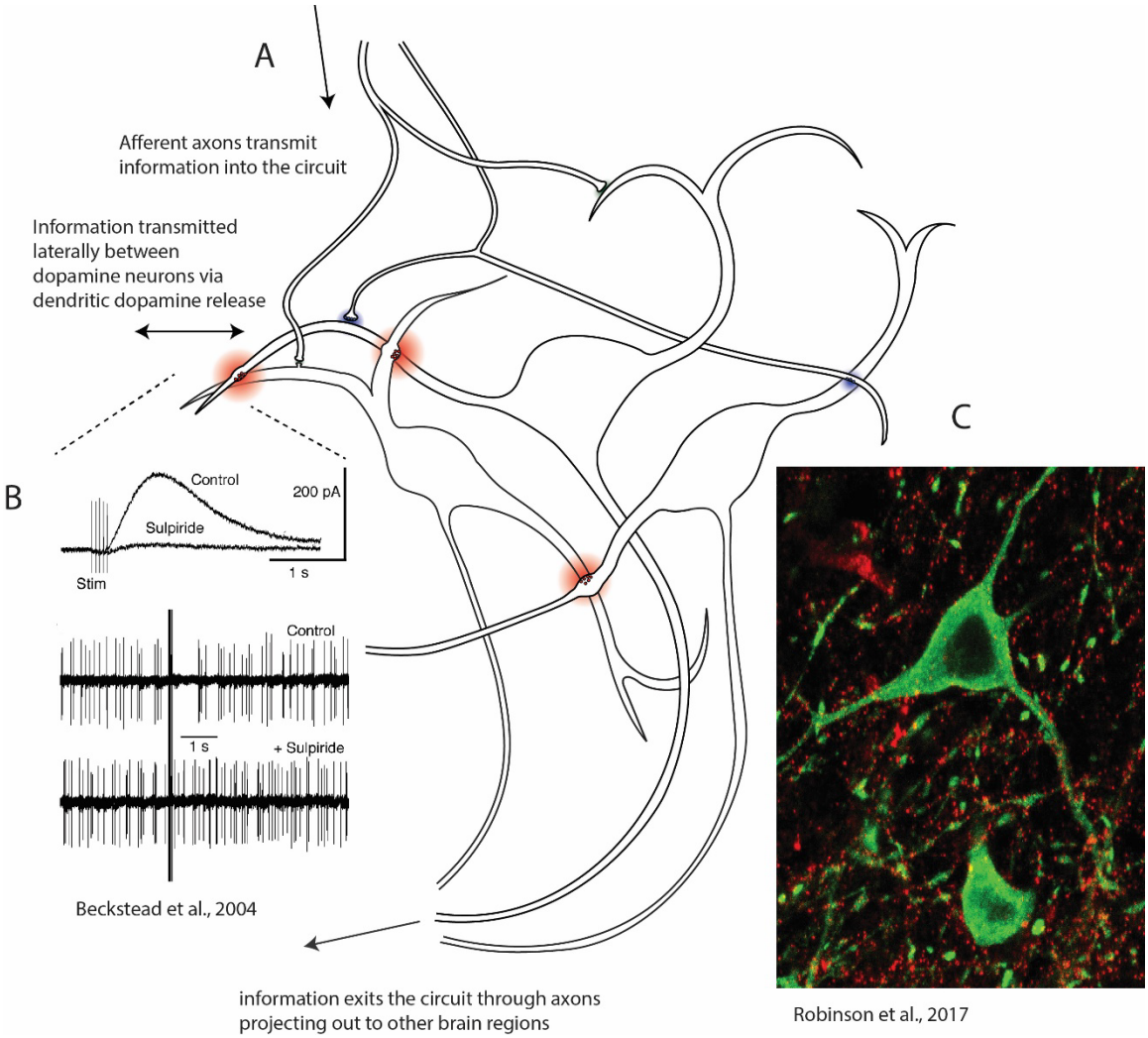

Figure 1-1 Schematic of Dopamine Neurons

A) Axons projecting from other brain regions make synapses on to dopamine neurons to control their excitability. Excited dopamine neurons release dopamine on to neighboring neurons as a form of lateral inhibition. Action potentials are generated based on the combination of afferent and local neurotransmission combined with intrinsic neuronal properties. Action potentials then travel down axons projecting to other brain regions to release dopamine in those regions. B) Dendrodendritic dopamine release between dopamine neurons produces a D2 dependent inhibitory post-synaptic current (Top; Beckstead et al., 2004). This “outward” potassium mediated current causes a voltage hyperpolarization to regulate dopamine neuron firing (bottom). C) Immunofluorescent labeling of dopamine neurons with tyrosine hydroxylase (a protein expressed in dopamine neurons) in green and D2 receptors in red (Robinson et al., 2017).

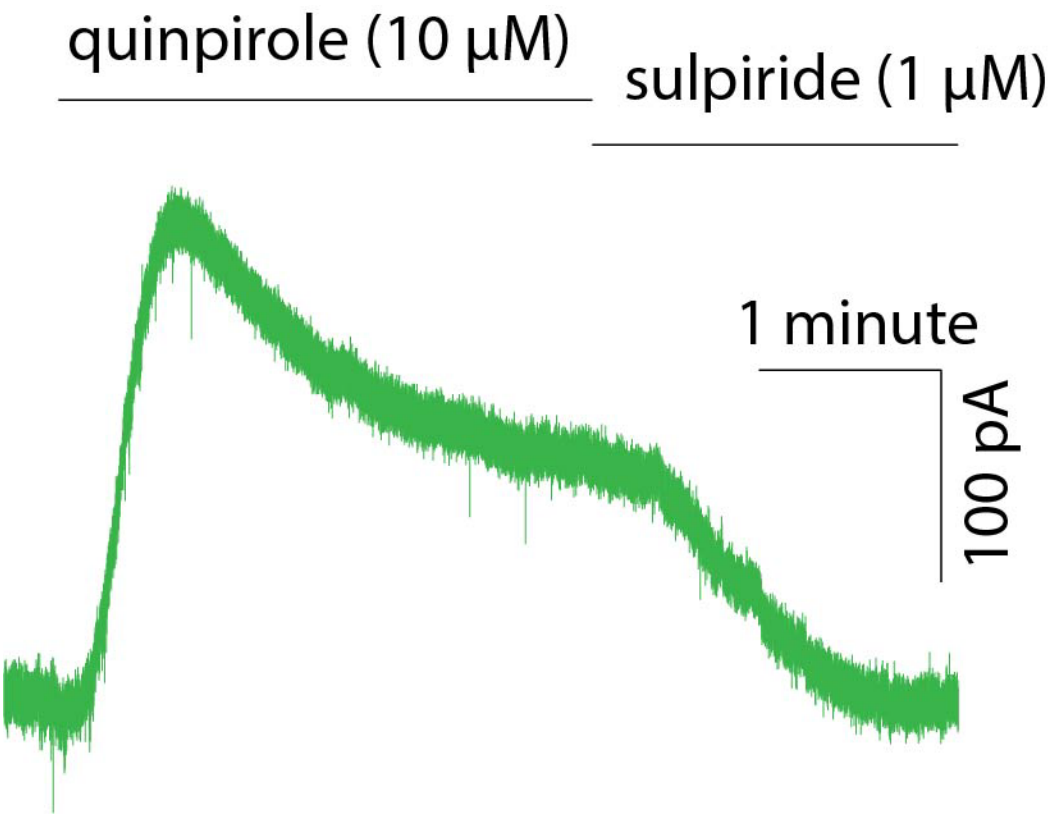

Figure 1-2 Desensitization of D2 receptor signaling

Example trace of a D2 dependent GIRK current generated by bath perfusing a D2 receptor agonist (quinpirole) and reversed with an antagonist (sulpiride). Desensitization of signaling can be seen by the decline in current amplitude in the continued presence of agonist.

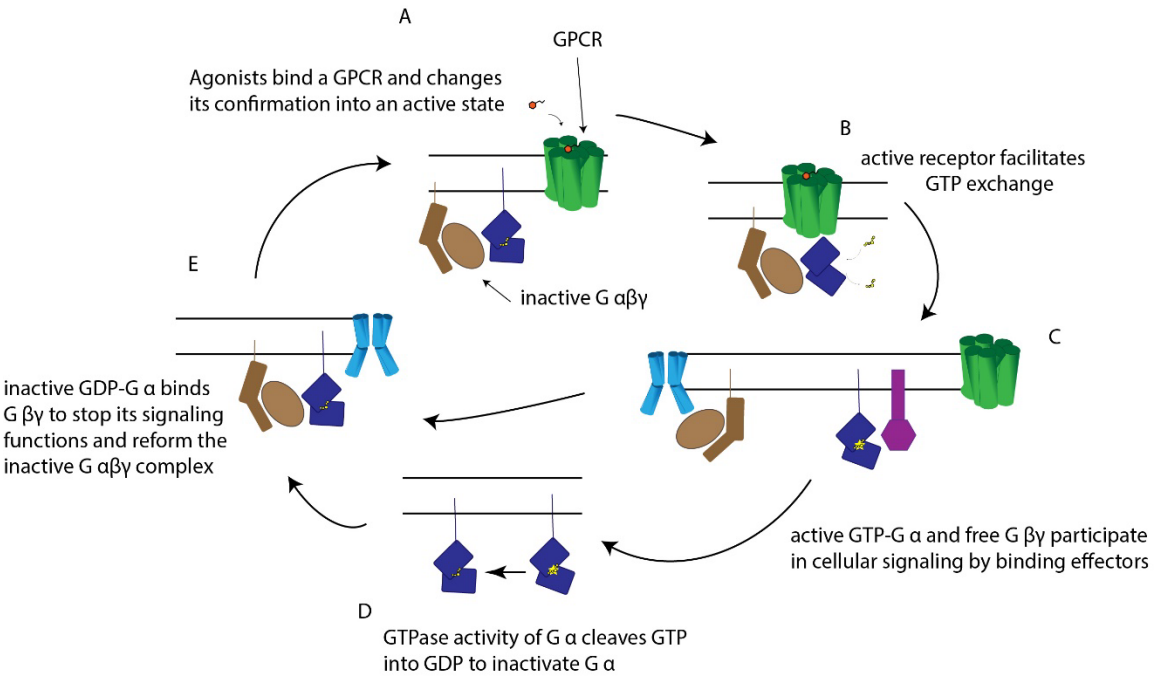

Figure 1-3 The G protein cycle of GPCR signaling

A) Agonists bind receptors which changes their confirmation into the active state. B) Active receptors associate with GDP-associated heterotrimeric G αβγ. Receptors then catalyze the exchange of GDP for GTP in the G α subunit, activating the G proteins. This catalysis does not inactivate the receptor so a single activated GPCR can catalyze GTP exchange for multiple G proteins depending on context. C) GTP-G α loses its affinity for G βγ and the two subunits split off, diffuse away, and participate in cellular signaling by binding effector proteins. In the case of inhibitory GPCRs, GTP-G αi will bind to and inhibit adenyl cyclase to broadly suppress cell excitability and G βγ interacts with a wide array of effector proteins including functions to suppress calcium channels or bind GIRK channels and induce inhibitory potassium currents. D) Over time, either through intrinsic GTPase activity or facilitation by RGS proteins, G α cleaves the terminal phosphate from GTP, converting it back into GDP which turns off G α signaling functions. E) GDP-G α then binds G βγ with high affinity and returning the heterotrimeric G protein to its basal inactive state at the start of the G protein cycle, ready to be reactivated by an active GPCR.

Chapter 2 – Materials and Methods

Slice preparation and whole-cell electrophysiology

Mice (male and female, C57BL/6J, 8-12 weeks) were deeply anesthetized with isoflurane and decapitated. Brains were removed and horizontal sections (222 µM) were cut using a Leica vibratome. Brains and sections were kept warm (32-34°C) throughout this process using Krebs buffer (with concentrations in mM, 126 NaCl, 1.2 $MgCl_2$, 2.4 $CaCl_2$, 1.4 NaH_2PO_4, 25 $NaHCO_3$, and 11 D-Glucose). Throughout all, bath solutions were bubbled with 95%/5% O_2/CO_2 gas. MK-801 (2.5 µM) was including in the cutting solution as well as the recovery bath (10 µM) where slices were allowed to recover for >30 minutes before they were hemisectioned and returned to Krebs without MK-801. For experiments, slices were perfused with Krebs (2-3 mL/minute) and maintained at 34-36 °C. Two internal recording solutions were used with different calcium buffers (concentrations in mM): EGTA (0.1 EGTA, 130 K-methanesulphonate, 20 NaCl, 1.5 $MgCl_2$, 10 HEPES(K), 2 ATP, 0.2 GTP, and 10 phosphocreatine) and BAPTA (10 BAPTA(4K), 90 K-methanesulphonate, 20 NaCl, 1.5 $MgCl_2$, 10 HEPES(K), 2 ATP, 0.2 GTP, and 10 phosphocreatine). Each experiment type used an even mix of the two recording solutions except for those in Figure 7.5 which only used the EGTA internal to more closely match endogenous calcium buffering. Recordings were made using glass electrodes (1.4-1.9 megaohm) and gigaohm seals were achieved prior to breaking into whole-cell configuration. Nigral dopamine neurons were first identified anatomically and verified by a combination of pacemaker firing while recording cell-attached and response to D2 and $GABA_B$ receptor agonists. Cells were maintained at -60 mV with voltage clamp using an Axopatch200A amplifier (Axon Instruments), continuously monitored with Chart 5.5.6 (AD Instruments, Colorado Springs, CO)., and individual trials using AxoGraph X. Input resistance and membrane resistance and capacitance were measured. For experiments involving electrical stimulation, a metal bipolar electrode (World Precision Instruments) was placed in the nigra and two 0.5 ms pulses (40 Hz) were used to elicit release.

Mice

All studies were conducted in accordance with the Institutional Animal Care and Use Committees at the VA Portland Health Care System (VAPORHCS) and Oregon Health & Science University (OHSU). Twelve mice (4 male and 8 female, 59–96 days old on day of surgery) were used in the study of the I212F mutation. Auto-D2-KO mice were bred at the VAPORHCS Veterinary Medical Unit by crossing Drd2loxP/loxP mice (Bello et al., 2011), obtained from Jonathan Javitch (Columbia University, USA), with heterozygous B6.SJL-Slc6a3tm1.1(cre)Bkmn/J mice(56) obtained from the Jackson Laboratory (JAX stock no. 006660). All lines are maintained on a C57BL/6 background. Mice were housed in standard plastic containers on a 12 h light/dark cycle with food and water available ad libitum. For expression of recombinant D2S receptors in dopamine neurons, auto-D2-KO mice were immobilized in a stereotaxic alignment system after injection of an anesthesia cocktail consisting of 7.1 mg/kg xylazine, 71.4 mg/kg ketamine, and 1.4 mg/kg acepromazine (10 mL/kg, i.p.). Mice received bilateral 500 nL injections of AAV-DIO-hD2S-WT or -I212F in the ventral tegmental area, at a rate of 200 nL/min, with the injection needle left in place for an additional 5 min before it was slowly withdrawn. The coordinates for injections were AP −3.26 mm, ML ±1.2 mm, DV −4.0 mm. After injections, mice recovered in individual (male) or group (female) housing for 2–3 weeks to allow for expression.

Mice with genetic deletion of the long splice variant of the dopamine D2 receptor (D2L-KO or D2L-/-) and the short variant of the D2 receptor (D2S-KO or D2S-/-) were used in this study in addition to wild types from each of these lines. Mice originated from the Borrelli laboratory (UC Irvine). For further information on creation of lines refer to Usiello et al. (2000) and Radl et al. (2013).

Bilateral stereotaxic injections of AAV9 (Syn dLight1.3b, Vigene Biosciences) into the substantial nigra were done in mice anesthetized with isoflurane. The coordinates were AP −2.3 from bregma: ML ± 1.3: DV −4.5 mm. Injection volume was 120 nl. Experiments were done 1-3 weeks following the surgery.

Pharmacology

Most drugs were applied with bath superfusion. CyHQ-O-dopamine was dissolved in DMSO (50 mM) and aliquoted for a fresh vial to be used daily. The working solution (50 µM) was recirculated over the slice for 5+ minutes prior to the start of experiments. Similar procedures were used for CDNI-GABA with a stock solution of 50 mM and working concentration of 50 µM. Photolysis of these caged compounds was induced by a ThorLabs M365LP1-C1 LED (3.8 mW, 265 nM, 2.5 ms for experiments in supplemental Figure 7.1, 0.2 mW). For iontophoresis, thin-walled glass electrodes (70-110 megaohm) were filled with 1 M DA or 500 uM GABA. GABA acidity was adjusted to 3 pH to reduce the zwitterion for easier electric control. Agonists were held in the pipette with a backing current (5 nA and 2 nA for DA and GABA respectively) and expelled from the pipette with a 200 nA pulse. For experiments using electrical stimulation, NBQX (1 µM) and picrotoxin (100 µM) to block AMPA and GABAA receptors respectively in addition to the pre-treatment with MK-801 to block NMDA receptors. All other drugs were applied by bath perfusion.

Forskolin was used to facilitate dopamine release specifically in experiments with the use of a single stimulus for the experiments in Chapter 6. This treatment increased the amplitude of the IPSC about 2-fold such that more accurate measurements of block by the CyHQ-sulpiride could be made. In previous publications forskolin have been shown to have little or no postsynaptic effect on the D2-receptor activation of potassium conductance. Given that the rate of current decay induced by CyHQ-sulpride was the same for the IPSC and the exogenously applied dopamine, the results indicate that forskolin had no postsynaptic action on the kinetics.

Recombinant cDNA Constructs

All human D2 receptor cDNA constructs (for work in Chapter 5) contained a signal peptide and a FLAG epitope tag at the receptor N-terminus. The wild type (WT) short (SF-hD2S) and long (SF-hD2L) isoforms of human D2 receptors as well as the SF-hD2L(I212F) and SF-hD2S(I212F) variants in pcDNA3 and the corresponding RLuc8 fusion proteins for arrestin BRET assays were described

previously (van der Weijden et al., 2021). Other plasmids for arrestin3 recruitment BRET assays (human arrestin3 fused to mVenus and human GRK2), for measuring G protein activation (Gαi1-91-RLuc8, V1-Gß1 and V2-Gγ2), and for inhibition of cAMP accumulation (pcDNA3l-His-CAMYEL; ATCC MBA-277) were previously described (Clayton et al., 2014; Jiang et al., 2007), except for the plasmid GαoA-91-RLuc8 (Marcott et al., 2018; Saulière et al., 2012) that was obtained from Jonathan Javitch (Columbia University, USA). For animal studies, recombinant adeno-associated viral (AAV8.2) vectors containing a Cre recombinase-dependent double-floxed inverted open reading frame (DIO) for hD2S-WT or -I212F, tagged at their C terminus with a self-cleaving 2A peptide and EGFP, were described previously (van der Weijden et al., 2021) and were produced by Virovek, Inc. (Hayward, CA, USA). To generate stable transfected HEK293 cells, pcDNA3.1[SF-hD2S-P2A-EGFP] was obtained from Jonathan Javitch (Columbia University, USA). Plasmids containing wild type and mutated D2L isoforms (pcDNA3.1[SF-hD2L-P2A-EGFP] and pcDNA3.1[SF-hD2L(I212F)-P2A-EGFP], respectively) and mutated D2S isoform (pcDNA3.1[SF-hD2S(I212F)-P2A-EGFP]) were generated by digesting pcDNA3.1[SF-hD2S-P2A-EGFP] with BstEII and PmlI (New England BioLabs, MA, USA). The purified 6.8 kb fragment was ligated to each 782 bp insert generated by BstEII/PmlI digestion of pcDNA3[SF-hD2L] and pcDNA3[SF-hD2L(I212F)] or 695 bp insert of pcDNA3[SF-hD2S(I212F)], using T4 DNA Ligase (New England BioLabs). All new constructs were verified by DNA sequencing at the OHSU Vollum DNA Sequencing Core Facility (Portland, Oregon, USA).

Cell Culture and Transfection Conditions

HEK293 cells obtained from Caroline Enns (Oregon Health & Science University, USA) were maintained in Dulbecco's modified Eagle's medium (DMEM) supplemented with 10% FetalClone I serum (FCS; Thermo Fisher Scientific; Waltham, MA, USA) at 37 °C in a 5% CO2 atmosphere. New cell cultures were initiated frequently from frozen stocks. Eighteen hours before transfection, HEK293 cells were plated in 100 mm dishes at 60–80% confluence. HEK293 cells were transfected with equal amounts of D2-WT or D2-I212F receptor DNA, except in some arrestin recruitment (Figure S5.1) and

D2-mediated inhibition of cAMP (Figure 5.3C,D) assays. Transient transfections were performed with polyethylenimine (PEI; MAX 40K reagent, Polysciences, Inc.; Warrington, PA, USA) in Opti-MEM I (Gibco by Life Technologies; Logan, UT, USA). In most cases, two 100 mm Petri dishes per condition were transfected to allow us to carry out BRET and radioligand binding assays using identically treated cells. Transfections were incubated for 5–6 h at 37 °C in the 5% CO2 humidified atmosphere, after which the medium was replaced by fresh DMEM plus 10% FCS. Cells were harvested 48 h post-transfection for BRET studies and frozen for radioligand binding assays.

To study quinpirole affinity of the D2 variants, stable HEK293 cells expressing either SF-hD2L/S-P2A-EGFP or SF-hD2L/S(I212F)-P2A-EGFP were generated by transfecting the respective plasmids with PEI in 12-well plates, as described above. Two days after transfection, cells recovered from each well were plated into two 100 mm dishes in supplemented DMEM containing 500 ug/mL of G-418 (Gold Biotechnology Inc.; MO, USA). Colonies were initially screened for EGFP expression by immunoblotting. Then, EGFP-positive clones were screened for Flag tagged-D2 expression by immunoblotting, using a rabbit polyclonal antibody anti-DYKDDDDKC epitope tag (Invitrogen; CA, USA), and radioligand binding assays as described below. Stable transfected cells were maintained in DMEM plus 10% FCS, with 500 ug/mL of G-418.

Bioluminescence Resonance Energy Transfer (BRET) Assays

For arrestin3 recruitment, cells were cotransfected with plasmids containing mVenus-Arr3 (2.5 µg) and the WT or I212F-mutated D2 receptor fused to RLuc8 (0.25 µg except for Figure S5.1, where D2-WT receptor DNA amounts were adjusted to yield similar levels of receptor expression for the allelic variants), with or without hGRK2 (2 µg). For G protein activation, cells were cotransfected with WT or I212F-mutated D2 receptor (0.5 µg), the G protein subunits V1-Gß1 (2 µg) and V2-Gγ2 (2 µg), and the Gα proteins Gαi1-91-RLuc8 (0.2 µg) or GαoA-91-RLuc8 (0.2 µg). For cyclic AMP accumulation, cells were cotransfected with WT (0.2 µg for WT-Low and 0.5 µg for WT-High) or I212F-mutated D2 receptor (0.5 µg) and the cyclic AMP sensor CAMYEL (2.5 µg). Control cells were

transfected with CAMYEL and nonspecific plasmid DNA. After 48 h, cells were harvested, washed, resuspended in PBS containing CaCl2, MgCl2, and 11 mM d-glucose, plated at 100 000–150 000 cells/well in 96-well OptiPlates (PerkinElmer Life Sciences), and incubated at 37 °C and 5% CO2 atmosphere for 1 h before adding the agonist quinpirole. Compound 101 (Cmpd101; HelloBio, Princeton, NJ) was initially dissolved in DMSO at 100 mM and subsequently diluted in PBS. For GRK2 inhibition during arrestin recruitment-BRET assays, HEK293 cells were pretreated with 30 μM of Cmpd101 or vehicle (DMSO diluted in PBS) 30 min before agonist addition. For D2-mediated inhibition of cyclic AMP, HEK293 cells were pretreated with the dopamine D1 receptor antagonist SCH 23390 (1 μM) and the β-adrenoceptor antagonist pindolol (0.1 μM; Sigma-Aldrich; MO, USA) before the addition of inverse agonist (10 μM sulpiride or 1 μM spiperone) and 10 μM forskolin (Sigma-Aldrich; MO, USA). Emission of the donor (460 μm) and acceptor (535 μm) was measured at room temperature several times after adding the luciferase substrate coelenterazine h, and BRET ratios were calculated as previously described (Clayton et al., 2014; Pfleger et al., 2006).

D2 Receptor Radioligand Binding

Membrane expression of the receptors was evaluated exactly as described previously (van der Weijden et al., 2021). Cells were lysed in ice-cold hypotonic buffer (1 mM HEPES, 2 mM EDTA, pH 7.4), scraped from the plate, and centrifuged at 17 000 × g at 4 °C for 20 min. The resulting pellet was resuspended in Tris-buffered saline (TBS: 50 mM Tris, 120 mM NaCl, pH 7.4) and homogenized for 10 s using a Polytron homogenizer (Brinkmann Instruments, Westbury, NY). Protein determination was performed using the BCA Protein Assay Kit (Thermo Scientific). Samples were incubated in TBS containing 0.002% BSA and [3H]spiperone at 37 °C for 1 h in a final volume of 1 mL before addition of ice-cold buffer and vacuum filtration. Nonspecific binding was assessed using (+)-butaclamol (2 μM). Competition binding assays were carried out using membranes prepared from HEK293 cells stably expressing each of the four receptor variants. The ability of various concentrations of quinpirole to

inhibit the binding of [3H]spiperone (~85 pM) was analyzed by nonlinear regression. IC50 values were converted to Ki according the method of Cheng and Prusoff (Yung-Chi and Prusoff, 1973).

2-photon microscopy

Imaging was carried out using a custom built 2-photon microscope with ScanImage software (Pologruto et al., 2003). Full frame images (128x128 pixels) were taken at a rate of 4 Hz. Line scans through areas of interest were taken at 2 ms/line.

Quantification and statistical analysis

Phasic currents were analyzed with AxoGraph. Peak currents were quantified by the find peak function and averaged ± 20 ms from peak (for more accurate estimate of slow currents). Traces that were analyzed for width were then heavily filtered (down to as low as 20 Hz) to a point where accurate readings could be measured due to the way AxoGraph measures peak width. Measurements of heterologous synaptic enhancement was also done using graph subtraction functions and integral transformations. Statistical analysis was done using GraphPad Prism 7. Desensitization and recovery from desensitization measures were analyzed by non-linear curve fit, respectively one-phase decay or association. T tests were used to compare data with two sample groups and 2way ANOVA with Sidak's multiple comparison test was used to analyze the experiments testing heterologous enhancement of synaptic currents (Figure 7.5). Further statistical detail can be found in the results section and figure legends.

Kinetic simulations of G βγ concentrations and interaction with GIRK

The equations and starting conditions for kinetic simulations were reproduced from Tauhara and MacKinnon 2018 and the G βγ-GIRK concentration response curve was modified from Wang et al 2016.

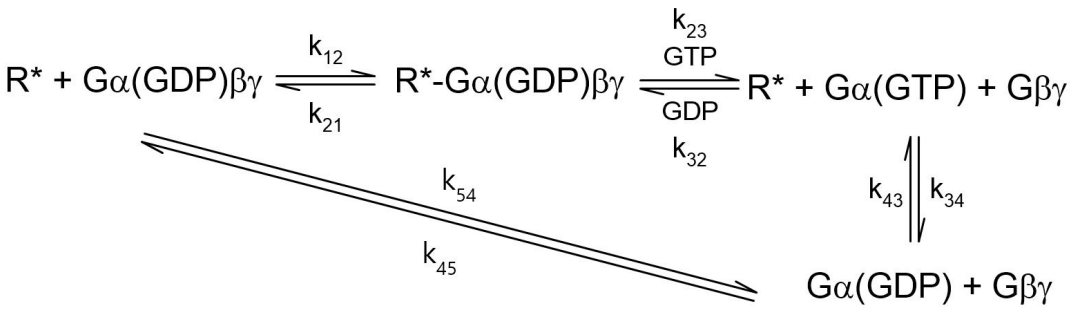

Table 2-1 G protein cycle reactions and rates used to model GPRC-GIRK interactions

Reaction	Forward-rate	Backward-rate
R* + Gα(GDP)βγ ⇌ R*-Gα(GDP)βγ	k_{12}: 1 μM^{-1} sec^{-1}	k_{21}: 1 sec^{-1}
R*-Gα(GDP)βγ⇌ R* + Gα(GTP) + Gβγ	k_{23}: 1 sec^{-1}	k_{23}: assumed irreversible
R* + Gα(GTP) + Gβγ⇌Gα(GDP) + Gβγ	k_{34}: 2 sec^{-1}	k_{43}: assumed irreversible
Gα(GDP) + Gβγ ⇌ Gα(GDP)βγ	k_{45}: 0.7x10^6 M^{-1} sec^{-1}	k_{54}: 0.002 sec^{-1}

The equations for change over time as a function of reactant concentration and rates were schematized in Mathematica and NDSolve was used to solve for reactant concentrations over time. The initial concentrations used for analysis in Tauhara and MacKinnon 2018 used receptor and heterotrimeric G proteins were concentrations of 10 and 20 micromolar, respectively. For the purposes of simulating phasic GPCR activation, receptor concentration was changed from static to a falling concentration with a time constant equal to dopamine concentration decay follow dendrodendritic release in the nigra (τ=223 ms, Supplemental Figure 7.2) as measured by dLight (Condon et al, 2021). As the G βγ-GIRK binding reaction is thought to be diffusion limited, this interaction was simplified and predicted GIRK activity was simulated merely by passing the G βγ concentrations throug8h the GIRK concentration response curve (Wang et al, 2016). It should be

noted that the affinity of G βγ for GIRK2/3 channels is not static. To gate the channel requires the coordinated actions of Na^+ ions, phosphatidylinositol 4,5-bisphosphate (PI(4,5)P2), and G βγ with each additional molecule increasing the affinity of others by stabilizing the open confirmation and thermodynamic linkage (Wang et al, 2016). This affect also increases the maximal conductance of the GIRK channels. For the purposes of simulating G βγ-GIRK interactions in this context, PIP2 concentrations are assumed to be static, matching the conditions of Wang et al 2016, and sodium concentration set to be that used in the internal solution of the recording pipette, 20 mM. Note, it is also worth mentioning that both works discussed here from the MacKinnon lab, Wang et al 2016 and Taurara et al 2018, convert 2D protein density in the membrane to 3D concentration close to the membrane by multiplying by a linear distance into the cytoplasm equal to the length of G βγ. These two papers use slightly different assumptions of this multiplier, so calculations from Wang et al 2016 are here converted into the distances used by Tauhara and MacKinnon 2018 (70 vs 80 Å). As described in the results sections, the concentrations of G βγ produced using a phasic pulse under these initial assumptions are relatively low, so if these concentrations were accurate to a dopamine neuron, tonic G βγ concentrations produced by low-level $GABA_B$ receptor activation would also be low. To simulate tone in a normalized fashion, low tonic G βγ was set to be equal to 30% and high tone equal to 100% of the peak concentration and from the associated phasic pulse in each condition (Supplemental Figure 7.2). As can be seen, this addition passed through the GIRK concentration-response curve does indeed show facilitation, however the level of facilitation is much greater than observed in dopamine neurons so already this first set of assumptions does not seem accurate to dopamine neurons.

To move beyond the set of assumptions from Tauhara et al 2018 which was attempting to model GPCR activation in CHO cells, conditions may be quite different in a dopamine neuron which natively uses GPCR-GIRK signaling. Whereas their set of assumptions produces a standing concentration of G βγ maxing out at ~5 μM, previous work from the MacKinnon lab gave estimates

of G βγ concentrations in dopamine neurons produced by maximal $GABA_B$ activation equal to 245 μM (280 μM as published but converted from 70 to 80 Å assumption of linear distance into the cytoplasm). Clearly, this concentration is much higher than would be possible with the base assumptions of receptor concentrations of 10 μM and G protein concentrations of 20 μM.

For the next set of assumptions attempting to match conditions in dopamine neurons, both receptor and G protein concentration must be increased. Only increasing one or the other bottlenecks the system such that it still cannot approach the 245 μM G βγ measured in dopamine neurons. Precise measurements of surface D2 or $GABA_B$ receptor density is not available, but detailed measurements of GABAB receptor density have been done with freeze-fracture EM for Purkinje neurons, another neuronal subtype where $GABA_B$ activation is coupled to GIRK channels (Luján et al, 2018). Here, authors give two density measurements, one for overall compartment-specific densities, and one for compartment-specific cluster densities. Tauhara and MacKinnon (2018) uses the assumption that overall receptor density is concentrated into 10% of the membrane based on the previous observation that single-particle GPCR-G protein interaction happen in membrane hotspots equal to about 10% of the membrane, even in non-specialized cells (Sungkaworn et al 2017). It is notable that the density estimates given by freeze fracture gold-particle labeling of $GABA_B$ receptor clusters vs total membrane are in reasonable agreement with this 10% hypothesis, though there is effect of cluster size affecting density. $GABA_B$ receptor density in spines was found to be 227.62 μM^{-1} or 2276.2 μM^{-1} cluster density by the 10% membrane hypothesis or 455.2 μM based on the Tauhara and MacKinnon (2018) conversions of membrane density to concentration at the membrane. Therefore, for the next model initial receptor concentration was simplified to 500 μM and G protein concentration was set at 600 μM (Supplemental Figure 7.3). With these conditions, G protein concentration peaks at ~55 μM. The same interactions with tonic G βγ can be seen here with facilitation of the amplitude and duration of GIRK response can be seen. However, given this model of receptor activation starts with full receptor occupancy that decays, this

nicely mimics what would be expected with a strong pulse of dopamine uncaging. Given comparison to real data, this set of assumptions still does not produce a high enough concentration of G βγ if max $GABA_B$ response produces 245 μM G βγ. The high tone condition also results in more facilitation than low tone, which is a potential contrast to experimental data which shows the facilitation effect on amplitude can saturate.

For the final model (Figure 7.6), initial receptor and G protein concentrations are kept at 500 and 600 μM, but reaction rates are increased. Critical rates complied and used by Tauhara and MacKinnon (2018) were measured at room rather than physiological temperatures. Rather than attempting to accurately guess the temperature sensitivity of each reaction, the forward reaction rate of G protein-receptor binding (k_{12}), GDP-GTP exchange (k_{23}), and G protein GTPase activity (k_{34}) were all multiplied by 10. This results in similar equilibrium concentrations, but equilibrium is reached much faster and the simulated response to the phasic receptor activation is much higher (peak of ~160 μM). As discussed in the results section, the specific numbers and assumptions foe each of these models are certainly wrong, but in every case, the models predict facilitation of GIRK current amplitude and prolongation of decay times, and this final model additionally predicts saturation of facilitation of amplitude.

D2 Receptor Homology Models and Molecular Dynamics Simulations

Homology modeling was performed using YASARA Structure (Krieger et al., 2002) that features a CASP- (Critical Assessment of Structure Prediction) approved protocol (Krieger et al., 2009). The inactive state of the D2 receptor was modeled using inactive structures of the β2-adrenoceptor (2RH1), the A2A adenosine receptor (3EML and 6GT3), the M2 muscarinic receptor (3UON), bovine rhodopsin (1GZM), and the D2 receptor (6CM4) as templates. The D2 receptor active state model was built using active-state structures of the M2 receptor (4MQS), the β2-adrenoceptor (3SN6 and 3P0G), the A2A receptor (2YDV and 5WF6), the CB1 receptor (6N4B), the μ-opioid receptor (6DDE), and rhodopsin (3PQR) as templates. Multiple D2 receptor models for inactive and

active states (48 and 45 models, respectively) were obtained, and side chain rotamers were optimized using backbone-dependent probabilities and knowledge-based force fields in YASARA (Krieger et al., 2004). The resulting models were further optimized for hydrogen bonding, refined using short molecular dynamics simulations, and ranked. Residue-specific quality graphs were calculated for each model, and a final hybrid model was developed through an iterative process, replacing poorly scoring regions in the best model with the corresponding regions from other models, with the goal of increasing the accuracy beyond each of the contributing models. The stereochemical properties of the homology models were verified using the PROCHECK module (Laskowski et al., 1993) of the PDBSum server, which examines protein quality based on parameters such as percentage of residues lying in favored and allowed regions, the number of glycine and proline residues, the orientation of dihedral angles including phi (ϕ) and psi (ψ), and backbone conformation. The VERIFY3D (Eisenberg et al., 1997) server was used to check the compatibility of atomic models (3D) with its own primary amino acid sequences (1D). The RSMD of the α-helical segments of the resulting active-state homology model of the D2 receptor was 1.62 and 1.63, respectively, relative to 6CM4 and the recently published active-state structure of the D2 receptor 6VMS (Yin et al., 2020).

To assess the potential functional impact of the I212F substitution on the active and inactive D2 receptor homology models, the system was simulated atomistically for 15 ns using the YASARA software package under an NPT ensemble with the AMBER14 force field (Ponder and Case, 2003), with a time step of 5.0 fs. Simulation conditions were conducted with periodic boundaries, at 0.9% NaCl concentration by mass, pH 7.4, 298 K, at atmospheric pressure. The water model employed was TIP3 equiv. Snapshots were saved every 100 ps. Structures were visualized using YASARA and the distances between the atom OE1 of E368 and HH1 and HH2 atoms of R132 were monitored during the simulation and plotted using Prism GraphPad software.

Chapter 3 – Tool development and characterization

Preface

In studying D2 autoreceptor plasticity, the method of agonist application must always be considered. Electrical stimulation to induce endogenous dopamine release introduces pre-synaptic plasticity as a variable and clouds interpretation of results. Bath perfusion of drugs is useful in studying D2 receptor desensitization, but it is a blunt instrument. The dense architecture of brain slices makes for slow wash in and wash out of any compound, but particularly with the drugs currently available for the D2 receptor. Dopamine iontophoresis is useful in applying phasic pulses of dopamine, but the thin glass tips are prone to variability in thickness, can be difficult to place precisely, and small changes in tip position can lead to large changes in response kinetics and amplitude. In short, as useful as it can be, iontophoresis cannot be considered a quantitative method of agonist application. Though not without its own consideration, an alternative method of fast exogenous drug application is the use of chemically "caged" compounds with photolabile linkers.

The following section is from a methods paper describing the synthesis and properties of such a caged compound, CyHQ-O-dopamine. This compound, designed and synthesized by the Dore Lab, is nearly inert at baseline, but following exposure to UV light, the CyHQ compound breaks off from the rest of the molecule, freeing dopamine to interact with the D2 dopamine receptor. My work on this paper was to characterize the properties of its use in brain slice as a tool to study dopamine neuron biology. In the context of this dissertation, I show that it is a well-behaved molecule that I then use throughout the rest of my work that can be repeatedly uncaged when recirculated without damaging the health of cells or with significant reduction in total concentration if using moderate intensity and duration UV flashes. One downside of this compound is that rather

than being totally inert, I found that it retains some level of low affinity or low efficacy interaction with the D2 receptor. This is exemplified by producing a standing outward current when applied to dopamine neurons. When used at lower concentrations (50 μM was my chosen working concentration, in part due to the findings of this study), this effect is minimal, but can be significant when used at sufficiently high concentrations. To confirm that the current produced by CyHQ-O-dopamine was not due to free dopamine, I used a high concentration and applied a D2 receptor antagonist. This treatment only partially reversed the current meaning sulpiride could only partially out compete the agonism. If the current produced by CyHQ-O-dopamine was due to a small amount of free dopamine, it would readily be reversed by sulpiride, but that sulpiride could only partially reverse this current suggested it was competing with a high concentration of a very low efficacy agonist. For the purposes of my future work, it simply meant I should choose a relatively low concentration for experiments.

Though the bulk of this publication was focused on CyHQ-O-dopamine, also included was work looking at CyHQ-sulpiride, a caged antagonist. It similarly seems to have some level of baseline activity, either from free sulpiride or lower affinity interaction with the D2 receptor, but it has been another tool I have been able to leverage to useful effect in studying dopamine signaling in the rest of this dissertation.

Photoactivatable Dopamine and Sulpiride to Explore the Function of Dopaminergic Neurons and Circuits

Naeem Asad,† Duncan E. McLain,†‡ **Alec F. Condon**,§ Sangram Gore,† Shahienaz E. Hampton,† Sauparnika Vijay,† John T. Williams,§ and Timothy M. Dore†‡

†New York University Abu Dhabi, Saadiyat Island, PO Box 129188, Abu Dhabi, United Arab Emirates

‡Department of Chemistry, University of Georgia, Athens, Georgia 30602, United States

§Vollum Institute, Oregon Health and Science University, Portland, Oregon 97239, United States

Acknowledgments

Part of this work was carried out using Core Technology Platform resources at New York University Abu Dhabi. We thank Davide Deodato, Brooks G. Robinson, David Weiner, and Samuel S.–H. Wang for helpful discussions.

This research was supported by New York University Abu Dhabi and in part by grants to T.M.D. from the U.S. National Institutes of Health (R01 NS070159) and the U.S. National Science Foundation (CHE-1012412 and CHE-1317760), to J.T.W. from the U.S. National Institutes of Health (R01 DA004523), and to A.F.C. from the U.S. National Institutes of Health (F31 DA047007).

[A portion of this manuscript is presented as published in (Asad et al., 2020), ACS Chemical Neuroscience, 2020, March 18, 11:939-951]

Results

Asad et al. states:

Photoactivation of Dopamine in Brain Slice

Midbrain dopamine neurons provide an ideal target for testing CyHQ-O-DA in acute brain slice. Substantia nigra pars compacta neurons express the inhibitory D2 receptor that activates the G protein-coupled inwardly rectifying potassium (GIRK) channel. These currents can be measured with whole cell voltage clamp recordings to provide a convenient readout of receptor activation. When recirculated over the slice (150 µM, 5 mL), flash photolysis of CyHQ-O-DA produced a robust GIRK-mediated outward current with a rapid activation phase and a slow decay (Figure 3.1). The response increased in amplitude and duration when cocaine was added, as would be expected with an inhibition of dopamine uptake, and all response was blocked with the addition of the D2 receptor antagonist sulpiride (500 nM).

The kinetics of the flash response were compared to synaptically released dopamine and iontophoretically applied dopamine (Figure 3.2). For medium-strength conditions for photoactivation (2.5 ms of a 1.8 mW pulse, 50 µM CyHQ-*O*-DA), picked because stronger pulses result in slower kinetics, the time the current response took to rise from 10 to 90% of the peak was 210 ms compared with 141 and 270 ms for synaptically released and iontophoretically applied dopamine, respectively. Although only the inhibitory postsynaptic current (IPSC) response was significantly faster than iontophoresis ($p = 0.002$ one-way ANOVA with Tukey's multiple comparison), the kinetics of the photolysis response represented a middle point between the two ($p = 0.08$ photolysis vs IPSC, $p = 0.13$ photolysis vs iontophoresis). The concentration of dopamine sensed by neurons in synaptic release is thought to be quite high (10–30 µM) with lower concentrations producing slower rise-time kinetics (Courtney and Ford, 2014). The kinetics of the photolysis response suggests an upper limit in effective dopamine concentration as lower than synaptic, but still in the micromolar

range. Comparison to iontophoresis concentration is difficult as iontophoresis pipettes cannot be directly proximal to a neuron.

CyHQ-O-DA was tested for any agonism in the absence of photolysis. A concentration–response curve was generated for CyHQ-O-DA (Figure 3.3). CyHQ-O-DA did elicit an outward current on its own at higher concentrations but was minimal at working concentrations. The current produced is unlikely to be due to free dopamine as the addition of sulpiride (1 μM) was unable to fully reverse the effect (Supplemental Figure 3.1). A low concentration of contaminating free dopamine would be easily blocked by sulpiride, but the data are consistent with a high concentration of a partial agonist competing with sulpiride.

Using a concentration of CyHQ-*O*-DA on the lower end of the concentration–response curve (50 μM), a flash–response curve was generated by sequentially increasing the flash durations and a cocaine concentration to reach maximal response (Figure 3.4A). Even this lower concentration of CyHQ-*O*-DA was able to effectively saturate the response of the cell with a 100 ms light flash. Note that cocaine itself produced a small current due to inhibiting removal of spontaneously released dopamine, which is consistent with cocaine-induced cell behavior in the absence of CyHQ-*O*-DA (Lacey et al., 1990). This current was included in the calculation of maximum response. To test for stability over time, CyHQ-*O*-DA was photolyzed once per minute with a 10 ms flash, which gave a half-maximal response in the flash-response experiment, for 15 min with no appreciable decline in response (Figure 3.4B). This indicates that a relatively small proportion of CyHQ-*O*-DA in the 5 mL of recirculating solution was photolyzed to produce the half-maximal response. This suggests that longer experiments can be feasible particularly with larger recirculation volumes.

Photoactivation of Sulpiride in Brain Slice

One of the uses for a caged antagonist is to probe the dissociation rates of agonists by measuring the decay constants of receptor signaling following photolysis. To test the properties of

CyHQ-sulpiride with dopamine neurons, dopamine (1 μM) or quinpirole (300 nM) was recirculated to activate D2 receptors. Following the period of initial application, CyHQ-sulpiride (5 μM) was added, which induced a small reduction in the D2 receptor dependent current, indicating a small amount of antagonism for the still-caged sulpiride (Supplemental Figure 3.2). For initial tests, CyHQ-sulpiride was photolyzed with a long flash (1 s) from and LED (6.5 mW) (Figure 3.5). The time constant of decay for quinpirole (τ = 635 ms) was significantly slower than that of dopamine (τ = 307 ms), which dissociates faster (koff = 1.69 min^{-1}, de Witte et al., 2018) than quinpirole (koff = 0.17 min^{-1}, Lepiku et al., 1997) ($p = 0.0011$ by t test, n = 4 and 2 for quinpirole and dopamine, respectively). The amplitude of the peak response of the agonists were not significantly different, so cannot be considered a confounding factor.

To enable more precise experiments such as those used for studying dopamine synaptic biology, we tested the ability of CyHQ-sulpiride to mediate D2 receptor signaling under more stringent conditions. A single 50 ms light pulse while CyHQ-sulpiride (5 μM) recirculates through the slice preparation is sufficient to block the dopamine IPSC, consisting of a 10–30 μM local concentration of dopamine near the receptors (Figure 3.6). This result and the previously observed kinetics of the block on the standing currents suggest CyHQ-sulpiride can be used to probe dopamine synaptic release and receptor signaling with fine temporal precision.

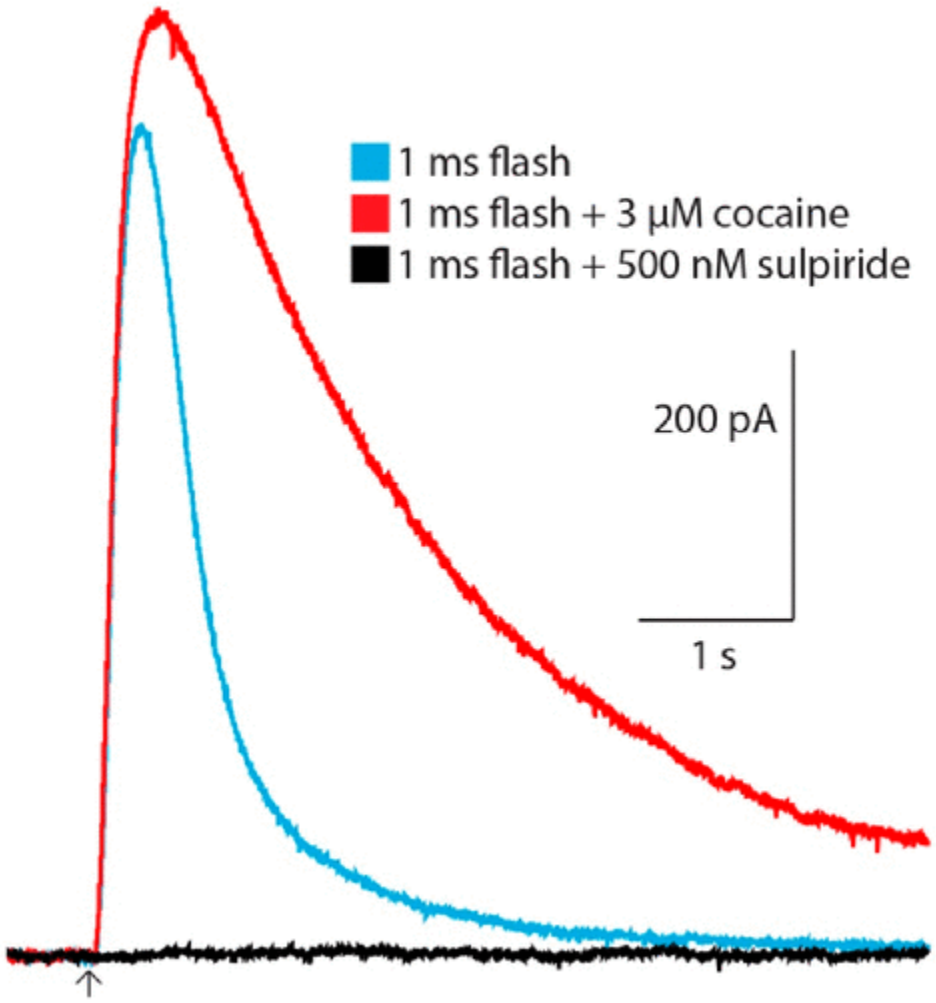

Figure 3-1 Activation of D2 receptors on substantia nigra dopamine neurons with 365 nm light.

Blue arrow indicates point of 1 ms flash. In blue is the response with CyHQ-O-DA (150 µM), in red is the response after the addition of cocaine (3 µM) to inhibit dopamine transport, and in black is the response after D2 receptors were blocked with sulpiride (500 nM).

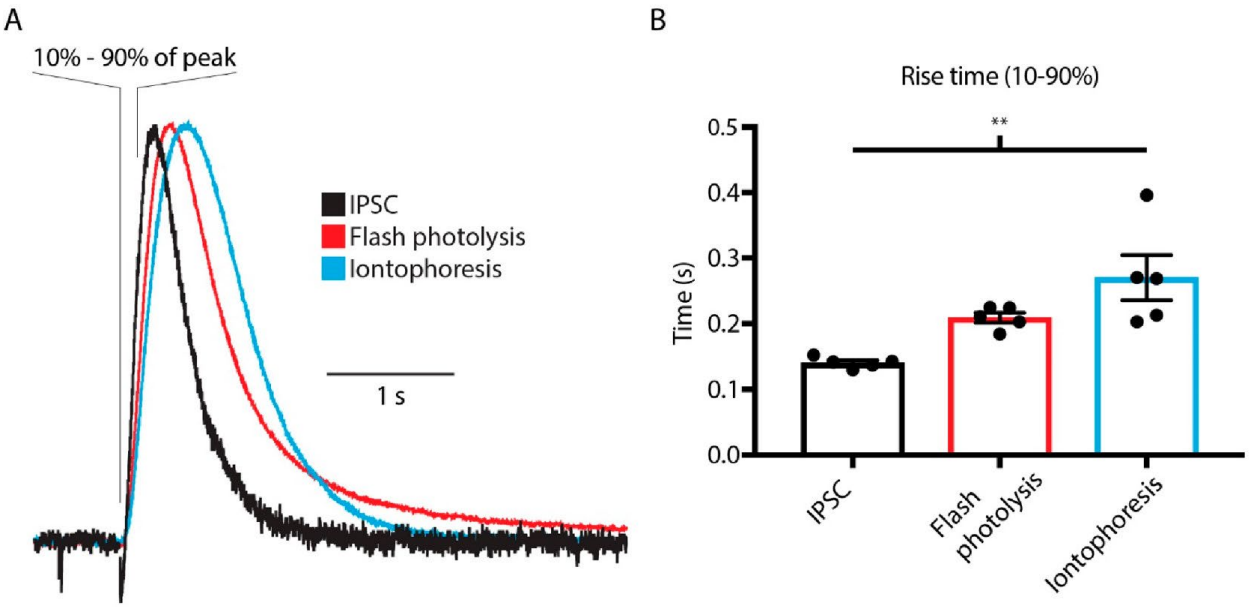

Figure 3-2 Kinetic comparison of normalized dopamine responses.

(A) Scaled responses to flash photolysis (2.5 ms, 1.8 mW) of CyHQ-O-DA (50 µM), electrically stimulated dopamine IPSC (single stimulation), and dopamine iontophoresis (1 M dopamine, 4 nA backing current, 10 ms of a 100 nA ejection pulse). (B) Rise times from 10 to 90% of peak current as outlined in A. There was a gradient of speed with the IPSC response being the fastest, then flash photolysis, then iontophoresis. Though only the IPSC response was significantly faster than iontophoresis (one-way ANOVA with Tukey's multiple comparison), the kinetics of the photolysis response were on the edge of significance on both ends ($p = 0.08$ vs IPSC, $p = 0.13$ vs iontophoresis).

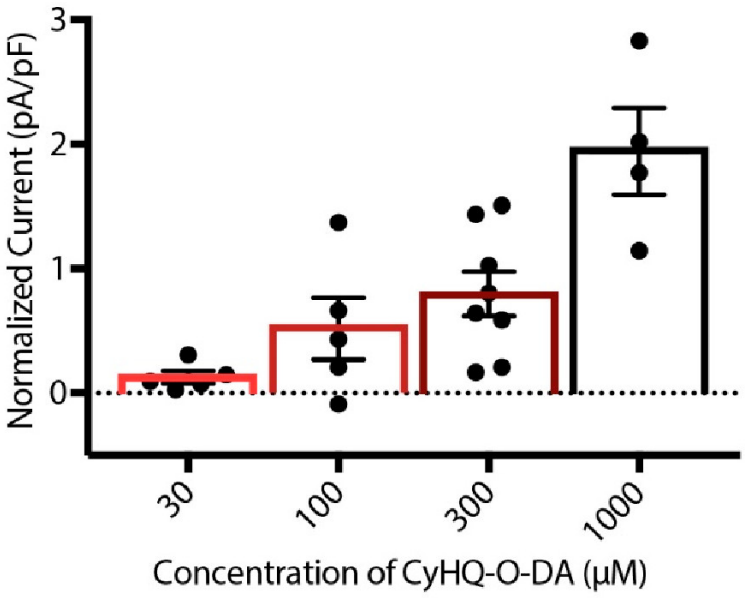

Figure 3-3 Concentration–response curve for CyHQ-O-DA applied to dopamine neurons in the absence of photolysis.

The current generated from adding CyHQ-O-DA was measured and normalized to the size of the cell as measured by capacitance in picofarads (pF).

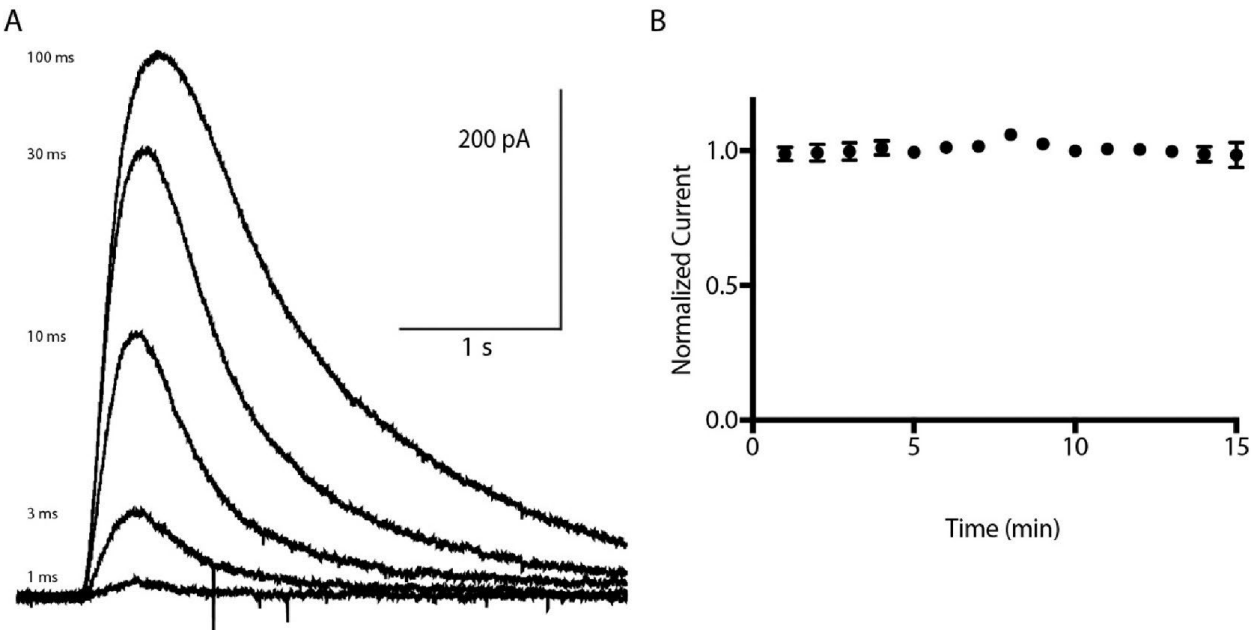

Figure 3-4 CyHQ-O-DA is effective at low concentrations.

(A) Electrophysiological response of CyHQ-O-DA (50 µM) when photolyzed by flashes of increased duration. (B) Electrophysiological response from repeated photolysis of CyHQ-O-DA (50 µM) with 10 ms light flashes every minute.

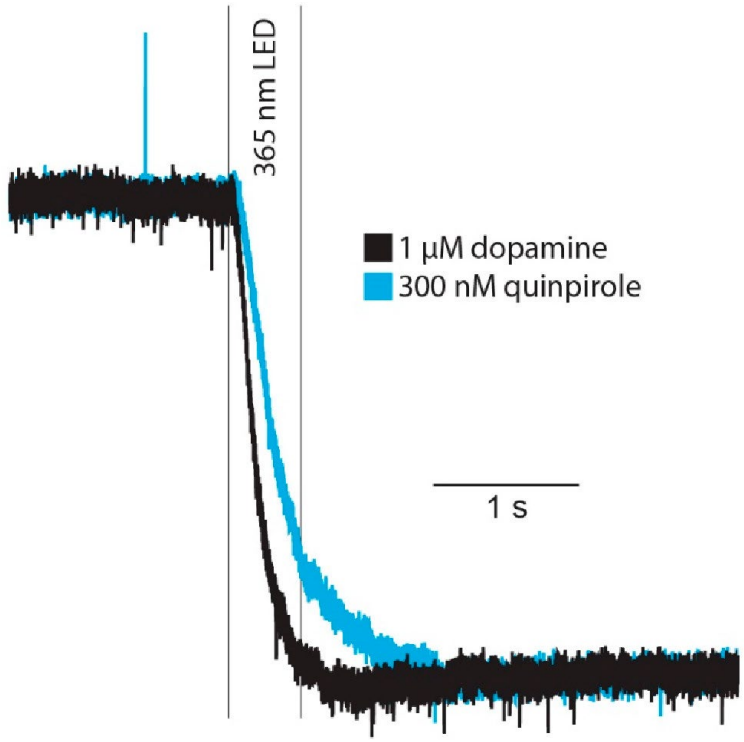

Figure 3-5 Photolysis of CyHQ-sulpiride can rapidly antagonize D2 receptors.

Representative traces of the effects of CyHQ-sulpiride photolysis on currents produced by the D2 receptor activated by quinpirole (300 nM) or dopamine (1 µM, currents have been scaled for better comparison of kinetics). The rate of decline for quinpirole was significantly slower for quinpirole than for dopamine ($p = 0.0011$, $\tau = 635$ and 307 ms, $n = 4$ and 2 for quinpirole and dopamine, respectively).

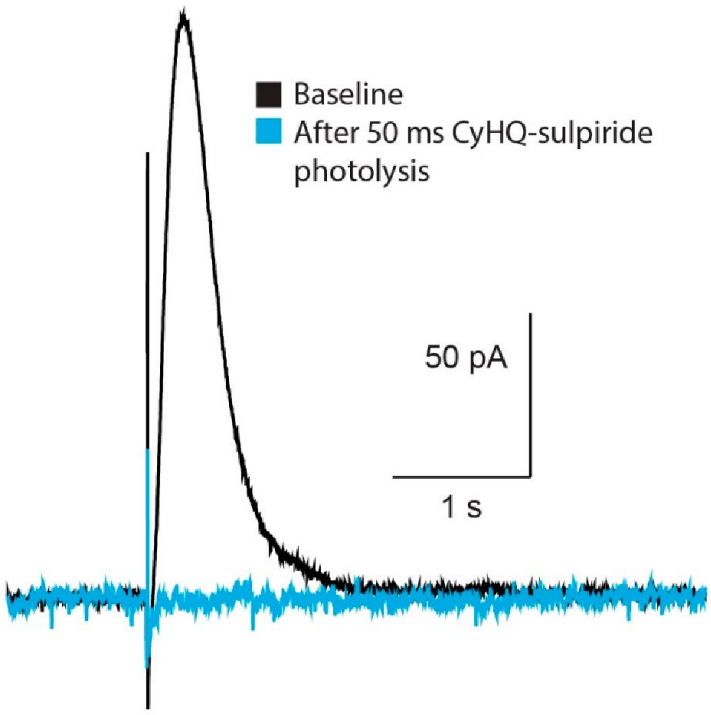

Figure 3-6 Short light pulses and CyHQ-sulpiride are effective at blocking synaptic activity.

The baseline IPSC with CyHQ-sulpiride (5 µM) recirculating over the slice is shown in black. The blue trace shows the complete block of the dopamine IPSC elicited 1 min after a single 50 ms flash of 365 nm light from an LED.

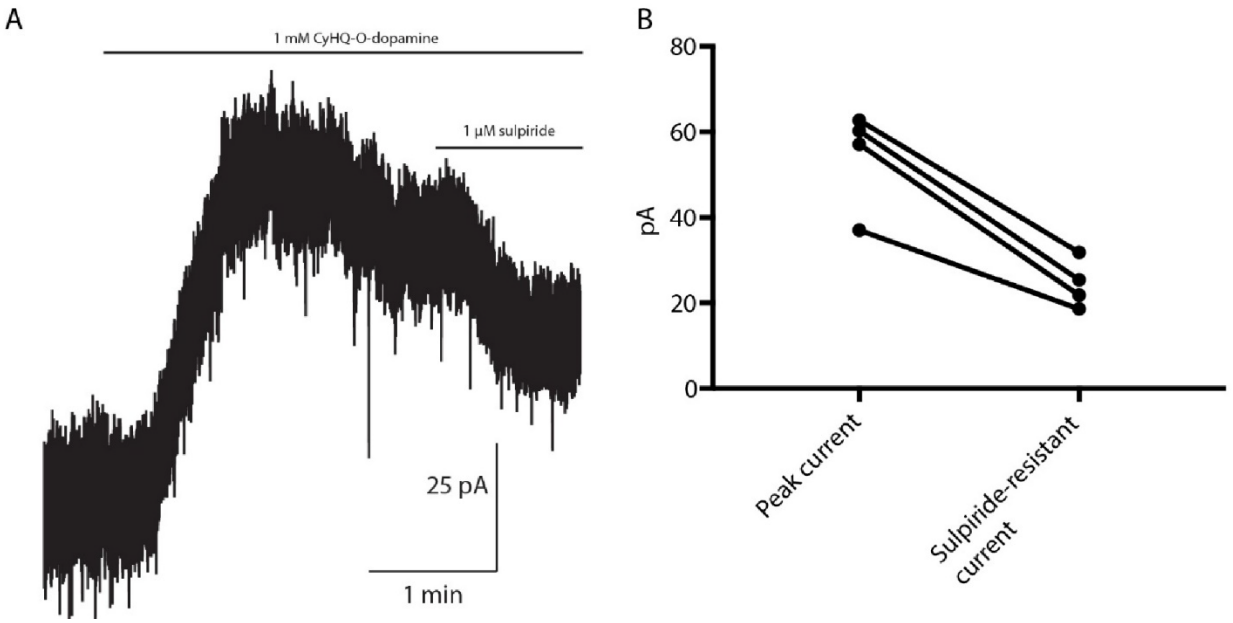

Supplemental Figure 3-1 The current produced by CyHQ-O-DA (1 mM) is not fully blocked by sulpiride

(A) Example trace produced from superperfusion of 1 mM CyHQ-O-dopamine in the dark. The current elicited reaches a peak in about a minute then the D2 response begins to desensitize. Antagonism with sulpiride (1 µM) only partially reverses the current, suggesting it is not due to a low concentration of free dopamine. (B) Summary data for the experiment depicted in (A). The peak current is matched with the remaining shift in baseline current after application of sulpiride.

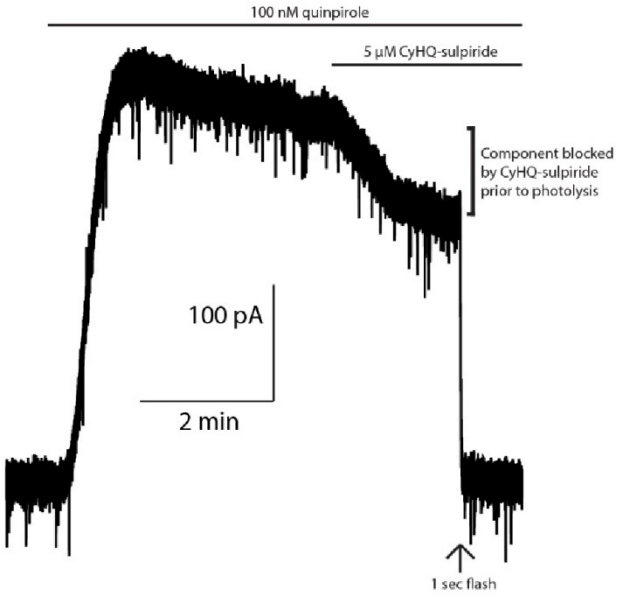

Supplemental Figure 3-2 CyHQ-sulpiride alone has a small level of antagonism prior to photolysis.

Quinpirole (100 nM) was recirculated at a low concentration, picked to emphasize any partial receptor block. CyHQ-sulpride (5 µM) was then added and a small amount of antagonism can be observed by an inward deflection of the outward current prior to photolysis.

Chapter 4 – D2 receptor isoforms

Preface

This chapter and the next are two largely separate stories but share a common theme in probing how D2 structure helps determine regulation and coupling to G proteins. The experiments featured in this chapter were some of the first I conducted in the Williams lab and were a joint effort between Dr. Robinson and myself. The study was part of a continuing effort comparing two splice variants of the D2 receptor, D2-short (D2S) and D2-long (D2L), to understand functional differences between the two isoforms. This work follows from a previous paper using virally expressed D2S and D2L (Gantz et al., 2015). One of the findings of this previous study was that D2S expressing neurons were sensitive to a calcium dependent desensitization which is also observed in WT conditions (Beckstead and Willaims, 2007), whereas desensitization D2L was insensitive to calcium. This calcium dependence was lost following a single treatment with cocaine the day prior to experiments in WT conditions, but not for D2S expressing neurons, leading to the hypothesis that cocaine treatment induces an adaptive shift in receptor subtype from D2S to D2L (Gantz et al., 2015). However, the results of this follow up study using genetic knock outs of either D2S or D2L, rather than overexpressing one or the other, differ in a few key ways including the finding that non-overexpressed D2L receptors maintain sensitivity to calcium dependent desensitization.

In the context of this dissertation, these data highlight several features of D2 receptor biology. First, it highlights the ability for the intracellular structure of the receptor to acutely regulate receptor plasticity in the form of desensitization. But one of the most interesting features here is the example it sets where changing the number of molecules involved in G protein signaling can produce dramatically different results. The different results seen between this study and the previous one using virally expressed versions of the same receptors (Gantz et al., 2015), can likely be explained by the increased copy number gained from viral overexpression. Subtleties of regulation of D2 receptor

signaling are lost when the system is pushed to extremes. This is a theme I take forward throughout the rest of this dissertation with an emphasis on using WT animals in experiments and using methods of agonist application that are more physiological than bath perfusion of agonist to maximally activate the systems of G protein signaling.

Cocaine-induced adaptation of dopamine D2S, but not D2L autoreceptors

Brooks G Robinson[1], **Alec F Condon[1]**, Daniela Radl[2], Emiliana Borrelli[2], John T Williams[1], Kim A Neve[3]

[1]Oregon Health & Science University, United States; [2]University of California, Irvine, United States; [3]VA Portland Health Care System, United States

Acknowledgements

This work was supported by NIH funding DA04523 (JTW), F32 DA038456 (BGR), and DA033554 (EB), INSERM (EB), and by Merit Review Award BX003279 from the US Department of Veterans Affairs, Veterans Health Administration, Office of Research and Development, Biomedical Laboratory Research, and Development (KAN).

[This Manuscript is presented as published in (Robinson et al., 2017), eLife, November 20, 2017, 6:e31924]

Abstract

The dopamine D2 receptor has two splice variants, D2S (Short) and D2L (Long). In dopamine neurons, both variants can act as autoreceptors to regulate neuronal excitability and dopamine release, but the roles of each variant are incompletely characterized. In a previous study we used viral receptor expression in D2 receptor knockout mice to show distinct effects of calcium signaling on D2S and D2L autoreceptor function (Gantz et al., 2015). However, the cocaine-induced plasticity of D2 receptor desensitization observed in wild type mice was not recapitulated with this method of receptor expression. Here we use mice with genetic knockouts of either the D2S or D2L variant to investigate cocaine-induced plasticity in D2 receptor signaling. Following a single in vivo cocaine exposure, the desensitization of D2 receptors from neurons expressing only the D2S variant was reduced. This did not occur in D2L-expressing neurons, indicating differential drug-induced plasticity between the variants.

Introduction

Dopamine D2 autoreceptors decrease neuronal excitability when activated by dendrodendritic release of dopamine in the midbrain. The D2 receptor has short (D2S) and long (D2L) splice variants that differ by a 29 amino acid section in the third intracellular loop. While both variants are expressed in dopamine neurons and function effectively as autoreceptors (Khan et al., 1998; Jang et al., 2011; Dragicevic et al., 2014; Jomphe et al., 2006; Neve et al., 2013), subtle differences have been reported suggesting the variants are not redundant. Agonist induced desensitization of the variants has been shown to differ in multiple reports. The D2S receptor desensitizes and internalizes to a greater degree than D2L (Liu et al., 1992; Itokawa et al., 1996; Ito et al., 1999; Morris et al., 2007; Thibault et al., 2011). Desensitization of the D2S receptor-dependent activation of G protein-gated inwardly rectifying potassium (GIRK) conductance was also greater and

was dependent on the level of intracellular calcium buffering (Gantz et al., 2015). Desensitization of the D2 receptor is decreased following in vivo acute drug exposure to ethanol (Perra et al., 2011), cocaine (Dragicevic et al., 2014; Gantz et al., 2015), or L-DOPA (Dragicevic et al., 2014). A reduction in desensitization following drug exposure would conceivably result in a more effective autoreceptor (and therefore reduced neuronal excitability) during the next high dopamine situation, which would have widespread effects on dopamine signaling throughout the brain. However, studies using viral expression of single D2 receptor variants in D2-KO mice were inconclusive in determining whether the plasticity induced by cocaine resulted from adaptation of a single variant, or perhaps an altered ratio of splice variant expression/function (Gantz et al., 2015). To resolve this issue, the present study used mouse models that express only the D2S (D2L-KO; Usiello et al., 2000) or D2L variant (D2S-KO; Radl et al., 2013). The results show that a single treatment of animals with cocaine reduced acute desensitization of the D2S variant. Treatment with cocaine did not alter the expression of either D2 receptor variant, and the desensitization of the D2L variant was not changed. Thus, it appears that plasticity in D2 receptor signaling induced by a single cocaine treatment results from adaptation of the D2S variant.

Results and discussion

The calcium sensitivity and desensitization of the short and long variants of the D2 receptor were effectively studied with the use of viral expression of D2S and D2L receptors in dopamine neurons of D2-KO mice (Gantz et al., 2015). However, the adaptation in D2 receptor desensitization following in vivo cocaine treatment could not be replicated with mice virally expressing D2 receptors (D2S, D2L, or a combination of both) and therefore there was uncertainty about the source of adaptation. To address the issue, D2L-KO and D2S-KO mouse lines were employed. These mice express a single D2 variant at physiological levels (Usiello et al., 2000; Radl et al., 2013). Whole-cell

recordings from dopamine neurons in brain slices containing the substantia nigra pars compacta (SNc) were used to measure desensitization. The selective D2 receptor agonist quinpirole (10 μM) was applied for 5 min and the decline from the peak outward D2-GIRK current was measured after 90 s. This experiment was done in slices taken from untreated and cocaine treated (20 mg/kg 24 hr prior) male mice between 61 and 106 days old. Each genotype was examined using two internal solutions, a weak calcium buffering EGTA (0.1 mM) and a strong calcium buffering BAPTA (10 mM) solution. The comparison of these two internal conditions allows the parsing of processes dependent on and independent of intracellular calcium signaling. Results from wild type littermates from both genotypes were combined as no differences between the groups were seen. D2-GIRK currents from wild type mice desensitized to a greater extent with the weak calcium buffering EGTA internal solution compared to the strong buffering BAPTA internal. With the use of EGTA (and not BAPTA) internal solution the D2-GIRK current desensitized significantly less in cells from animals that were treated with cocaine (Figure 4.1A). This confirms previous results obtained in wild type mice (Gantz et al., 2015). The results from experiments with the D2L-KO mice (expressing D2S only) were similar to experiments in wild type mice. The decline in the quinpirole current with EGTA internal was greater than with BAPTA internal and was significantly reduced following in vivo cocaine treatment (Figure 4.1B). In D2S-KO mice (expressing only D2L), some calcium sensitivity in current decline was still present (EGTA currents declined significantly more than BAPTA currents), but treatment with cocaine had no effect in these animals (Figure 4.1C). Representative traces of currents from naïve or cocaine-treated mice of each of the three genotypes in Figure 4.1 further demonstrate that D2S, and not D2L, adapts following cocaine exposure. Desensitization is measured 90 s post peak. This initial phase of desensitization is calcium sensitive and differs between D2 receptor variants (52.7 ± 5.1% vs. 36.1 ± 2.9% decline with EGTA internal $p<0.01$ with Student's t-test, comparison not depicted). In the wild type and D2L-KO genotypes, the initial decline from peak becomes substantially shallower following cocaine exposure indicating an adaptation in a calcium-sensitive aspect of desensitization.

The calcium sensitivity of D2 autoreceptors remains incompletely understood. The L-type calcium channels (Dragicevic et al., 2014; Gantz et al., 2015) and intracellular calcium stores (Perra et al., 2011; Gantz et al., 2015) are two sources of calcium that impact D2 receptor signaling. However, there are likely calcium binding proteins that act as intermediaries between the ion and the D2 receptor. Indeed, the intracellular domains of the D2 receptor can bind calmodulin (Bofill-Cardona et al., 2000; Liu et al., 2007), NCS-1 (Kabbani et al., 2002; Dragicevic et al., 2014; Pandalaneni et al., 2015), and S100B (Liu et al., 2008; Dempsey and Shaw, 2011) among other potential calcium sensitive proteins. The present results show that while the D2S is more calcium sensitive than D2L, the long variant maintains some calcium sensitivity as evidenced by decreased desensitization when calcium is strongly buffered by the BAPTA internal solution. One explanation is that the calcium sensitivity of the D2 receptor involves multiple sources. Recent imaging of endogenous D2 receptors revealed a clustered and static localization (Robinson et al., 2017). It is possible that an array of proteins, potentially including several that are calcium sensitive, forms a complex with D2 receptors modulating their placement and signaling.

Importantly, the desensitization of GABAB receptor-induced GIRK currents with baclofen (30 μM) was not sensitive to the two different internal solutions and did not change in any genotype following cocaine exposure (Figure 4.3A–C). Thus, the calcium sensitive desensitization and the cocaine-induced adaptations are specific to the D2 receptor and not general to Gi-coupled GPCRs or GIRK channels.

Adaptation in one D2 receptor variant but not the other is relevant to studies in humans that have identified two intronic single nucleotide polymorphisms (SNPs) in the DRD2 gene that cause an increase in D2L expression relative to D2S. These SNPs have been found to be associated with cocaine (Moyer et al., 2011; Levran et al., 2015), alcohol (Sasabe et al., 2007), and opioid abuse (Clarke et al., 2014; Levran et al., 2015). This has been interpreted mainly as altering the balance

between striatal postsynaptic D2 receptor activation (assumed to be D2L) vs. dopamine neuron autoreceptor activation (assumed to be D2S), but our data call into question this hypothesis about the dichotomous function of the D2 receptor splice variants (current results; Neve et al., 2013; Gantz et al., 2015). However, because dopamine neurons can express either variant, the ratio of D2 autoreceptor variants could very well be important in drug related behaviors. Increased presence of the D2L variant as the autoreceptor would alter the dopamine reward circuitry because this variant desensitizes less (suggesting it is a more efficacious autoreceptor) and does not appear to adapt following a single cocaine exposure. Furthermore, following cocaine exposure desensitization of the D2S variant adapts to resemble the D2L variant. In this assay, preexisting prevalence of the D2L variant would resemble a previous cocaine experience.

The present results are in some respects at odds with the previous study that used viral D2 receptor variant expression and found no calcium-dependent desensitization of D2L and no cocaine-induced adaptation of either variant (Gantz et al., 2015), rather than decreased calcium-dependent desensitization of D2L and selective cocaine-induced adaptation of D2S. A possible explanation is that virally transduced D2 receptors have altered expression levels (often superphysiological) resulting in reduced sensitivity to adaptive mechanisms. It must be noted, however, that we cannot exclude the possibility of developmental abnormalities in mice that are constitutive knockouts of D2S, D2L or both D2 variants. One clear advantage of the D2S- and D2L-KO mice used in this study over viral receptor expression is the maintenance of physiological levels of expression. Figure 4.2 shows the current densities in pA/pF (a reliable measure of expression) of D2-GIRK currents from wild type, D2L-KO, and D2S-KO animals. While viral receptor expression is not well controlled and often much higher than physiological levels (Gantz et al., 2015), the KO animals were in the same range, or lower (Figure 4.2B–C) compared to wild type (Figure 4.2A). The previously shown trend of GIRK currents having increased amplitude upon strong calcium buffering is clearly present (Figure 4.2A–B), however in the D2S-KO genotype, there is no significant difference between current

densities in the EGTA and BAPTA groups (Figure 4.2C). Additionally, a comparison between D2L-KO and D2S-KO groups reveals an overall significant effect of genotype on current density ($F(1, 28)=5.27$, $p=0.029$, two-way ANOVA). This effect is likely not due to differences in GIRK channel expression because GABAB-GIRK current density was not different between the groups (in pA/pF D2L-KO EGTA 16.3 ± 2.3, BAPTA 18.2 ± 3.6 vs. D2S-KO EGTA 16.0 ± 0.6, BAPTA 18.8 ± 1.2, $p>0.05$ two-way ANOVA, data not shown). Because of the similarity of D2S-mediated responses to responses of neurons from wild type mice, despite the presence of mRNA for both subtypes (Khan et al., 1998; Jang et al., 2011; Dragicevic et al., 2014) and the ability of both to activate GIRKs (Jomphe et al., 2006; Neve et al., 2013; Gantz et al., 2015), it was speculated that D2L function is in some way occluded under basal conditions (Gantz et al., 2015). The lower current density for D2L in this study, despite similar levels of expression of the splice variants in these two lines of mice (D. Radl, M. Chiacchiaretta, R. Lewis, K. Brami-Cherrier, L. Arcuri, & E. Borrelli, manuscript in preparation), is consistent with this notion. Alternatively, the lower current density for D2L and lack of calcium-dependent desensitization could both be explained if the D2L receptor were constitutively desensitized.

Concluding remarks

A genetic strategy was used to address the outstanding question of how the desensitization of dopamine D2 autoreceptors adapts following in vivo cocaine exposure. Mice with either the long or short splice variant of the D2 receptor constitutively knocked out were employed to show that the cocaine-induced decrease in D2 receptor desensitization occurs when D2S is the only variant expressed. This mimics the wild type phenotype and does not occur when only the D2L variant is expressed.

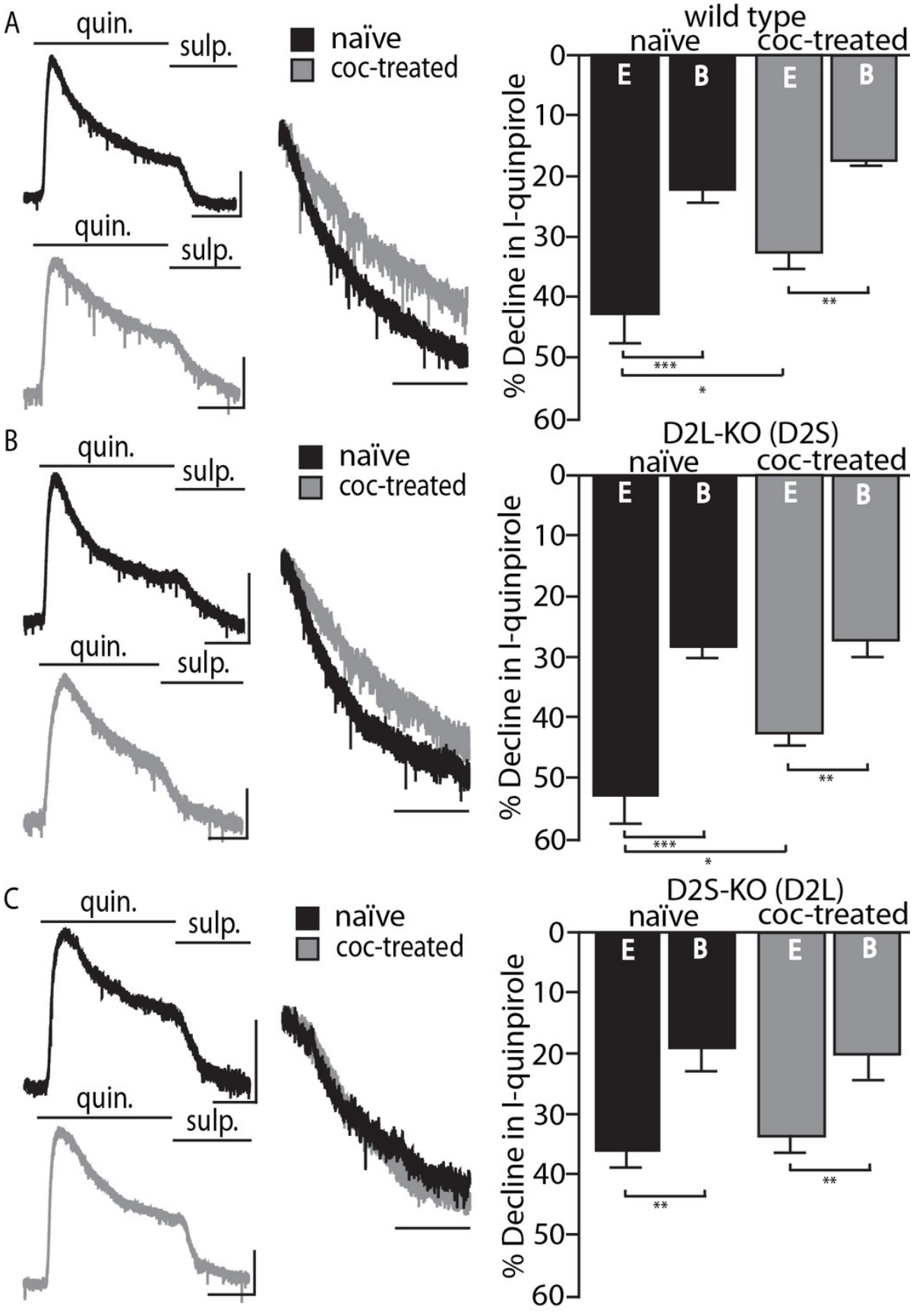
A
quin.
sulp.
quin.
sulp.
naïve
coc-treated
wild type
naïve
coc-treated
% Decline in l-quinpirole
0
10
20
30
40
50
60
E
B
E
B
***
*
**
B
quin.
sulp.
quin.
sulp.
naïve
coc-treated
D2L-KO (D2S)
naïve
coc-treated
% Decline in l-quinpirole
0
10
20
30
40
50
60
E
B
E
B
***
*
**
C
quin.
sulp.
quin.
sulp.
naïve
coc-treated
D2S-KO (D2L)
naïve
coc-treated
% Decline in l-quinpirole
0
10
20
30
40
50
60
E
B
E
B
**
**

Figure 4-1 Cocaine-induced adaptation in D2 receptor desensitization.

Shown on the left are representative traces from naïve and cocaine-treated groups in all genotypes of quinpirole (quin., 10 μM)-induced D2 receptor-GIRK currents (I-quinpirole) reversed by sulpiride (sulp., 600 nM) recorded from dopamine neurons in the SNc using EGTA internal solution. For further comparison, scaled and peak aligned current declines are also shown (horizontal scale bars = 90 s, vertical scale bars = 100 pA). (A) In wild type animals there were significant overall effects of internal solution ($F(1, 30)=23.57$, $p<0.001$) and cocaine treatment (20 mg/kg, $F(1, 30)=4.259$, $p=0.048$) on the decline of I-quinpirole. Post-hoc analyses indicate that in both treatment conditions the decline using BAPTA (B) internal was less than that using EGTA (E, $p<0.001$ for naïve and coc-treated). Additionally, with EGTA internal there was significantly reduced decline following cocaine treatment ($p=0.049$, n = 7–9 neurons from 5 to 8 mice). (B) In mice in which the long isoform of the D2 receptor has been knocked out (D2L-KO), there was an overall effect of internal solution ($F(1, 32)=37.09$, $p<0.001$), but not of cocaine treatment ($F(1, 32)=2.917$, $p=0.097$). In post hoc analyses, there was significantly more decline when using EGTA internal than BAPTA internal in both treatment conditions ($p<0.001$ for naïve, $p=0.002$ for cocaine-treated), and the decline was significantly reduced following drug exposure when EGTA internal was used ($p=0.021$, n = 8–12 neurons from 4 to 7 mice). (C) In animals with the short isoform of the D2 receptor knocked out (D2S-KO), there was an overall effect of internal solution ($F(1, 28)=21.24$, $p<0.001$) with EGTA currents declining significantly more that those of BAPTA in both treatment conditions ($p=0.001$ for naïve, $p=0.007$ for coc-treated, n = 7–9 neurons from 4 to 7 mice). Cocaine treatment caused no change in desensitization of the D2-GIRK current in this genotype. Comparisons were done using two-way ANOVAs followed by Fisher's LSD when $p<0.05$. *$p<0.05$, **$p<0.01$, ***$p<0.001$.

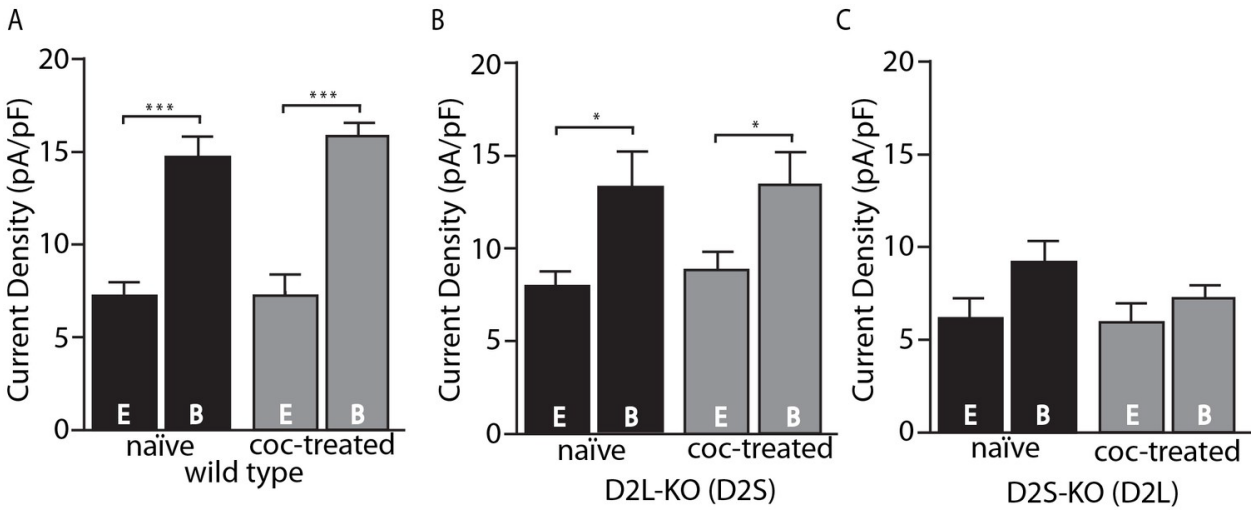

Figure 4-2 Amplitude of D2-GIRK currents.

(A) In wild type mice, there was an overall significant effect of internal solution on D2-GIRK current density (pA/pF, $F(1, 30)=76.32$, $p<0.001$). The current density was greater when using the strong calcium buffering BAPTA (B) internal solution compared with the weak buffering EGTA (E) internal solution ($p<0.001$ for naïve and coc-treated, n = 7–11 neurons from 5 to 7 mice). There was no difference between naïve and cocaine-treated groups. (B) From D2L-KO mice, there was an overall significant effect of internal solution ($F(1, 32)=12.85$, $p=0.001$). The current density of the BAPTA group was significantly larger than that of EGTA in both naïve and coc-treated conditions ($p=0.016$ for naïve, $p=0.016$ for coc-treated, n = 7–12 neurons from 4 to 7 mice), however there was no difference between treatment conditions. (C) In D2S-KO mice, there was no significant effect of internal solution or drug treatment (n = 7–9 neurons from 5 to 7 mice). Analyses were done by two-way ANOVAs followed by Fisher's LSD when $p<0.05$. *$p<0.05$, **$p<0.01$, ***$p<0.001$.

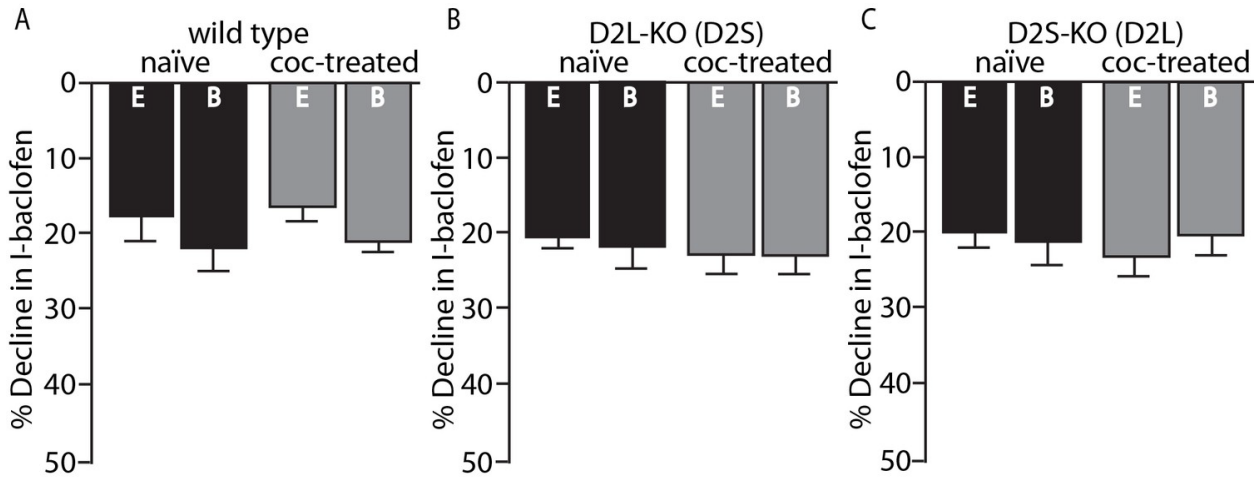

Figure 4-3 No change in GABAB desensitization following cocaine exposure.

GABAB receptor decline/desensitization was measured by bath application of baclofen (30 µM) for ~5 min. There were no significant effects of EGTA (E, 0.01 mM) versus BAPTA (B, 10 mM) internal solution or treatment condition (naïve versus coc-treated) on the decline in GABAB-GIRK currents (I-baclofen) from (A) wild type mice, (B) D2L-KO mice, or (C) D2S-KO mice ($p<0.05$, n = 5–9 neurons from 3 to 6 mice). Analyses were done using two-way ANOVAs

Chapter 5 – A constitutively active D2 receptor

Preface

This chapter describes work studying a spontaneously occurring mutation in the D2 receptor found in a Dutch family presenting with a hyperkinetic movement disorder (van der Weijden et al., 2021). Sequencing found that this novel disorder was due to a single amino acid substitution in the D2 receptor, I212F, a position at the N-terminus of the third cytoplasmic loop. Initial work from the Neve lab using heterologous expression systems in cell culture suggested this was a constitutively active receptor, notably useful in understanding how the D2 receptor couples to G proteins. To further characterize this mutation, the Neve lab virally expressed D2-I212F in dopamine neurons lacking native D2 receptors and collaborated with us for *ex vivo* slice work. Dr Robinson and I recorded various aspects of D2-I212F biology either with endogenously released dopamine or with exogenously applied dopamine or sulpiride. Work with the IPSC done by Dr Robinson working with the IPSC was published in an initial paper, which included descriptions of the patients' phenotypes (van der Weijden et al., 2021). This chapter consists of the second publication, which went further into descriptions of molecular interactions, molecular dynamic simulations comparing D2-WT and D2-I^{221}F, and my work characterizing its behavior in dopamine neurons. In agreement with Dr Robinson's findings with the IPSC, my work found evidence for constitutive activity when expressed in dopamine neurons, yet an even more pronounced effect in prolonging responses to agonist exposure. These findings can be explained by the molecular dynamic simulations, which found I^{212} was near an ionic lock holding the intracellular face of the D2 receptor in the off position. The I212F mutation weakens this interaction causing the receptor to spontaneously open and presumably contribute to the deficiency in turning off when agonists unbind or when constitutive activity is reversed by the inverse agonist sulpiride.

This chapter ends with some unpublished data generated in these experiments where I apply baclofen to activate $GABA_B$ receptors in mutant and WT D2 receptor expressing neurons following the experiments published in Chapter 5/Rodriguez-Contreras et al. (2021). The reduced amplitude and current decline of these $GABA_B$ currents suggest the constitutive activity and increased sensitivity of D2-I212F induces tonic heterologous desensitization of $G_{i/o}$-coupled GPCR activity in dopamine neuron, an effect predicted by work I'll show in chapter 7 where I present work studying D2 receptor desensitization. This tonic desensitization may also explain the smaller peak current amplitudes seen in D2-I212F expressing neurons in response to dopamine.

Signaling-Biased and Constitutively Active Dopamine D2 Receptor Variant

Dayana Rodriguez-Contreras[1], **Alec F. Condon[2]**, David C. Buck[3], Naeem Asad[4], Timothy M. Dore[4], Dineke S. Verbeek[5], Marina A.J. Tijssen[6], Ujwal Shinde[7], John T. Williams[2], and Kim A. Neve[1]

[1]Research Service, VA Portland Health Care System, and Department of Behavioral Neuroscience, Oregon Health & Science University, United States; [2]Vollum Institute, Oregon Health & Science University, United States; [3]Research Service, VA Portland Health Care System, United States; [4]New York University Abu Dhabi, United Arab Emirates; [5]Expertise Center Movement Disorders and Department of Genetics, University of Groningen, The Netherlands; [6]Expertise Center Movement Disorders and Department of Neurology, University of Groningen, The Netherlands; [7]Department of Chemical Physiology & Biochemistry, Oregon Health & Science University, United States.

Acknowledgements

Support for this research was provided by the National Institute of Neurological Disorders and Stroke (R21NS117713), the National Institute on Drug Abuse (F31DA047007 and R01DA004523), the US Department of Veterans Affairs, Veterans Health Administration, Office of Research and Development, Biomedical Laboratory Research and Development (Merit Review Award BX003279), and New York University Abu Dhabi.

[This Manuscript is presented as published in (Rodriguez-Contreras et al., 2021), ACS chemical neuro, May 11, 2021, 12:1873-1884]

Abstract

A dopamine D2 receptor mutation was recently identified in a family with a novel hyperkinetic movement disorder. Compared to the wild type D2 receptor, the novel allelic variant D2-I212F activates a $G\alpha_{i1}\beta_1\gamma_2$ heterotrimer with higher potency and modestly enhanced basal activity in human embryonic kidney (HEK) 293 cells and has decreased capacity to recruit arrestin3. We now report that omitting overexpressed G protein-coupled receptor kinase-2 (GRK2) decreased the potency and efficacy of quinpirole for arrestin recruitment. The relative efficacy of quinpirole for arrestin recruitment to D2-I212F compared to D2-WT was considerably lower without overexpressed GRK2 than with added GRK2. D2-I212F exhibited higher basal activation of $G\alpha_{oA}$ than $G\alpha_{i1}$ but little or no increase in the potency of quinpirole relative to D2-WT. Other signs of D2-I212F constitutive activity for G protein-mediated signaling, in addition to basal activation of $G\alpha_{i/o}$, were enhanced basal inhibition of forskolin-stimulated cyclic AMP accumulation that was reversed by the inverse agonists sulpiride and spiperone and a ~4-fold increase in the apparent affinity of D2-I212F for quinpirole, determined from competition binding assays. In mouse midbrain slices, inhibition of tonic current by the inverse agonist sulpiride in dopamine neurons expressing D2-I212F was consistent with our hypothesis of enhanced constitutive activity and sensitivity to dopamine relative to D2-WT. Molecular dynamics simulations with D2 receptor models suggested that an ionic lock between the cytoplasmic ends of the third and sixth α-helices that constrains many G protein-coupled receptors in an inactive conformation spontaneously breaks in D2-I212F. Overall, these results confirm that D2-I212F is a constitutively active and signaling-biased D2 receptor mutant and also suggest that the effect of the likely pathogenic variant in a given brain region will depend on the nature of G protein and GRK expression.

Introduction

The dopamine D2 receptor is a G protein-coupled receptor that signals through both Gαi/o and arrestin to regulate movement and motivated behavior (Beaulieu et al., 2005; Donthamsetti et al., 2020; Rose et al., 2018). The D2 receptor is a target of virtually all antipsychotic drugs currently in use and also a frequent drug target in the treatment of movement disorders such as Parkinson's disease and chorea (Cepeda et al., 2014; Moritz et al., 2018). The D2 receptor has long (D2L) and short (D2S) splice variants; if and in what way the splice variants are functionally distinct is an active area of research (Gantz et al., 2015; Radl et al., 2018).

We recently described a four-generation family with an autosomal dominant genetic disorder characterized by chorea and cervical dystonia, in which affected family members carry the novel D2 receptor missense variant DRD2 (c.634A > T;p.I212F) (Van derWeijden et al., 2021). Ile212 (Ile2125.61 according to the Ballesteros-Weinstein numbering scheme) (Ballesteros and Weinstein, 1995) is in the cytoplasmic extension of the fifth transmembrane α-helix, at the N-terminus of the D2 receptor third cytoplasmic loop. A deep mutational analysis of the β2-adrenoceptor identified position 5.61 as being one of the top four mutationally intolerant positions at the β2-Gαs interface and also in a part of the receptor where many mutations are activating or inactivating (Jones et al., 2020). Mutations introduced in this region of the D2 receptor decrease the binding of at least three D2 receptor-interacting proteins: arrestin (Lan et al., 2009; Clayton et al., 2014), calmodulin (Liu et al., 2007), and S100B (Liu et al., 2008; Lee et al., 2021). Our initial studies demonstrated that recruitment of arrestin by D2L/S-I212F in human embryonic kidney (HEK) 293 cells is decreased compared to wild type D2L/S (D2 L/S-WT), whereas D2L/S-I212F activation of a Gαi1β1γ2 heterotrimer and inhibition of cAMP accumulation are enhanced (Van derWeijden et al., 2021).

G-protein-coupled receptor (GPCR) kinases (GRKs) facilitate arrestin recruitment by phosphorylating serine and threonine residues on the intracellular domains of GPCRs, typically

leading to receptor desensitization, internalization, and either degradation or resensitization, and also promoting arrestin-mediated signaling (Moor et al., 2007). GRK is frequently cotransfected in cellular studies of arrestin recruitment to maximize the signal. GRK2/3 are ubiquitously expressed GRKs that are the major subtypes interacting with the D2 receptor (Kim et al., 2001; Gurevich et al., 2016; Namkung et al., 2009). Thus, our previous arrestin recruitment studies were performed with overexpressed GRK2.

Similarly, we assessed D2 receptor activation of a G protein heterotrimer containing Gαi1 even though the D2 receptor activates both Gαi and Gαo (Neve et al., 2004). Gαo is the most abundant Gα subunit in mammalian brain, comprising about 1% of total membrane protein (Jiang and Bajpayee, 2009). Furthermore, Gαo knockout mice have greatly decreased dopamine-stimulated GTPγS binding and a complete loss of GTP-sensitive dopamine binding in brain, suggesting that Gαo contributes importantly to dopamine signaling (Jiang et al., 2001). Both Gαi and Gαo mediate D2 receptor signaling in brain, with the contribution of specific subtypes varying among brain regions (Marcott et al., 2018).

We now report that D2L/S-I212F receptors have a more stringent requirement than D2-WT for GRKs, so that the novel allelic variant had a more profound loss of arrestin recruitment, compared to that of D2-WT, in the absence of overexpressed GRK2 than when the kinase was overexpressed. We also describe the effect of the mutation on D2 receptor activation of GαoA, which differed from Gαi1 activation in effects on both agonist potency and basal activity. Furthermore, the mutation increased constitutive inhibition of cyclic AMP accumulation in HEK293 cells and increased the apparent affinity of quinpirole for the D2 receptor. In midbrain dopamine neurons expressing D2-I212F, photoactivated sulpiride inhibited a substantial tonic current, consistent with both the constitutive activity and enhanced agonist potency suggested by studies of the novel variant in HEK293 cells. Molecular dynamics (MD) simulations indicate that these effects of

the mutation are associated with the breaking of an “ionic lock” that constrains many unliganded GPCRs in an inactive conformation.

Results and Discussion

Arrestin3 Recruitment by D2-I212F Depends Heavily on GRK2

We previously investigated the ability of D2S/L-I212F receptors to recruit arrestin3 under the most favorable conditions by overexpressing GRK2, which enhances arrestin recruitment to the D2 receptor (Kim et al., 2001). We reported that recruitment of arrestin3 by D2S/L-I212F is reduced by about 30–50% compared to that of D2S/L-WT receptors, whereas the potency of quinpirole is modestly enhanced at D2S/L-I212F (van der Weijden et al., 2021). We now describe arrestin3 recruitment in the absence of GRK2. HEK293 cells were transiently cotransfected with D2S/L-WT or D2S/L-I212F fused with RLuc8 (BRET donor) and mVenus-tagged arrestin3 (BRET acceptor). Previous results with overexpressed GRK2 are shown for comparison. Quinpirole-induced recruitment of arrestin3 by both D2 receptor splice variants was substantially decreased for D2L/S-I212F with or without overexpressed GRK2 (Figure 5.1A,B; Table 5.1), whereas the potency of quinpirole was modestly increased for all conditions compared to D2-WT (Table 5.1). The mutation-induced reduction in maximal recruitment of arrestin was considerably larger in the absence of expressed GRK2 for both splice variants. Thus, with added GRK2, Emax for D2L/S-I212F was decreased by 44% (D2L) or 27% (D2S), but in the absence of overexpressed GRK2, Emax for D2L/S-I212F was decreased by 73% (D2L) and 64% (D2S) compared to the corresponding condition for D2-WT (Table 5.1). In contrast, omitting GRK2 decreased the potency similarly for all variants, ranging from a 4.2-fold decrease for D2s-WT to a 6.7-fold decrease for D2L-I212F (Table 5.1).

In the presence of overexpressed GRK2, maximal arrestin recruitment peaked by the first measurement, (1 min after adding coelenterazine h, which was approximately 4 min after addition of quinpirole), whereas maximal recruitment was delayed without overexpressed GRK2, particularly for D2S/L-WT (Figure 5.1C,D). Emax decreased more rapidly for D2L/S-I212F than for D2L/S-WT and more rapidly without overexpressed GRK2 than with GRK2 transfection. Thus, a significant interaction among the three factors of time, GRK2 condition, and genotype was determined by 3-way RM ANOVA (D2L: F ((6, 60) = 17.77, $p < 0.0001$; D2S: F (6, 60) = 6.689, $p < 0.0001$). This was followed by 2-way RM ANOVAs to assess the interaction between genotype and time (D2L + GRK: F (6, 24) = 69.15, $p < 0.0001$; D2L No GRK: F (6, 36) = 81.08, $p < 0.0001$; D2S + GRK: F (6, 36) = 118.9, $p < 0.0001$; D2S No GRK: F (6, 24) = 12.49, $p < 0.0001$) and between GRK treatment and time (D2L-WT: F (6, 30) = 103.7, $p < 0.0001$; D2S-WT: F (6, 30) = 71.26, $p < 0.0001$; D2L-I212F: F (6, 30) = 16.62, $p < 0.0001$; D2S-I212F: F (6, 30) = 19.16, $p < 0.0001$). Consistent with our previous report (van der Weijden et al., 2021), expression of D2L/S-I212F was only 35–40% of D2L/S-WT (Table S5.1).

Decreased Arrestin3 Recruitment by D2-I212F Was Not Due to Lower Receptor Expression

Based on unpublished data mentioned previously (van der Weijden et al., 2021), we considered it unlikely that the reduced arrestin recruitment by D2L/S-I212F was simply due to lower receptor expression. Furthermore, the mutation-induced instability of the interaction with arrestin (Figure 5.1C,D) and the greater dependence of arrestin recruitment to D2L/S-I212F on GRK2 are difficult to explain as simply due to lower receptor number. Nevertheless, to confirm that reduced arrestin recruitment by D2-I212F was not a consequence of lower receptor expression, we repeated these experiments with D2L under conditions where the wild type and mutant variants were expressed at similar levels and observed a similar mutation-induced decrease in Emax (Figure S5.1). At this lower level of D2 receptor expression, GRK2 overexpression had no effect on Emax for D2-WT but continued to regulate quinpirole potency at D2-WT.

Contribution of Endogenous GRK to Arrestin3 Recruitment

To determine if endogenous GRK2/3 contributes significantly to arrestin recruitment in this assay, we repeated the experiments above with D2L-WT and D2L-I212F, adding a condition in which cells were pretreated with the GRK2/3 inhibitor Compound 101 (Cmpd101). In the absence of Cmpd101 (Table S5.2), results were indistinguishable from those presented above and replicate prior results for D2L-WT and D2L-I212F with overexpressed GRK2 (Table 5.1). Inhibiting endogenous GRK2/3 significantly decreased the maximal response for both allelic variants with (Figure S5.2A,C) or without (Figure S5.2B,C) overexpressed GRK2. Nevertheless, maximal arrestin recruitment by D2L-I212F was always less than the corresponding condition for D2L-WT (Table S5.2). In contrast, quinpirole potency was decreased by either omitting overexpressed GRK2 or adding Cmpd101, but there was no detectable additivity (Figure S5.2D; Table S5.2).

GRK2 has both phosphorylation-dependent and phosphorylation-independent effects on D2 receptor function (Namkung et al., 2009a; Namkun et al., 2009b). Inhibition of arrestin recruitment by the active-site inhibitor Cmpd101 (Thal et al., 2011) may suggest that at least some of the observed effects of GRK2 require D2 receptor phosphorylation, although it is notable that translocation of GRK2 to the μ-opioid receptor can be inhibited by Compd101 (Gondin et al., 2019; Miess et al., 2018). Observed effects of overexpressed GRK2 despite the presence of Cmpd101 may reflect phosphorylation-independent processes.

D2-I212F Receptor Expression Increased Basal GαoA Protein Activation

We assessed G protein activation using a Gαo energy donor (GαoA-91-RLuc8), a Gβ1/Gγ2 acceptor (mVenus-Gβ1γ2), and D2S/L-WT or D2S/L-I212F transiently expressed in HEK293 cells. Quinpirole produced a concentration-dependent increase in GαoA protein activation for both D2S/L-I212F and D2S/L-WT receptors (Figure 5.2A,B). For D2L, no significant difference in the potency of quinpirole at D2L-WT and D2L-I212F receptors was observed, whereas quinpirole was slightly but

significantly more potent at D2S-WT (1 nM) than at D2S-I212F (2 nM; Table 5.2). On the other hand, basal GαoA activation by D2L-I212F (43% of maximal stimulation) or D2S-I212F (57%) was markedly higher than for D2S/L-WT (set as 0%; Figure 5.2A,B; Table 5.2). Enhanced basal activity was observed despite lower expression of D2S/L-I212F than D2S/L-WT (Table S5.1).

Because the effect of the I212F mutation on GαoA protein activation differed in several respects from what we observed previously using Gαi1 (van der Weijden et al., 2021), we repeated those experiments with D2L-WT and D2L-I212F (Figure 5.2C; previously published results for D2S shown in Figure 5.2D for comparison). Whereas quinpirole potency for activating GαoA was not substantially changed by the I212F mutation, we confirmed our previous observation that the potency of D2L-I212F for activating Gαi1 (3 nM) is markedly increased compared to that of D2L-WT (21 nM; Figures 5.2C and 5.3A). Basal activity of Gαi1 was enhanced by 25% of WT Emax in cells expressing D2L-I212F (Figure 5.2C). This enhanced basal activity associated with D2-I212F expression was significantly lower than that observed for GαoA for both splice variants (Figure 5.3B).

Quinpirole was considerably more potent at GαoA than at Gαi1 for D2-WT, consistent with prior work (Gazi et al., 2003). The G protein subtype-specific effect of the mutation on agonist potency is particularly interesting in light of recent findings that Gαo mediates a relatively high-affinity response to dopamine in the mouse nucleus accumbens that is eliminated by repeated treatment with cocaine (Marcott et al., 2018). This is in contrast to a lower-affinity, cocaine treatment-insensitive response in the dorsal striatum that is mediated by Gαi. In our results, the mutation-induced shift in potency of quinpirole at Gαi1 eliminated the difference between the G protein subtypes (Figure 5.3A; Table 5.2). Thus, mice expressing D2-I212F might display higher sensitivity responses to dopamine in both nucleus accumbens and dorsal striatum, responses that would perhaps be unaffected by repeated cocaine treatment.

Constitutive Inhibition of Cyclic AMP Accumulation

Increased basal activation of G proteins by D2-I212F could be indicative of a higher constitutive activity than that of D2-WT. To test this hypothesis, we measured the ability of D2 receptors to inhibit forskolin-stimulated cyclic AMP accumulation in the absence of agonist. HEK293 cells were transiently cotransfected with the BRET-based cylic AMP sensor, CAMYEL (Jiang et al., 2007) and D2L/S-WT or D2L/S-I212F. Compared to control cells, cells transfected with a higher amount of D2L/S-WT plasmid DNA (0.5 μg) or D2L/S-I212F showed reductions in cyclic AMP accumulation that were greater for D2-I212F (41–50%) than for D2-WT (17–21%) (Figure 5.3C,D; D2L = 83 ± 7% of control for WT High vs 59 ± 6% for D2L-I212F; D2S = 79 ± 2% of control for WT High vs 50 ± 5% for D2S-I212F). Preincubation with either of the inverse agonists sulpiride and spiperone not only reversed the constitutive inhibition of cyclic AMP accumulation but also yielded significantly enhanced cyclic AMP levels that were highest for D2L/S-I212F (Figure 5.3C,D; D2L-I212F = 126 ± 11% of control for sulpiride and 128 ± 12% of control for spiperone; D2S-I212F = 128 ± 12% for sulpiride and 132 ± 14% for spiperone). We hypothesize that increased FSK-stimulated cyclic AMP accumulation in the presence of inverse agonists reflects heterologous sensitization of adenylyl cyclase resulting from prolonged constitutive activation of Gαi/o by D2-I212F (Watts and Neve, 1996; Watts and Neve, 2005).

Enhanced Affinity of D2-I212F for Quinpirole

Receptor constitutive activity is commonly reflected in increased affinity for agonists (Parker and Ross, 1991; Kjelsberg et al., 1992; Wilson et al., 2001). We carried out competition binding assays to compare the apparent affinity of D2-WT and D2-I212F for quinpirole in membranes prepared from HEK293 cells stably expressing the receptors (Figure 5.S3). In four experiments, the geometric mean for quinpirole Ki decreased from 1.5 to 0.4 μM (D2L-WT and D2L-I212F, respectively; $p = 0.0027$) and from 1.9 to 0.5 μM (D2S-WT and D2S-I212F, respectively; $p = 0.0005$).

Thus, the affinity of D2L/S-I212F for quinpirole was increased roughly 4-fold compared to that of D2L/S-WT.

Altered D2-I212F Receptor-GIRK Currents in Mouse Midbrain Slices

To characterize effects of the mutation in a native environment for brain D2 receptors, we used AAV-mediated expression of DIO-Flag-D2S-WT or -I212F to restore D2 receptor function in dopamine neurons of auto-D2-KO mice and characterized D2 receptor activation of G-protein-regulated inward-rectifying potassium channels (GIRKs). We used D2S for these studies because of evidence that this splice variant might contribute more than D2L to autoreceptor activity (Gantz et al., 2015; Radl et al., 2018). The effect of the mutation on D2 receptor function in HEK293 cells was qualitatively similar for both splice variants. Values for both basal G protein activation and maximal arrestin recruitment were greater compared to D2L/S-WT for D2S-I212F than for D2L-I212F, although for most experiments there was neither a significant main effect of splice variant nor an interaction with genotype. The only statistically significant difference among the data presented here was a greater relative efficacy of D2S-I212F for recruitment of arrestin in the presence of GRK2 compared to that of D2L-I212F ($p = 0.001$).

In midbrain slices prepared two weeks after AAV injection, the GIRK response to iontophoretically applied dopamine (Figure 5.1A) was smaller in amplitude (Figure 5.1B), slower in rise time, and longer in duration (Figure 5.1C) for D2S-I212F-expressing neurons compared to that of D2S-WT transduced controls. Despite the smaller peak amplitude, the prolonged duration of the response meant that total charge transfer was higher for D2S-I212F (409 ± 92 pC) than for D2s-WT (207 ± 29 pC; Figure 5.1D).

Photolytic release of sulpiride from CyHQ-sulpiride (Asad et al., 2020) produced a small inhibition of a tonic GIRK current in cells expressing D2-WT (−9 pA) and a much larger inhibition in cells expressing D2-I212F (−62 pA; Figure 5.2A,B). The tonic current could reflect constitutive

activation of G proteins, similar to what we observed in HEK293 cells (Figure 5.2 and Figure 5.3D), or it could reflect the heightened sensitivity of D2-I212F to agonist that is suggested by data for activation of Gαi1 (Figure 5.2C,D) and inhibition of cAMP accumulation (van der Weijden et al., 2021). To distinguish between these possibilities, we treated slices with reserpine to deplete endogenous dopamine. Reserpine treatment abolished or greatly decreased the response to sulpiride in cells expressing D2-WT or D2-I212F, respectively (Figure 5.2B,C), indicating that most of the tonic current is due to endogenous dopamine to which D2-I212F is more sensitive but that D2-I212F also displayed some constitutive activity in the presumed absence of dopamine. Because the mutation increased agonist potency for activation of Gαi1 but not Gαo in HEK293 cells, this may indicate that D2 receptor signaling in SNc dopamine neurons is mediated by Gαi. Interestingly, the current decay in response to sulpiride photoactivation was slower for D2-I212F than for D2-WT even following reserpine treatment and the presumed absence of dopamine (Figure 5.2D), suggesting that relaxation of the receptor or uncoupling of the signaling machinery is inherently slower for the mutant receptor.

Molecular Dynamics Simulations with D2 Receptor Homology Models

One feature of many GPCRs is an "ionic lock" between an Arg residue at the cytoplasmic end of the third transmembrane domain (TM3, Arg132 in the D2 receptor) and a Glu residue at the cytoplasmic end of TM6 (Glu368 in the human D2L receptor) (Ballesteros et al., 2001). These residues are Arg3.50 and Glu6.30 in the Ballesteros-Weinstein index (Ballesteros and Weinstein, 1995). This ionic lock contributes to maintaining the unliganded receptor in an inactive conformation; the lock is broken in the agonist-activated receptor and, conversely, breaking the lock frequently creates a constitutively active receptor (Ballesteros et al., 2001; Rasmussen et al., 1999; Alewijnse et al., 2000). We used crystal structures of the D2 receptor (Wang et al., 2018) and other $G\alpha_{i/o}$-coupled GPCRs to build homology models of the human D2 receptor in both inactive and active

conformations, with either Ile212 or Phe212. As depicted in Figure 5.6, the side chains of Arg132 and Glu368 are in sufficient proximity to form an ionic bond or salt bridge in both inactive models but are too distant for salt bridge formation in both active models. After MD simulations for 15 ns, the Glu368 side chain separated from Arg132 in the inactive D2-I212F model, breaking the ionic lock (Figures 5.6 and 5.7).

During the MD simulation with the inactive D2-I212F model (Figure 5.8), a comparison of snapshots obtained at t = 0.5 ns (left panel) or 7.5 ns (right panel) shows that, initially, the Phe212 side chain extends very close to TM3 residue Ser129 (Ser3.47; not shown), whereas Ile212 in the inactive D2-WT model is more distant from TM3 (Figure 5.6). A steric effect of the close Ser129-Phe212 interaction may provide some of the energy needed to separate the ionic lock residues. As depicted in Figure 5.8 (right panel), Arg132 appeared to strengthen its interaction with Asp131 (D3.49) likely through ionic interactions (Ballesteros et al., 2001). Concomitantly, the ionic lock between residues Glu368-Arg132 was disrupted as Glu368 moved away from Arg132 with the rotation and translocation of TM6, perhaps interacting with other residues in TM6. The Phe212 side chain was reoriented toward a possible interaction with Leu216.

These results provide a structural rationale for the effects of the mutation on G protein activation; separation of the lock residues would better enable the conformational rearrangement of TM6 that creates space for binding of Gα (Ballesteros et al., 2001; Kling et al., 2016; Farrens et al., 1996; Rasmussen et al., 2007). Activating mutations of the ionic lock residues also renders the receptor less stable, which is often reflected in decreased expression (Rasmussen et al., 1999; Alewijnse et al., 2000; Gether et al., 1997) as observed here (Table S5.1).

Constitutive activation of the receptor potentially explains decreased recruitment of arrestin to D2-I212F, particularly if one speculates that enhanced binding of Gα might competitively inhibit binding of arrestin (Mafi et al., 2020; Huang et al., 2020; status et al., 2020). However, we have also

described concurrent reductions in arrestin recruitment and G-protein-mediated signaling for a D2 receptor with a targeted mutation in this part of the receptor (Clayton et al., 2014), in contrast to the reciprocal effects described here; therefore, it may be that distinct mechanisms underlie the observed effects on arrestin and G protein interaction with D2-I212F. For example, abundant data support a model in which arrestin has separate binding determinants for negatively charged phosphorylated residues on the receptor ("phosphorylation sensor") and for receptor sites that are exposed by receptor activation ("activation sensor") (Gurevich and Gurevich, 2006; Zhuang et al., 2013; Hilger at el., 2018). We have proposed that non-natural mutations in this intracellular extension of the fifth α-helical domain selectively affect presentation of the activation sensor (Lan et al., 2009). Decreased engagement of the activation sensor could increase reliance on the phosphorylation sensor, which might explain why arrestin recruitment by D2-I212F has a greater dependence on GRK2 and GRK2-catalyzed phosphorylation.

Conclusions

The data presented here are consistent with a model in which substitution of Ile212 with a Phe residue in the dopamine D2 receptor breaks an interhelical salt bridge that constrains the unliganded receptor. As a result, D2-I212F constitutively activates Gαi/o and mediates high-potency agonist activation of at least one Gαi/o subtype in HEK293 cells and in dopamine neurons. D2-I212F is biased toward G protein-mediated signaling, because the enhanced Gαi/o activation was combined with reduced arrestin recruitment that was particularly profound under conditions where GRK2 activity was limited. A hyperactive D2 receptor would be predicted to cause overinhibition of D2 receptor-expressing medium spiny neurons of the neostriatum and nucleus accumbens. Mice in which the activity of these neurons is genetically inhibited show increased locomotor activity (Bateup et al., 2010). Furthermore, overstimulation of G-protein-mediated signaling by the D2 receptor exacerbates, and overexpression of arrestin3 protects against, L-DOPA-induced dyskinesia

in mice (Urs et al., 2015). This D2 receptor variant c.634A > T;p.I212F is carried by patients with a hyperkinetic movement disorder characterized by both chorea and dystonia (van der Weijden et al., 2021); we speculate that both constitutive activity and G protein bias of D2-I212F contribute to the clinical phenotype and that an effective treatment should target these characteristics of the receptor.

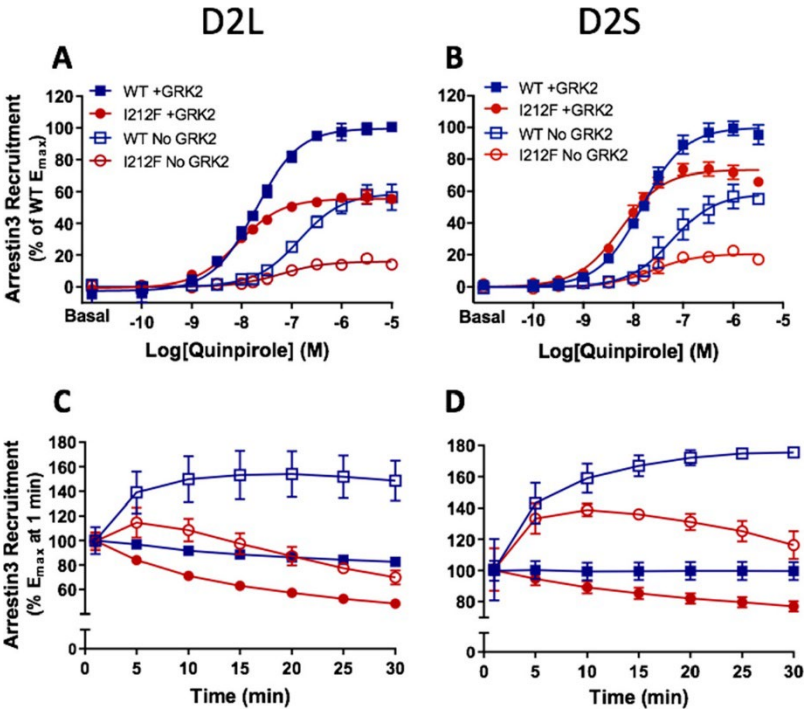

Figure 5-1 Dose–response curves for quinpirole-induced arrestin3 recruitment mediated by D2L/S-WT and D2L/S-I212F.

Arrestin3 recruitment was measured in HEK293 cells cotransfected with GRK2 (+ GRK2) or nonspecific plasmid DNA (No GRK2). Values plotted are the means ± SD of three to four independent experiments performed in quadruplicate. (A, B) Quinpirole concentration–response curves measured at 10 min. Data from each independent experiment were normalized by subtracting the baseline and expressed as a percentage of maximum arrestin3 recruitment by D2-WT+GRK2. Data for +GRK2 are from the data set described in van der Weijden et al. (2021), where results were shown after 20 min of agonist stimulation. (C, D) Change in Emax values over 30 min, with each condition normalized to Emax for that condition at 1 min. Data for +GRK2 were previously described in van der Weijden et al. 2021,

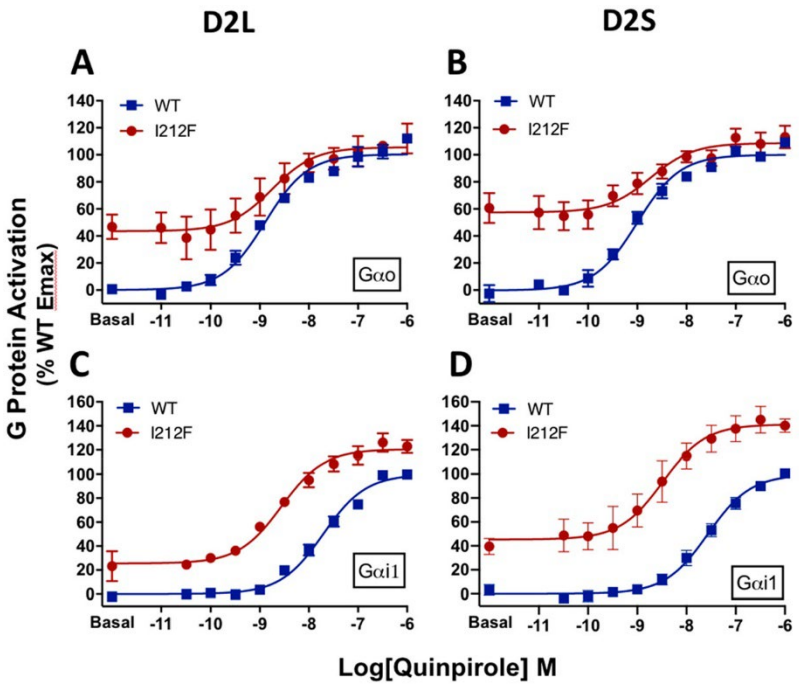

Figure 5-2 Concentration–response curves for Gαi/o protein activation mediated by D2-WT and D2-I212F in response to stimulation with quinpirole.

Results are expressed as the percentage of maximum G protein activation by D2-WT, measured 10 min after adding coelenterazine h. (A) Activation of GαoA by D2L-WT/I212F. (B) Activation of GαoA by D2S-WT/I212F. (C) Activation of Gαi1 by D2L-WT/I212F. (D) Data from van der Weijden et al. (2021) for activation of Gαi1 by D2SWT/I212F. Values plotted represent means ± SD of three (panel C) or four (panels A, B, D) independent experiments performed in quadruplicate.

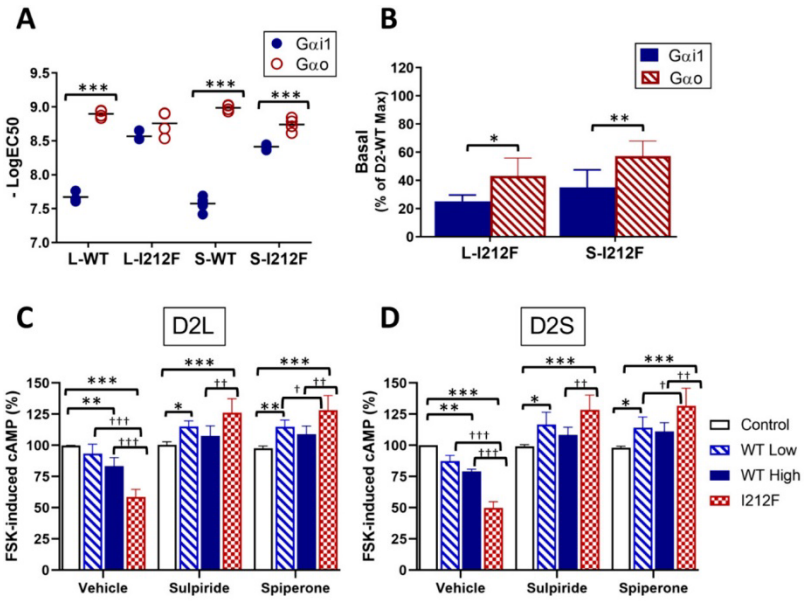

Figure 5-3 Increased constitutive activity of D2-I212F.

Concentration–response curves for Gαi/o protein activation mediated by D2-WT and D2-I212F were analyzed by nonlinear regression to determine quinpirole potency. (A) This was expressed as the – log EC50, and (B) activation in the absence of quinpirole was expressed as the percentage of Emax for D2-WT. Data are from Table 5.2. Statistical differences were determined as described in Table 5.2 (*p < 0.05, **p < 0.01, ***p < 0.001). (C, D) Cyclic AMP accumulation was measured in the presence of 10 µM forskolin (FSK) in HEK293 cells transfected with the cyclic AMP biosensor CAMYEL and either control plasmid DNA (control), a high (0.5 µg, WT High) or low (0.2 µg, WT Low) amount of D2L/S-WT DNA, or D2 L/S-I212F plasmid DNA (0.5 µg, I212F). Measurements were taken 10 min after addition of either vehicle, sulpiride (10 µM) or spiperone (1 µM), FSK (10 µM), and coelenterazine h. Results are expressed as a percentage of cyclic AMP accumulation by control cells treated with the inverse agonist vehicle. Values plotted are mean ± SD of four independent experiments performed in sextuplicate. Statistical differences were determined by 2-way ANOVA followed by Turkey's posthoc test (*p < 0.05, **p < 0.01, ***p < 0.001 compared to the corresponding control condition; †p < 0.05, ††p < 0.01, †††p < 0.001 compared to D2-WT).

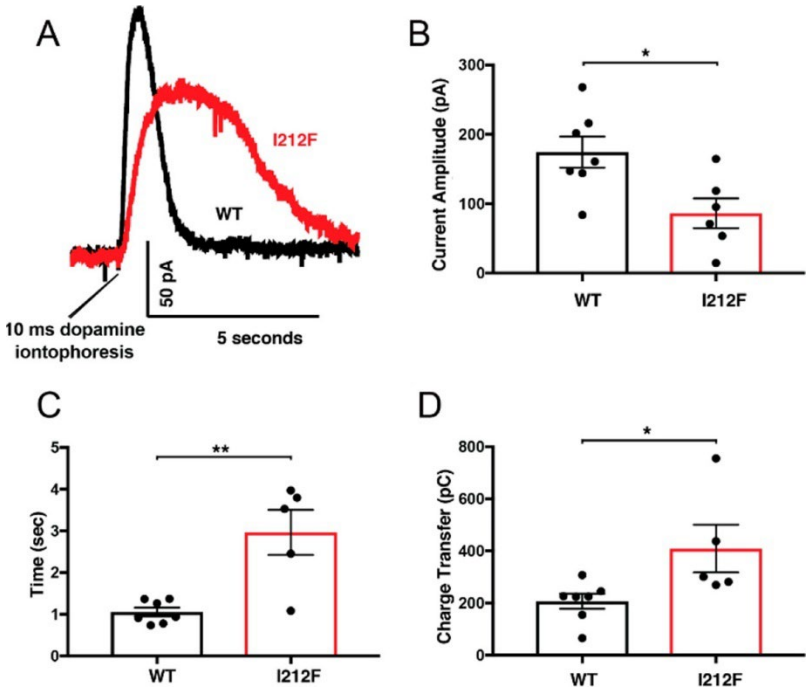

Figure 5-4 Activation of GIRK currents by dopamine iontophoresis was assessed in mouse midbrain slices.

AAV-DIO-D2$_S$-WT or -D2$_S$-I^{212}F was used to restore D2 receptor expression in dopamine neurons of auto-D2-KO mice. (A) Representative outward currents in response to iontophoresis of dopamine (1 M) for 10 ms. Mean ± SEM is shown for (B) current amplitude, (C) peak half-width, and (D) charge transfer. The number of cells differs among panels for D2-I^{212}F, because kinetics in the lowest amplitude response in panel B could not be accurately resolved. Student's *t*-test: *$p < 0.05$, **$p < 0.01$.

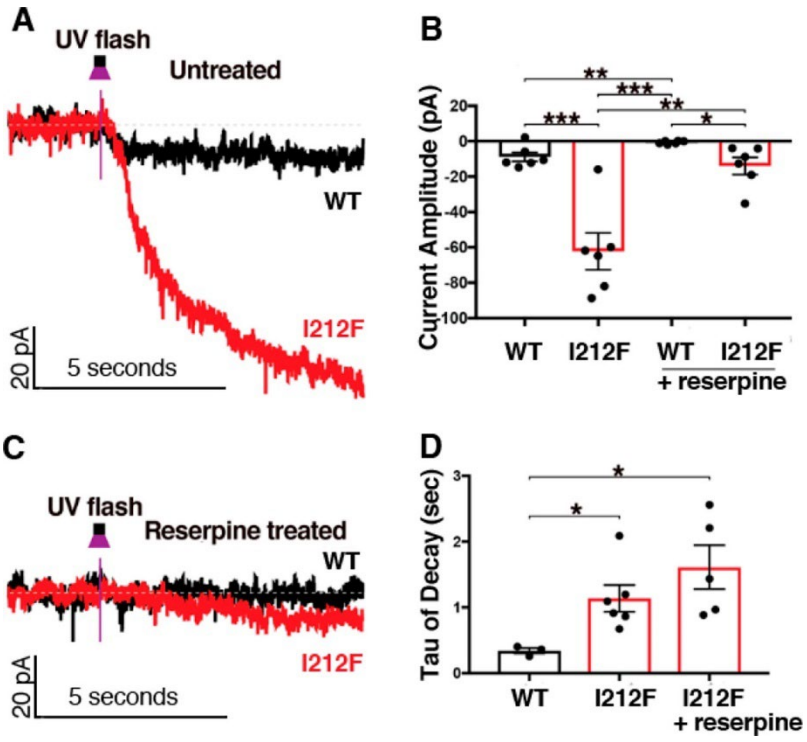

Figure 5-5 CyHQ-sulpiride photolysis

AAV-DIO-$D2_S$-WT or -$D2_S$-$I^{212}F$ was used to restore D2 expression in dopamine neurons of auto-D2-KO mice. CyHQ-sulpiride (5 µM) was circulated over a midbrain slice, and photolysis was induced by a 50 ms flash (365 nm) from a 6.5 mW LED light. The left panels depict representative traces for untreated slices (A) and slices incubated with reserpine to deplete endogenous dopamine (C). The right panels depict the mean ± SEM of the decreased current amplitude (B) and the rate of decay of the current after photorelease of sulpiride (D) in control slices and in slices pretreated with reserpine. It was not possible to calculate a decay rate for reserpine-treated slices from mice expressing D2-WT. For some conditions, the number of cells differs between panels B and D, because kinetics could not be accurately resolved in the lowest amplitude responses in panel B. Student's *t* test: *$p < 0.05$, **$p < 0.01$, ***$p < 0.001$.

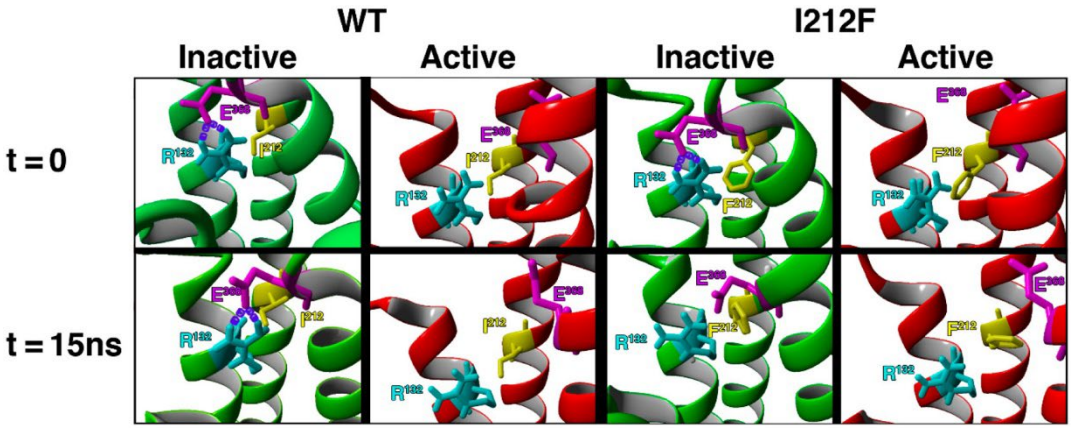

Figure 5-6 Eight panels show TM3-6 ionic lock residues Arg132 (light blue) and Glu368 (magenta), as well as the variant residue Ile/Phe212 (yellow).

Models are shown before (t = 0) and after (t = 15 ns) MD simulations for 15 ns. At t = 0, the distances between OE1 of Glu368 and HH1 and HH2 of Arg132 are short enough to form salt bridges (purple) in both inactive models but are too far apart in both active models. After 15 ns MD simulations, the WT model is essentially unchanged, whereas the presence of Phe212 separates the side chains of Arg132 and Glu368, preventing maintenance of the ionic lock in inactive D2-I212F. The cytoplasmic face is up.

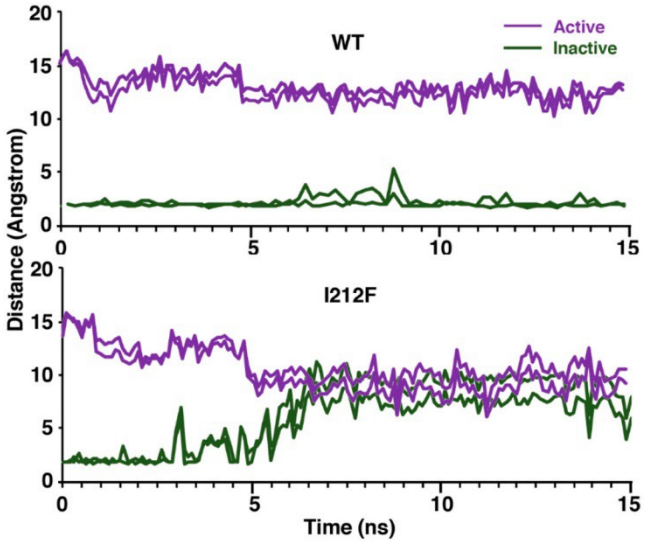

Figure 5-7 Distances between the atoms that form the two bonds of the ionic lock are shown for all four models during 15 ns MD simulations.

Note that the distances are relatively stable for the active and inactive D2-WT models, whereas the distances increased 6–8 Å in the inactive D2-I212F model and decreased ~5 Å in the active model.

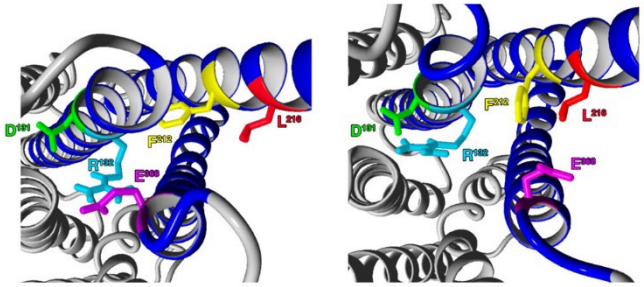

Figure 5-8 Residues involved in the disruption of the ionic lock are shown at t = 0.5 ns (left panel) and 7.5 ns (right panel) during MD simulation with the inactive D2-I212F model.

Ballesteros-Weinstein numbering for the colored residues is Asp1313.49 (green), Arg1323.50 (light blue), Phe2125.61 (yellow), Leu2165.65 (red), and Glu3686.30 (magenta).

Table 5-1 Arrestin Recruitment: Requirement for Overexpressed GRK2[a]

	arrestin recruitment			
	+GRK2[b]		**no GRK2**	
receptor	**–log EC_{50}**	**E_{max} (% of WT+GRK2)**	**–log EC_{50}**	**E_{max} (% of WT+GRK2)**
$D2_L$-WT	7.69 ± 0.05	100 ± 2	6.85 ± 0.05†††	59 ± 4†††
$D2_L$-$I^{212}F$	8.06 ± 0.03**	56 ± 1*** (−44%)	7.22 ± 0.08**,†††	16 ± 1***,††† (−73%)
$D2_S$-WT	7.83 ± 0.01	100 ± 3	7.20 ± 0.13†††	59 ± 2†††
$D2_S$-$I^{212}F$	8.24 ± 0.04**	73 ± 2*** (−27%)	7.59 ± 0.09*,†††	21 ± 0.4***,††† (−66%)

[a]Quinpirole potency is shown as −log EC_{50}. E_{max} was calculated by subtracting basal response from maximal response at 10 min after adding the substrate coelenterazine *h* and is shown as the percentage of D2-WT with added GRK2. For D2-$I^{212}F$, the percent reduction compared to the corresponding D2-WT E_{max} is included in parentheses. *N* = three to four independent experiments for each condition. Data are presented as mean ± SEM.

[b]From the data set described in van der Weijden et al. (2021), except after 10 min instead of 20 min of agonist stimulation. Statistical differences were calculated by 2-way ANOVA followed by Turkey's posthoc test (*$p < 0.05$, **$p < 0.01$, ***$p < 0.001$ compared to D2-WT; $^{\dagger\dagger\dagger}p < 0.001$ compared to the corresponding +GRK2 condition).

Table 5-2 Gα Protein Activation in HEK293 Cells [a]

	–log EC_{50}		**basal activity (% of WT max)**	
receptor	**$G\alpha_{i1}$**	**$G\alpha_{oA}$**	**$G\alpha_{i1}$**	**$G\alpha_{oA}$**
$D2_L$-WT	7.7 ± 0.05	8.9 ± 0.03	0 ± 0.01	0 ± 0.02
$D2_L$-$I^{212}F$	8.6 ± 0.04***	8.8 ± 0.09	25 ± 3**	43 ± 6***
$D2_S$-WT	7.6 ± 0.05[b]	9.0 ± 0.02	0 ± 0.01[b]	0 ± 0.02
$D2_S$-$I^{212}F$	8.4 ± 0.02[b]***	8.7 ± 0.05**	35 ± 6[b]***	57 ± 5***

[a]Quinpirole potency is shown as −log EC50. Basal activity for D2L/S-I212F is expressed as a percentage of the respective D2-WT maximal response. Data are presented as mean ± SEM of three (Gαi1-D2L) or four (Gαo-D2L/S) independent experiments performed in quadruplicate.

[b]Data are from van der Weijden et al. 2021 Statistical differences were calculated by 2-way ANOVA followed by Turkey's posthoc test (**p < 0.01, ***p < 0.001 compared to D2-WT).

Suplemental Table 5-1 D2 receptor density in HEK293 cells

Receptor	Arrestin Recruitment (No GRK)		Gαo Activation		Gαi Activation	
	B_{max}	N	B_{max}	N	B_{max}	N
$D2_L$-WT	2.6 ± 0.5	7	2.3 ± 0.5	7	2.3 ± 0.8	2
$D2_L$-I^{212}_F	0.9 ± 0.1*	6	1.1 ± 0.2**	7	1.0 ± 0.2	2
$D2_S$-WT	2.5 ± 0.3	3	4.6 ± 1.0	7	3.2 ± 0.6[a]	3
$D2_S$-I^{212}_F	1.0 ± 0.01	2	2.3 ± 0.5**	7	1.1 ± 0.2[a],***	3

For most experiments included in Tables 5.1 and 5.2, replicate plates were prepared for analysis of receptor density. Bmax values (Mean ± S.E.M., pmol/mg of membrane protein) were determined by saturation analysis of the binding of [3H]spiperone to a crude membrane fraction. In some BRET experiments, the number of cells was not sufficient to start replicate plates for binding. In some experiments, the number of replications (N) for radioligand binding was greater than the number of replications of the G protein activation and arrestin recruitment assays because results from replicate plates of both donor-only and donor+acceptor conditions were included as separate measurements. a from van der Weijden et al. 2021. Student's t-test: *p

Suplemental Table 5-2 Arrestin recruitment: Cmpd101 pretreatment

Receptor $D2_L$	**Arrestin Recruitment** (n=3)			
	$-LogEC_{50}$		E_{max} (% of WT+GRK)	
	+GRK2	No GRK2	+GRK2	No GRK2
WT Vehicle	7.8 ± 0.02	6.8 ± 0.02†††	100 ± 2	61 ± 3†††
I212F Vehicle	8.2 ± 0.03*	7.2 ±0.04**,†††	55 ± 2*** (-45%)	19 ± 1***,††† (-69%)
WT Cmpd101	6.9 ± 0.03	6.7 ± 0.04	28 ± 2	17 ± 1††
I212F Cmpd101	7.5 ± 0.04***	7.3 ± 0.2***	12 ± 1*** (-57%)	6 ± 1*** (-65%)

HEK293 cells were pretreated with vehicle or the GRK2/3 inhibitor Cmpd101 (30 μM), 30 min before adding quinpirole and coelenterazine *h*. Data are presented as mean ± SEM. E_{max} was calculated as described in Table 1, and is expressed as a percentage of E_{max} for $D2_L$-WT with added GRK2. For D2-$I^{212}F$, the percent reduction compared to the corresponding D2-WT E_{max} isincluded in parentheses. N = 3 independent experiments for each condition. B_{max} values (pmol/mg protein) were 1.68 ± 0.08 ($D2_L$-WT, no GRK2), 0.57 ± 0.03 ($D2_L$-$I^{212}F$, no GRK2),
2.27 ± 0.16 ($D2_L$-WT, + GRK2), and 0.93 ±0.25 ($D2_L$-$I^{212}F$, + GRK2). Statistical differenceswere calculated by 2-way ANOVA followed by Turkey's post-hoc test (*p<0.05, **p<0.01, ***p<0.001 compared to the corresponding D2-WT condition; ††p<0.01, †††p<0.001 compared tothe corresponding + GRK2 condition).

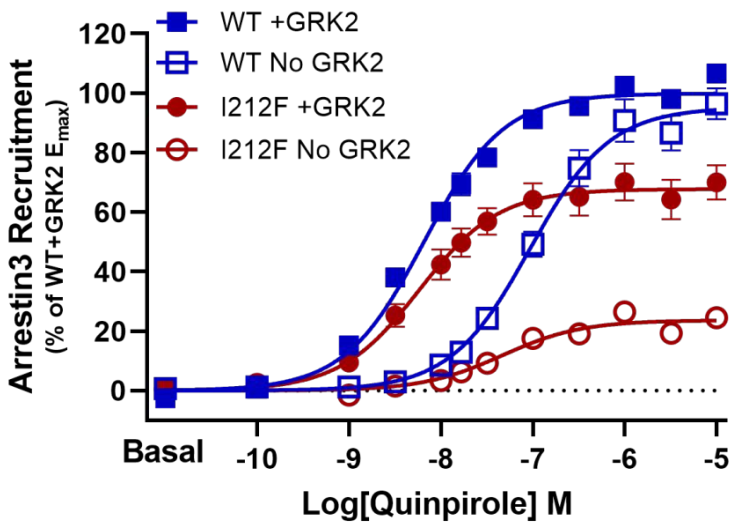

Supplemental Figure 5-1 Arrestin recruitment with matched receptor expression levels.

Arrestin3 recruitment was measured in HEK293 cells co-transfected with D2L-WT (50 ng plasmid DNA) or D2L-I212F (250 ng plasmid DNA) and with GRK2 (+GRK2) or nonspecific plasmid DNA (No GRK2). Values plotted are the means ± SD of 3-4 independent experiments performed in quadruplicate. Data from each independent experiment were normalized by subtracting the baseline and expressed as a percentage of maximum arrestin3 recruitment by D2-WT+GRK2.
D2 receptor Bmax values were 0.46 ± 0.05 pmol/mg protein (D2-WT, No GRK2), 0.48 ± 0.04 pmol/mg (D2-WT, +GRK2), 0.55 ± 0.01 pmol/mg (D2-I212F, No GRK2), and 0.54 ± 0.07 pmol/mg (D2-I212F, +GRK2). Omitting overexpressed GRK2 decreased arrestin recruitment for D2-I212F by 65%, whereas there was no significant effect of omitting GRK2 on maximal response for D2-WT at this lower level of expression. On the other hand, the potency of quinpirole at D2-WT decreased from 6 nM in the presence of GRK2 to 100 nM in the absence of GRK2, and at D2-I212F from 6 nM to 50 nM.

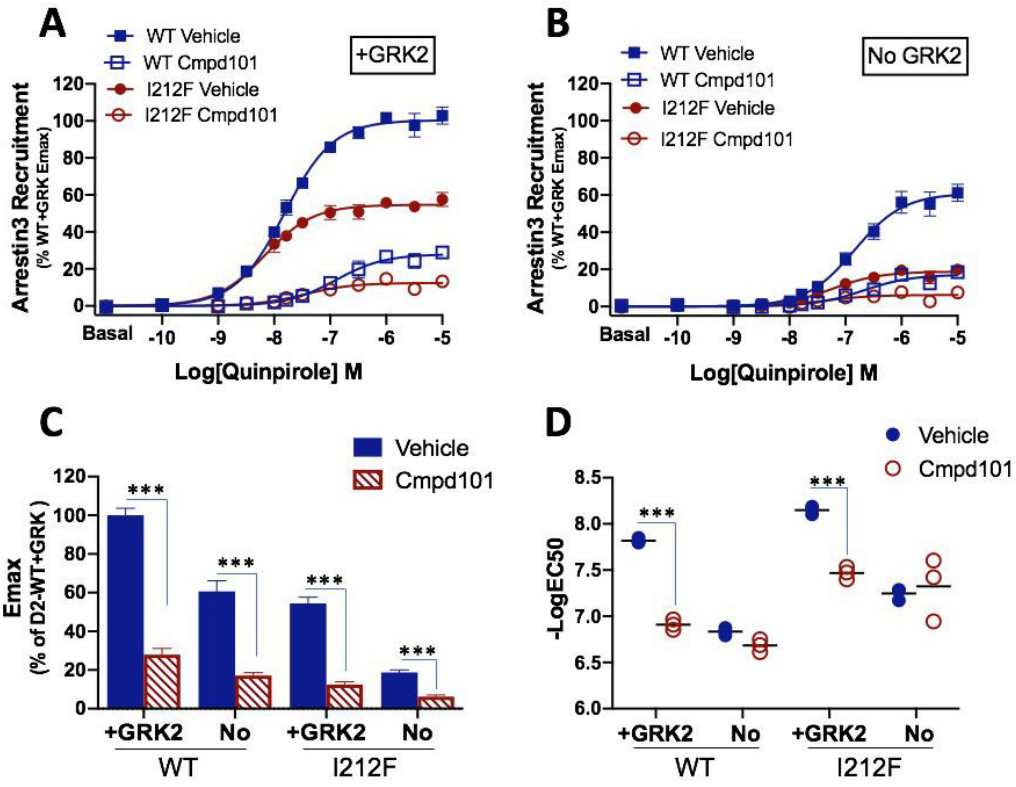

Supplemental Figure 5-2 Effect of Cmpd101 on Arrestin3 recruitment by D2L.

Arrestin3 recruitment was measured in HEK293 cells co-transfected with GRK2 (+GRK2) or nonspecific plasmid DNA (No GRK2) and pretreated with vehicle or the GRK2/3 inhibitor Cmpd101 (30 M, 30 min). A and B, quinpirole concentration-response curves for D2L-WT (WT) or D2L-I212F (I212F) with GRK2 (A) or in the absence of overexpressed GRK2 (B). Data from each independent experiment were normalized by subtracting the baseline and expressed as a percentage of maximum arrestin3 recruitment by D2-WT +GRK2. Values plotted are the means ± SD of 3 independent experiments performed in quadruplicate. C and D, values from Table S2 for D2L- WT (WT) or D2L-I212F (I212F) with (+GRK2) or without (No) GRK2, in the presence (Cmpd101) or absence (vehicle) of Compound 101. C, Emax, expressed as the percentage of Emax for D2-WT with GRK2, and D, quinpirole potency, expressed as the –LogEC50. Statistical differences determined as described in Table S2 (***$p < 0.001$).

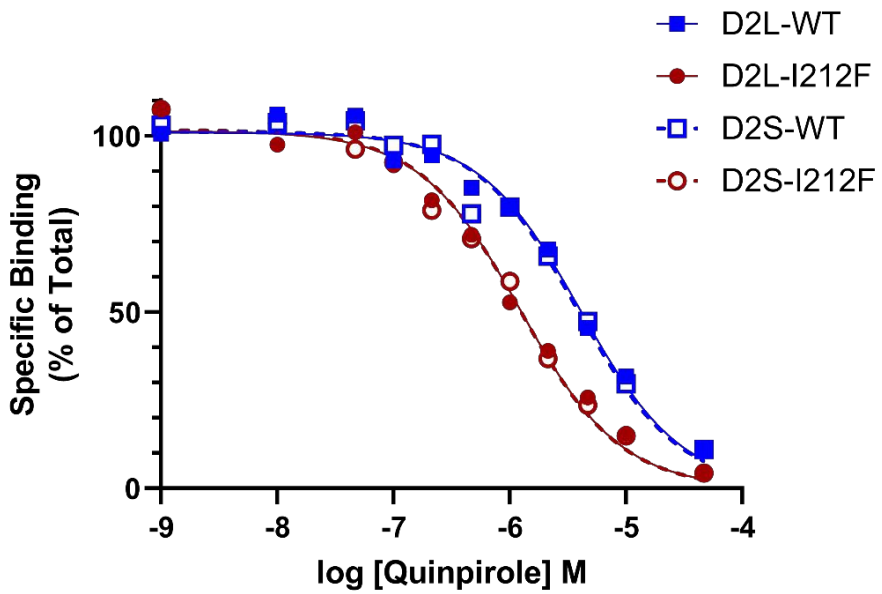

Supplemental Figure 5-3 Quinpirole competition binding curves.

Representative curves are shown for inhibition of the binding of [3H]spiperone (87 pM) by various concentrations of quinpirole in membranes prepared from HEK293 cells stably expressing each of the variants. Ki values in this experiment were 1.24 ±M (D2L-WT), 0.35 ±M (D2L-I212F), 1.19 ±M (D2S-WT), and 0.39 ±M (D2S-I212F). The leftward shift in the quinpirole competition curves for D2L/S-I212F relative to D2L/S-WT indicates that the mutation increased the affinity of the D2 receptor for that agonist, consistent with many studies of constitutively active GPCRs.

Additional Experiments

In Chapter 7, I will discuss findings that D2 receptors largely desensitize by an unknown heterologous mechanism that appears to inhibit GPCR-GIRK coupling. This desensitization is heterologous as it is inducible by and inhibits both D2 and $GABA_B$ receptors. To test if this constitutive D2 receptor activity might affect $GABA_B$ receptor signaling, I applied baclofen at the end of the experiments featured previously in this chapter (same cells/recordings that had previously been exposed to DA ionto and sulpiride). Results of these experiments (Figure 5.9) show the I212F responses to baclofen had smaller peak amplitudes and smaller current decline ($p = 0.0063$ by two-way ANOVA for peak amplitude genotype factor, but no individual group was significantly different than another by Sidak's multiple comparison, means ± SEM = 439.3 ± 22.9, 389.7 ± 93.99, 246.5 ± 84.28, 179.8 ± 45.17 pA for WT untreated, WT reserpinized, I212F untreated, and I212F reserpinized respectively, n = 6, 6, 5, and 6; $p = 0.0141$ by two-way ANOVA for normalized remaining current 90 s after peak, but no individual group was significantly different than another by Sidak's multiple comparison, means ± SEM = 0.7777 ± 0.0262, 0.7612 ± 0.0347, 0.9363 ± 0.0884, 179.8 ± 0.0392 for WT untreated, WT reserpinized, I212F untreated, and I212F reserpinized respectively, n = 5, 6, 5, and 5).

With qualitative observation, in some cells currents would seem to reach peak currents as in a WT cell, but then drift upwards instead of declining. This effect is captured in normalized remaining current (Figure 5.9 F), but the simple number undervalues how odd some currents behaved by increasing amplitude following what appears to be fully equilibrated baclofen currents (peak amplitude in other cells). Sensitization in the continued presence of baclofen may be consistent with altered $GABA_B$ receptor activity, but it should be noted that a second possibility is that sulpiride begins to unbind. The removal of the inverse agonist would allow for constitutive activity to up G

protein concentrations, increasing current by itself or participating in heterologous facilitation (described in Chapter 7). This constitutive activity induced constitutive desensitization may also account for smaller peak responses to iontophoretically applied dopamine in D2-$I^{212}F$ expressing neurons (Figure 5.4 A,B). However, as I had not yet published the paper discussing heterologous desensitization, this observation was left out of the manuscript, potentially to published later or to help guide future experiments studying this mutant receptor.

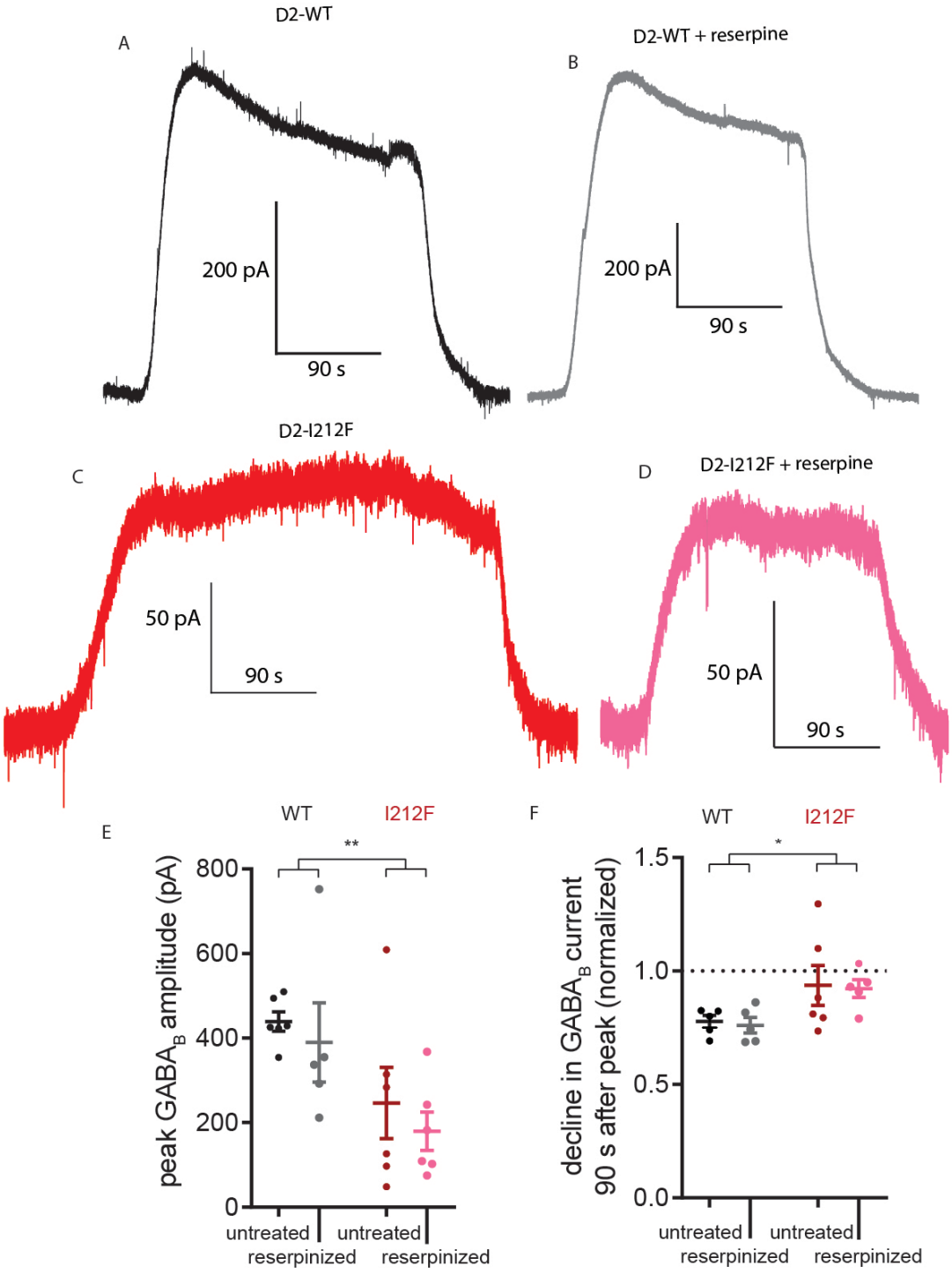

Figure 5-9 Baclofen Currents in D2-WT vs D2-I212F expressing neurons

Baclofen (30 µM) was perfused over the slice followed by reversal with CGP-55845 (1 µM). A) Example baclofen response in D2-KO neurons virally transduced with D2-WT (D2S). B) Example trace

from neurons expressing D2-WT with reserpine pretreatment. C) Example trace from neurons expressing D2-I212F. D) Example trace from neurons expressing D2-I212F with reserpine pretreatment. E) Group data for peak amplitude of the $GABA_B$ receptor current. There was a significant effect of genotype on amplitude ($p = 0.0063$ by two-way ANOVA), but no individual group was significantly different than another by Sidak's multiple comparison (means ± SEM = 439.3 ± 22.9, 389.7 ± 93.99, 246.5 ± 84.28, 179.8 ± 45.17 pA for WT untreated, WT reserpinized, I212F untreated, and I212F reserpinized respectively, n = 6, 6, 5, and 6) F) decline in amplitude of the $GABA_B$ receptor current 90 s after peak current. There was a significant effect of genotype on amplitude ($p = 0.0141$ by two-way ANOVA), but no individual group was significantly different than another by Sidak's multiple comparison (means ± SEM = 0.7777 ± 0.0262, 0.7612 ± 0.0347, 0.9363 ± 0.0884, 179.8 ± 0.0392 pA for WT untreated, WT reserpinized, I212F untreated, and I212F reserpinized respectively, n = 5, 6, 5, and 5). Note: n's differ between peak current and decline due to some cells having a reliable peak current, but losing the cell before 90 s after peak.

Chapter 6 – Dopamine-D2 receptor interactions

Preface

The study presented in this chapter is the result of advances in tool development with the production of photosensitive caged-sulpiride (CyHQ-sulpiride) and fluorescent sensors for dopamine (dLight1.3). Following directly from the work I did characterizing CyHQ-sulpiride (Chapter 3), Dr. Williams, Dr Robinson, and I began to have discussions for the potential use of such a tool. Rapid application of antagonist has a history of use determining the time course of agonist-receptor interactions (Lester et al., 1990). To dissect the functional time course of dopamine-D2 interactions within the IPSC, I performed experiments where I uncaged sulpiride before or just after stimulating dopamine release to induce an IPSC. I then sequentially shifted the timing of antagonism and measured the portion of the IPSC that was blocked. I showed that after about 100 ms, uncaging sulpiride no longer would affect the peak of the IPSC and only affect the decline. That means that dopamine produces this peak current from no more than 100 ms of interaction with the receptor, despite the current itself peaking at ~300+ milliseconds post-stimulation. I also found that when I uncaged sulpiride, I could reliably see a very small 1-2 pA current suggesting there was tonic dopamine interacting with receptors.

Here seems the right time to note that not a single datum of this work was actually used in this following paper. Ultimately, both of these findings were surprising as the lab as a whole was skeptical of tonic dopamine and previous work had showed that a high concentration of dopamine transiently interacts with receptors with diffusion not substantially contributing. These previous views seemed in potential contrast to functional interaction lasting 100 ms. I was balancing a number of different projects at the time, so Dr Williams took over this project. Different

electrophysiology recording stations have their own characteristics, key here being different UV light paths and strengths, so he repeated my experiments using the same settings I had identified as effective. Dr Williams recapitulated and expanded upon my results, producing the data here presented. He then took advantage of the recently developed dLight1.3 dopamine sensor, a heavily mutated D1 dopamine receptor with a circularized GFP attached such that rearrangements upon dopamine binding produce green fluorescence. He was able to use this tool to find sites of dopamine release and compare the time course of extracellular dopamine with the time course of functional dopamine-D2 receptor interaction.

Ultimately, the bulk of the credit for this paper has to go to Dr Williams; in another world he would be both the first and last author of this paper. But the credit I can claim is in collection of preliminary data, experimental design and discussion during the experiments, and a major contribution to writing and editing the manuscript.

The residence of synaptically released dopamine on D2 autoreceptors

Alec F. Condon[1], Brooks G. Robinson[1], Naeem Asad[2], Timothy M. Dore[2], Lin Tian[3], John T. Williams[1]

[1]The Vollum Institute, Oregon Health Sciences University, Portland, OR, USA; [2]New York University Abu Dhabi, Saadiyat Island, P.O. Box 129188, Abu Dhabi, United Arab Emirates; [3]Department of Biochemistry and Molecular Medicine, School of Medicine, University of California, Davis, Davis, CA, USA

Acknowledgments

This work was supported by the National Institutes of Health (R01 DA04523 to J.T.W., U01NS103522 to L.T., F31 DA047007 and K99 DA044287 to B.G.R.) and the Core Technology Platform resources at New York University Abu Dhabi (T.M.D.). We thank Drs. Kim Neve, Joseph Lebowitz, and Christopher Ford for insightful discussions.

[This manuscript is presented as published in (Condon et al., 2021), *Cell Press*, August 3, 2021, 36:109465]

Summary

Neuromodulation mediated by synaptically released endogenous transmitters acting in G-protein-coupled receptors (GPCRs) is slow primarily because of multistep downstream signaling. What is less well understood is the spatial and temporal kinetics of transmitter and receptor interaction. The present work uses the combination of the dopamine sensor, dLight, to detect the spatial release and diffusion of dopamine and a caged form of a D2-dopamine receptor antagonist, CyHQ-sulpiride, to rapidly block the D2 autoreceptors. Photoactivation of the CyHQ-sulpiride blocks receptors in milliseconds such that the time course of dopamine/receptor interaction is mapped onto the downstream signaling. The results show that highly localized release, but not dopamine diffusion, defines the time course of the functional interaction between dopamine and D2 autoreceptors, which determines downstream inhibition.

Introduction

It has been known for decades that the activation of D2 autoreceptors with the exogenous application of agonists cause a potassium conductance-mediated inhibition of neurons in the substantia nigra and ventral tegmental area (Lacey et al., 1987). In more recent years, electrical stimulation has been used to evoke endogenous dopamine release to drive a D2-autoreceptor-dependent inhibitory postsynaptic current (IPSC, Beckstead et al., 2004). The lack of identifiable recurrent collaterals extending from dopamine neurons led to the conclusion that dopamine release in substantia nigra was from dendrites (Hajdu et al., 1973; Wilson et al., 1977; Groves and Linder 1983). The release of dendritic dopamine appears to be mechanistically similar to axonal release from projections in that it is calcium dependent, vesicular, exhibits spontaneous release, and is dependent on RIM, a key scaffolding protein linked to transmitter release (Gantz et al., 2013; Robinson et al., 2019). However, the lack of clearly identifiable anatomical sites of dendrodendritic

transmission has created controversy and limited the understanding of this from of endogenous modulation (Cragg and Rice 2004; Wiencke et al., 2020).

The present investigation addressed the spatial and temporal substrates of dendrodendritic transmission in the substantia nigra using the combination of the dopamine sensor, dLight (Patriarchi et al., 2018) and a photoactivatable D2 receptor antagonist, CyHQ-sulpiride (Asad et al., 2020). Imaging of dLight fluorescence following electrical stimulation found small, isolated sites of intense fluorescence that followed stimulation. Photoactivation of CyHQ-sulpiride was used to rapidly block D2 autoreceptors (Asad et al., 2020). The timing of photoactivation relative to the electrical stimulation used to activate the IPSC was used to determine the time course of dopamine/D2-autoreceptor activation. The results show the peak amplitude of the IPSC was blocked or reduced by antagonism of D2 receptors with photolysis up to 90 ms after electrical stimulation. The amplitude of the IPSC was not affected with photoactivation of CyHQ-sulpiride at times later than 90 ms. Thus, the functional interaction between dopamine and the D2 receptor occurred at spatially defined spots of dopamine release that preceded the peak of the IPSC. Together, the results reveal that the IPSC reaches a peak amplitude after localized spots of dopamine activate D2 autoreceptors for about 100 ms. This approach using CyHQ-sulpiride defines the period of dopamine/receptor interaction that is independent of the slower (by 10 times) downstream processes that underlie the IPSC and suggests the viability of generalizing these methods to other GPCR synapses.

Results and Discussion

The release of extracellular dopamine triggered by electrical stimuli was measured using the viral expression of dLight1.3b. Imaging was carried out using a 2-photon microscope with full field frame scans (20 × 20 µm) at a single z-plane (about 1 µm). With this approach widely isolated spots (1.5–3 µm in diameter) of fluorescence following electrical stimulation required extensive searching and were strikingly obvious once encountered (Figure 6.1). The density of release sites found in the

substantia nigra was distinctly lower than that found in the striatum. This was expected since the amount of release in the striatum measured with voltammetry is close to 1,000 times greater than in the substantia nigra (Ford et al., 2010). Thus, although the density of release sites observed with dLight in the substantia nigra was low and scattered the results suggest that the high concentration of dopamine that is required to mediate the D2-receptor-dependent IPSC is very localized. The fluorescence increase measured in the full field returned to baseline in about 2 frames and remained a low level (Figure 6.1). Treatment with cocaine (10 μM) increased the duration of the fluorescence indicating that dopamine reuptake controlled the extent of diffusion in the midbrain (Figure S6.1).

The fluorescence in the distinct spots rose and fell in a single frame (200 ms, 5 Hz, Figure 6.1). To obtain the kinetics of the rise and fall of fluorescence in the isolated hotspots, line scans (2 ms/line) were carried out (Figure 6.1). The initial increase in fluorescence following stimulation peaked in 10 ms after a single stimulus (n = 4) and 45 ms (n = 6) following 2 stimuli (@ 40 Hz) and decayed with a time constant of 120 ms (n = 3, single stimulus) and 182 ± 44 ms (n = 6, 2 stimuli, Figure 6.1). The rise and fall of extracellular dopamine in the substantia nigra were similar to high concentration of dopamine found in spots of fluorescence reported in the striatum using dLight1.2 (Patriarchi et al., 2018).

Prior to probing of the interaction between endogenously released dopamine and D2 autoreceptors with CyHQ-sulpiride, the time course of D2 receptor blockade with photoactivation of CyHQ-sulpiride was examined using exogenous application of dopamine. Recordings were made from neurons in the substantia nigra and dopamine (10 μM) was added to a recirculating solution containing CyHQ-sulpiride (15 μM, recirculated for at least 5 min prior to use). Photolysis was accomplished with a full field flash of light through the objective (50 ms, 365 nm, 10 mW). Following photo-release of sulpiride, the outward current induced by dopamine was completely blocked with a time constant of 228 ± 28 ms (mean ± SD, n = 7, Figure 6.2). There was a small delay between the

onset of light exposure and current suppression. Following the onset of the flash, the time it took to reach 5% of the total decline in current was 106 ± 17 ms (n = 7, Figure 6.2). A visible deflection of current commenced by the end of the 50 ms flash. The delay in the onset of current decline is likely the combination of the off rate of dopamine from the receptor and the GTPase activity of Gα and the rebinding of Gβγ subunits.

Next, transient outward currents were induced with focal iontophoretic application of dopamine (20 nA, 5–20 ms). Photolysis of CyHQ-sulpiride to block the dopamine-induced current that was dependent on the relative timing of the iontophoretic pulse and the start of the 50 ms flash (Figure 6.2). Photolysis before the onset of the iontophoretic pulse completely blocked the outward current (data not shown). The time constant of the sulpiride-induced decay in the current induced by dopamine (223 ± 43 ms, n = 12) was independent of the amplitude of the outward current (Figure 6.2). One striking observation was that the time it took to reach the peak outward current induced by the iontophoretically applied dopamine was dependent on the timing of the flash (Figure 6.2). As the timing of the flash approached the peak of the outward current, the latency to the onset of decline in the dopamine current decreased. There are two possible explanations for the change in latency. First there is a latency of about 50 ms between the application of dopamine and the initial rise in current, a rate inherent to the signal transduction. Second, at early time points photoactivation of sulpiride and dopamine compete for receptor occupation. At later times, the concentration of dopamine is falling such that the latency to current decline was dependent on dopamine leaving the receptor. In all cases, despite changes in the latency of decline, the time constant of the sulpiride induced current decay was the same. The results indicate that CyHQ-sulpiride can be used to determine the time course of interaction between dopamine and D2 receptors that mediate the IPSC.

Next, the inhibition of the IPSC induced by CyHQ-sulpiride was examined. As previously reported the kinetics of the dopamine-dependent IPSC in the substantia nigra scale with amplitude (Figure 6.2, supplement; Beckstead et al., 2004; Courtney and Ford, 2014). The IPSC had a latency of about 50 ms, peaked in 275 ± 28 ms (n = 21, mean ± SD), the duration measured at the half amplitude was 403 ± 86 ms, and the time constant of decay that was 355 ± 82 ms. Each of these measures did not consistently vary with increased stimulus intensity and current amplitude. The kinetics of IPSCs evoked by single, pairs (25 ms interval), and trains (5 @ 40 Hz) of electrical stimulation was examined. In each case, the time course of the IPSCs were unchanged with the intensity of the stimulus (Figure S6.2).

The IPSC was examined in experiments using systematic antagonism of the D2 receptors with photolysis of CyHQ-sulpiride before and following electrical stimulation. Initial experiments used a single electrical stimulus (1/min) to maximize temporal resolution. A solution of CyHQ-sulpiride (15 μM) was recirculated for a period for at least 5 min. A single flash (50 ms, 10 mW) was sufficient to completely block the IPSC for at least 10 min, followed by partial recovery over about 30 min. Thus, each experimental replicate required a separate slice preparation. The timing of the flash was moved in steps ranging from 100 ms before the electrical stimulus to 500 ms after the stimulation. In each experiment, the effect of photolysis of CyHQ-sulpiride on the IPSC was compared with the previous IPSC as control. The amplitude of the IPSC induced in conjunction with photolysis was plotted relative to the preceding (control) IPSC (Figure 6.3).

The results show that photolysis of CyHQ-sulpiride before or simultaneous with the single electrical stimulus blocked the IPSC. Thus, receptors were blocked within ms following photolysis of CyHQ-sulpiride. As the time of photoactivation of sulpiride was moved to 30, 60, and 90 ms following the stimulus, the inhibition became partial such that amplitude of the IPSC increased (Figure 6.3). After 90 ms, the amplitude of the IPSC was almost unchanged by photolysis of the CyHQ-sulpiride.

Thus, extracellular dopamine contributes to the peak of the IPSC for ~90 ms. Although the duration of the IPSC measured at 50% of the peak decreased following photoactivation of sulpiride at different time points, the time constant of current decay following the flash was the same across all experiments (Figure 6.3). In addition, the time it took to reach the peak current after photolysis was about 200 ms in experiments where the timing of the flash was less than 90 ms after the electrical stimulation. In experiments where photolysis was 90 ms or later, the time to reach the peak amplitude decreased (Figure 6.3). This observation is similar to that obtained using iontophoretic application of dopamine (Figure 6.2) with the exception that the kinetics of the synaptically released dopamine contributing to peak current was dramatically faster than exogenously applied dopamine. Taken together the results suggest that a high concentration (30–100 μM, Ford et al., 2009) of synaptically released dopamine binds to the D2 autoreceptor in less than 30 ms to set in motion the downstream processes that activate the GIRK conductance. The consistency of flash-induced time-to-peak relative to the timing of the photolytic flash at the early stages of the IPSC suggests the concentration of dopamine must stay high in order to continue producing the same rate of rise in the IPSC. Though dopamine concentration is falling in this time frame, as seen both by dLight (Figure 6.1) or conceptual modeling (Cragg and Rice 2004; Wiencke et al., 2020), concentrations must still be high enough to almost maximally activate receptors during the time that defines the rising phase of the IPSC. This conclusion is also supported by experiments using excised macropatches of dopamine neurons where the duration of ligand-receptor interaction was found to determine the full amplitude of GIRK conductance (Ford et al., 2009: Courtney and Ford, 2014). The sulpiride induced block of receptors 30 and 60 ms following electrical stimulation decreased the amplitude of the IPSC but the initial rate of rise was the same as in control indicating that a high concentration of dopamine reached the receptors.

Pairs and trains of stimuli (2 or 5 at 40 Hz) were examined next. A flash 90 ms after a single stimulus decreased the IPSC to 82% ± 3% (n = 3) of control but following a pair of stimuli or train of

stimuli (5 @ 40 Hz) the IPSC was reduced to 69% ± 15% (n = 4) and 51% ± 13% (n = 7) of control (n = 4), respectively. Photolysis 120 ms after the start of a train of stimuli reduced the IPSC amplitude to 61% ± 18% of control (n = 7) and flashing at 240 ms was 90% ± 7% of control (n = 5). The results suggest that dopamine release continues with each stimulus so that the timing of receptor blockade by sulpiride moves to later time points. This result is notable due to the fact that the duration of the IPSC is the same after 1, 2, and 5 stimuli (Figure S6.3).

The decline in potassium current induced by photolysis of CyHQ-sulpiride is more rapid than the decline of the IPSC. The time constant of decline in the IPSC was 304 ± 6 ms (n = 78), whereas the time constant decline in the IPSC following photolysis was 253 ± 6 ms (n = 36). Thus, the duration of the IPSC was greater than the termination of the IPSC induced by CyHQ-sulpiride even when photolysis was late enough to have no effect on peak amplitude (ANOVA, $p < 0.001$, Tukey post hoc). The decline in current induced by exogenous application of dopamine was 220 ± 41 ms (n = 28, $p > 0.05$ ANOVA, Tukey post hoc). Thus, under normal circumstances the duration but not the peak of the IPSC is dependent on the continued presence of dopamine that could be the result of rebinding of dopamine or diffusion away from the release site.

One unexpected consequence of experiments using the CyHQ-sulpiride was a small (6.8 ± 4.0 pA, n = 21) and reproducible inward current that decayed with a time constant of about 200 ms. This inward current was larger in experiments following the viral overexpression of D2 receptors or the application of cocaine (3 µM, 25.2 ± 13.8 pA, n = 12). The inward current was only observed once in each slice, but was not observed following the superfusion of sulpiride or after treating the slice with reserpine to deplete vesicular dopamine (Rodriguez-Contreras et al., 2021). The results indicate that there was a very low level of D2-receptor activation and GIRK conductance resulting from tonic levels of extracellular dopamine.

The activation of the GIRK conductance mediated by GPCRs is dependent on both the concentration and the duration of agonist application. Short-duration applications (5–10 ms) of a saturating agonist concentration result in currents that peak in 100–300 ms. Longer applications (50–150 ms) result in larger amplitude currents with similar rise times (Sodickson and Bean, 1996; Ford et al., 2009; Courtney and Ford, 2014). The results of the present study indicate that synaptically released dopamine acts on the D2 autoreceptors for about 90 ms so that the IPSC reaches a peak in 200–300 ms (Figure 6.4). With continued release induced by trains of stimuli, the IPSC scales to that induced by a single stimulus (Figure S6.2), indicating, as observed with exogenous application of dopamine, that the duration of the current induced by receptor activation is dependent on downstream processes.

Given that the affinity of the Gßγ subunits for GIRK is very low (100 s of μM) both the peak amplitude and duration of GIRK conductance is dependent on the sequestration rate of Gßγ subunits by GDP-bound Gα subunits (Wang et al., 2016; Touhara and MacKinnon, 2018). By increasing the duration of dopamine release using a train of stimuli for up to 125 ms (5 pulses at 40 Hz) more Gßγ subunits are liberated thus increasing the number of Gßγ-bound GIRK channels.

The decline could be determined by the affinity of dopamine for the receptor and/or GTPase activity of the Gα subunits. Experiments with the photoactivation of sulpiride on the current induced by noradrenaline showed that the decline in current was more rapid than currents induced by dopamine (Figure S6.3). The suggestion is that the affinity of noradrenaline for the D2 autoreceptor is less than that of dopamine. Thus, the decline in the IPSC is at least in part dependent on the affinity of dopamine.

Taken together, the concentration of dopamine following dendritic release peaks and declines more rapidly than the activation of the GIRK-dependent IPSC (Ford et al., 2009). The rise to the peak of the IPSC is dependent on a concentration approximating 100 μM for roughly 90 ms, 150

ms prior to the peak amplitude of the IPSC. The decay of the IPSC is somewhat longer than expected based on the block of receptors by photoactivated sulpiride. Thus, the time course of the IPSC is determined by both the GTPase activity of the Gα subunits and the decline in the concentration of dopamine in the extracellular space. The late component of the IPSC is most likely the result of the trailing component (200–300 ms) of extracellular dopamine measured with dLight (Figure 6.4). Measures of the amplitude and kinetics of the IPSC were slowed in slices taken from animals that expressed dLight (Figure S6.4). This observation was taken as an indication that dLight buffered the released dopamine and increased the duration of the presence of dopamine as it dissociated from dLight.

That dopamine transmission is mediated by a synaptic or volume-dependent mechanism has been debated and modeled on multiple occasions (Cragg and Rice 2004; Wiencke et al., 2020). Dopamine-dependent transmission is clearly different from a truly synaptic mechanism. For example, glutamate is present in the synaptic cleft for less than 1 ms, and the time course of the NMDA-dependent transmission is dependent on the off rate of glutamate from the receptor (tau = 250–400 ms, Lester et al., 1990). Dopamine, on the other hand, must be present for about 100 ms to achieve the full amplitude of the IPSC. Given that the affinity of dLight1.3b for dopamine is roughly the same as the D2 receptors, the time course of the dLight transient correlates well with the functional experiments using the photoactivation of sulpiride. The dLight experiments also indicate that the concentration of dopamine (30–100 μM) is present in highly localized spots for the required time (100 ms) to induce the IPSC. Thus, the diffusion of dopamine beyond the highly localized spots of release is not a major contributor to the amplitude of the IPSC.

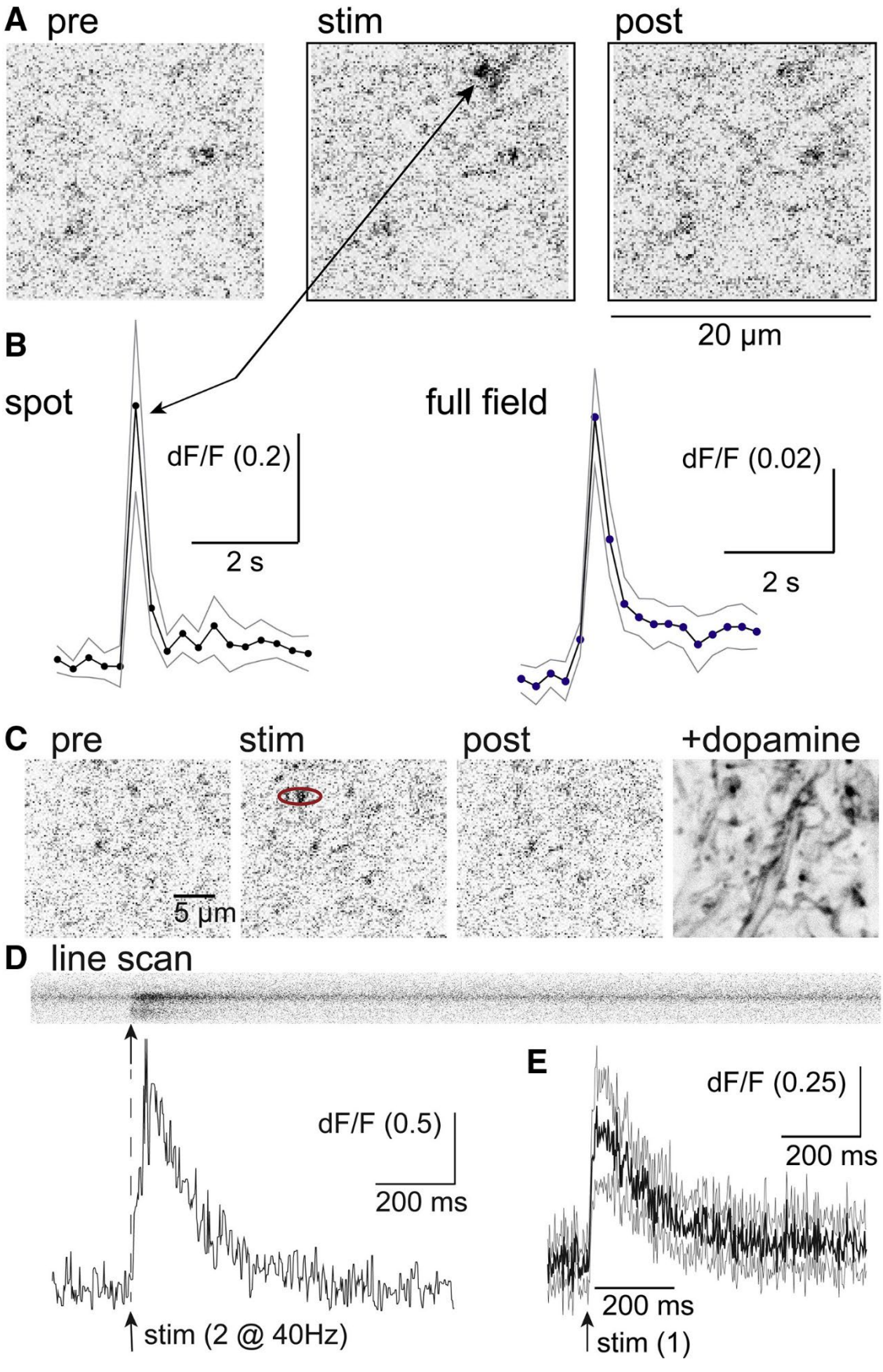
A pre
stim
post
20 µm
B
spot
dF/F (0.2)
2 s
full field
dF/F (0.02)
2 s
C pre
stim
post
+dopamine
5 µm
D line scan
dF/F (0.5)
200 ms
stim (2 @ 40Hz)
E
dF/F (0.25)
200 ms
200 ms
stim (1)

Figure 6-1 Location and kinetics of dopamine release measured with dLight1.3b

(A) Images of the activation of dLight upon electrical stimulation (frame rate 4 Hz). At frame 9 a pair of electrical stimuli were applied. Scale bar, 20 μm.

(B) The fluorescence increase in a spot was measured in each frame and plotted below. The fluorescence for the entire frame (full field) is plotted on the right.

(C) Images of the activation of dLight upon electrical stimulation. A line scan was carried out along the spot in the red ellipse. Scale bar, 5 μm.

(D) High temporal resolution measure of the rise and fall of dopamine measured with a line scan through a spot of dLight1.3b fluorescence. Blow is the rise and fall of the fluorescence measured using the line scan above.

(E) Summary of the time course of dLight fluorescence obtained from line scans of 4 different spots (4 slices, 3 animals). The dark line is the mean change in fluorescence, and the gray lines are the 95% confidence limits.

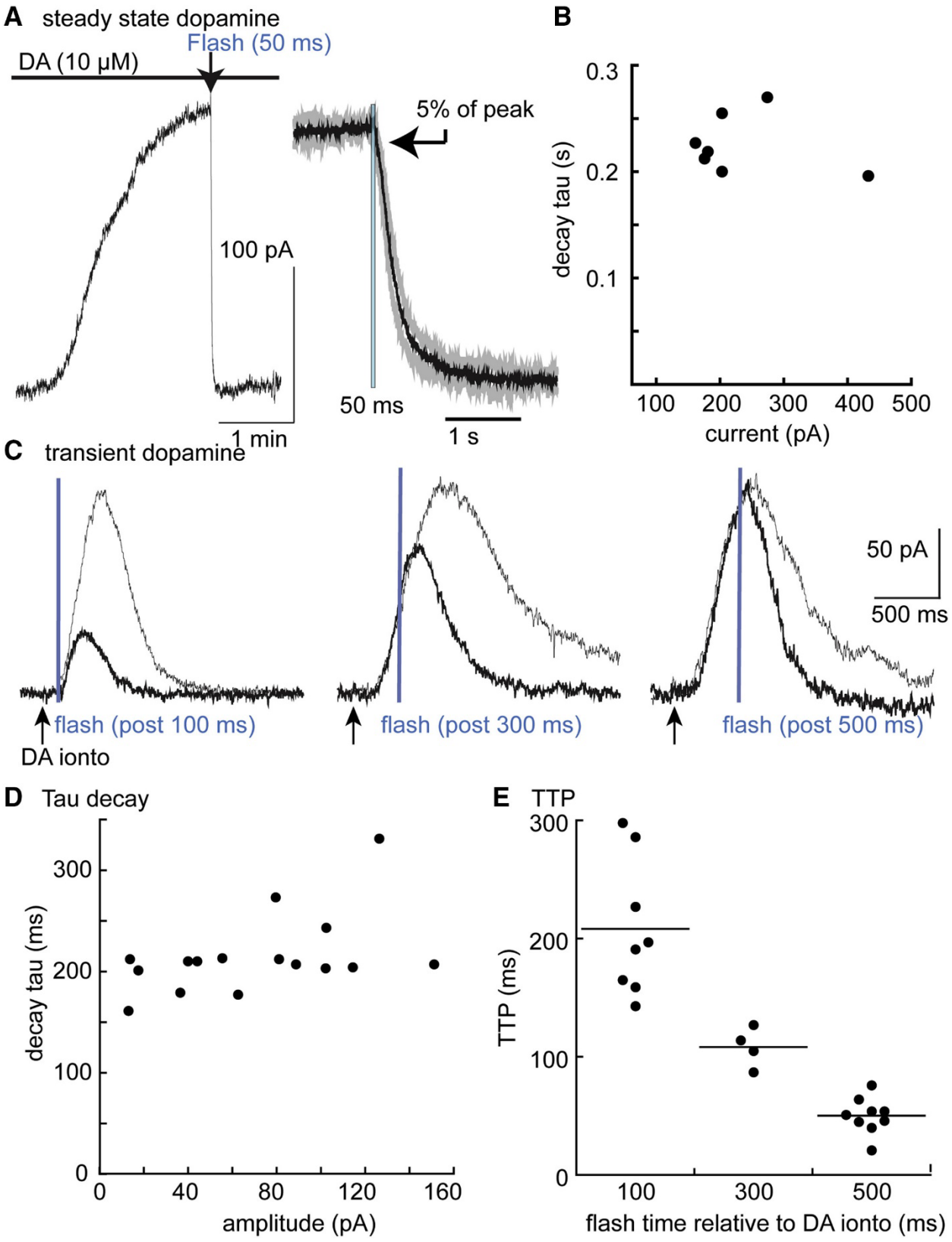
A steady state dopamine
Flash (50 ms)
DA (10 µM)
5% of peak
100 pA
50 ms
1 min
1 s
B
0.3
0.2
0.1
decay tau (s)
100
200
300
400
500
current (pA)
C transient dopamine
50 pA
500 ms
flash (post 100 ms)
flash (post 300 ms)
flash (post 500 ms)
DA ionto
D Tau decay
300
200
100
0
decay tau (ms)
0
40
80
120
160
amplitude (pA)
E TTP
300
200
100
0
TTP (ms)
100
300
500
flash time relative to DA ionto (ms)

Figure 6-2 Photolysis of CyHQ-sulpiride blocked D2-autoreceptor activation of GIRK

(A) Left: an experiment where dopamine (10 μM) was applied in the presence of CyHQ-sulpiride (15 μM) and a flash (365 nm, 5 mW, 50 ms) was applied at the arrow. The right side is a summary of results (n = 7) where the current induced by sulpiride was normalized and averaged. The black line is the mean and the gray lines are the 95% confidence limits. The arrow indicated the point at which the current declined to 5% of the maximum (106 ± 17 ms following the onset of the 50 ms flash).
(B) Summary of experiments illustrating the time course of current block as a function of the amplitude of the current induced by dopamine (10 μM).
(C) Traces showing individual experiments with a control current induced by iontophoretic application of dopamine (gray line) superimposed on the current induced by dopamine followed by photolysis of CyHQ-sulpiride (black line). The flash was applied at different times (100, 300, 500 ms) following the iontophoretic application of dopamine.
(D) Plot of the decay of the outward current induced by photolysis of CyHQ-sulpiride as a function of the amplitude of the outward current.
(E) Summarized results showing the time to reach the peak current relative to the onset of the flash.

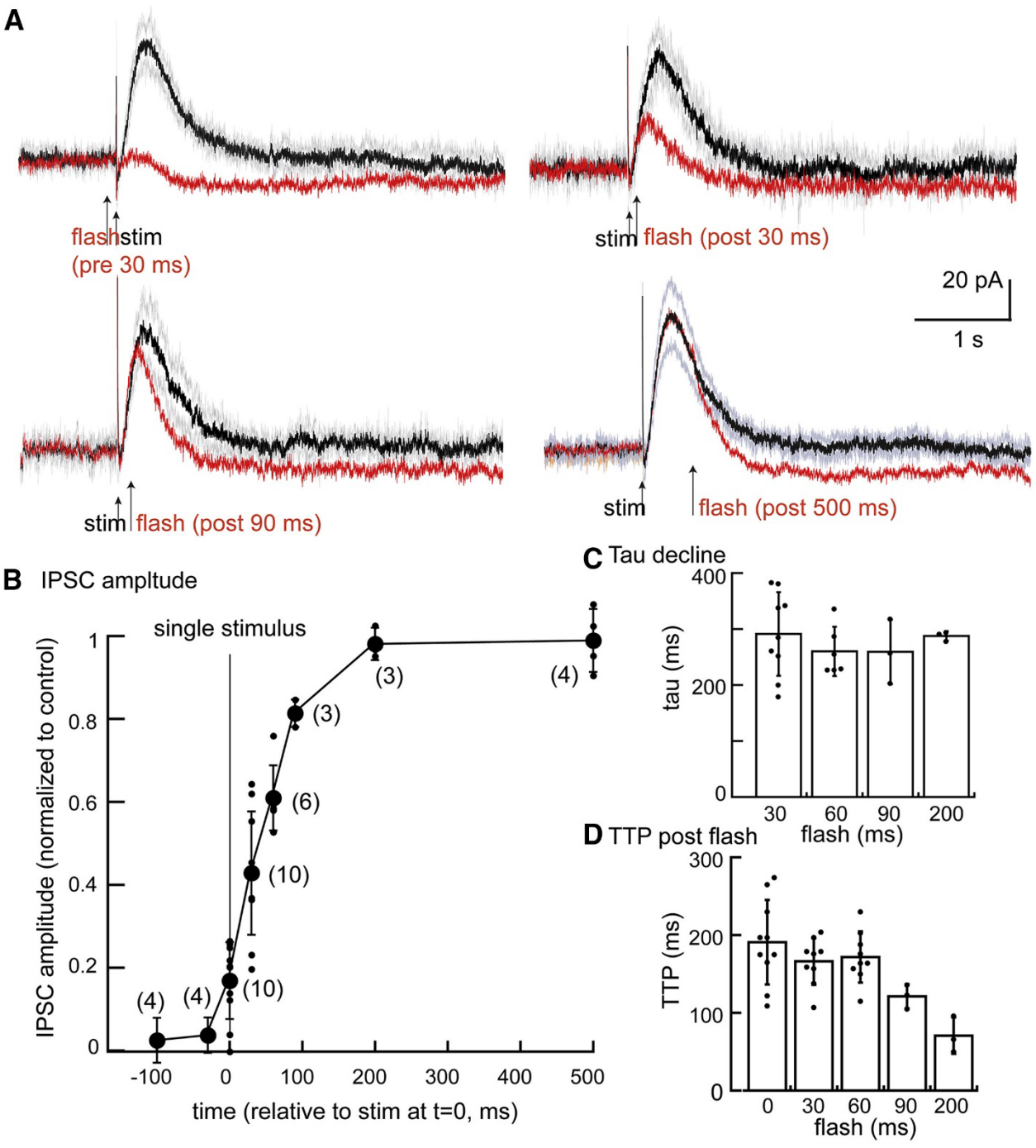

Figure 6-3 Photolysis of CyHQ-sulpiride blocks the D2-autoreceptor IPSC in a graded manner dependent on the timing of the flash.

(A) Summary of experiments where photolysis was applied at 30 ms prior to the electrical stimulus, 30, 90, and 500 ms post stimulus. Each point is from a separate slice.

(B) Plot of the amplitude of the IPSC following photolysis relative to the prior (control) IPSC. The electrical stimulus was applied a 0 ms, and photolysis was induced at the indicated times on the x axis (mean ± SD).

(C) Plot showing the time constant of decay following the flash was not dependent on the timing of the flash (mean ± SD).

(D) Plot of the time it takes to reach the peak of the IPSC relative to the onset of the flash (mean ± SD).

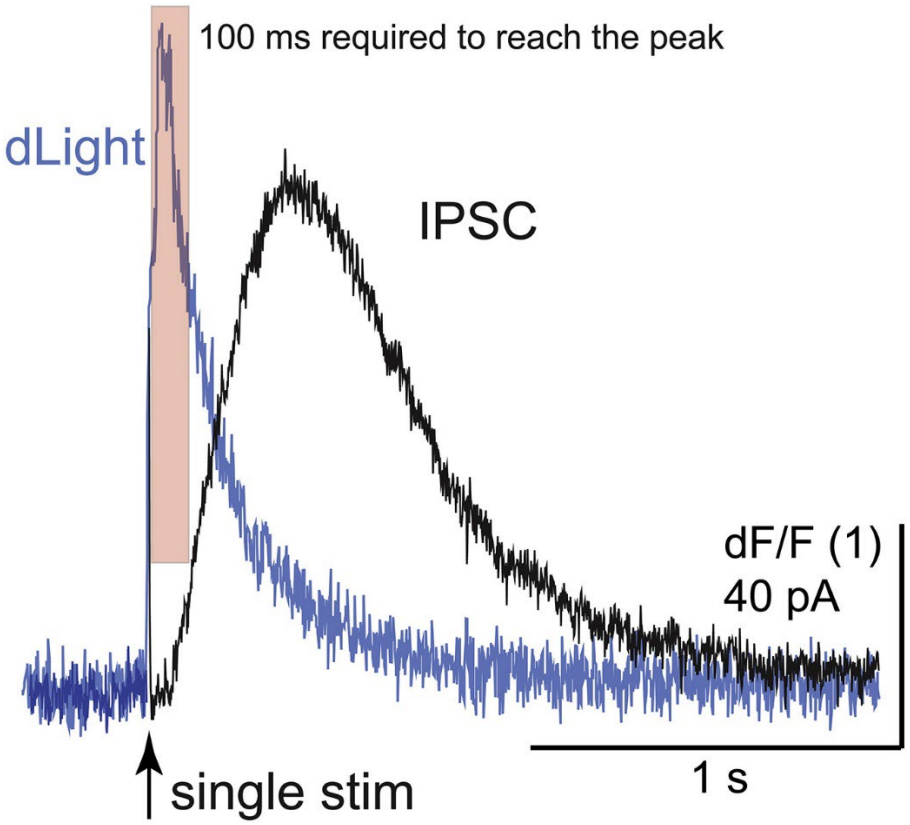

Figure 6-4 Illustration of the relative time course of the rise and fall of extracellular dopamine measured with dLight superimposed on the IPSC

This illustration is taken from two different experiments (dLight imaging, IPSC recording). The shaded red box indicates the 90 ms where most of the amplitude of the IPSC is induced. The remainder of the fall in extracellular dopamine is suggested to result in prolongation of the IPSC.

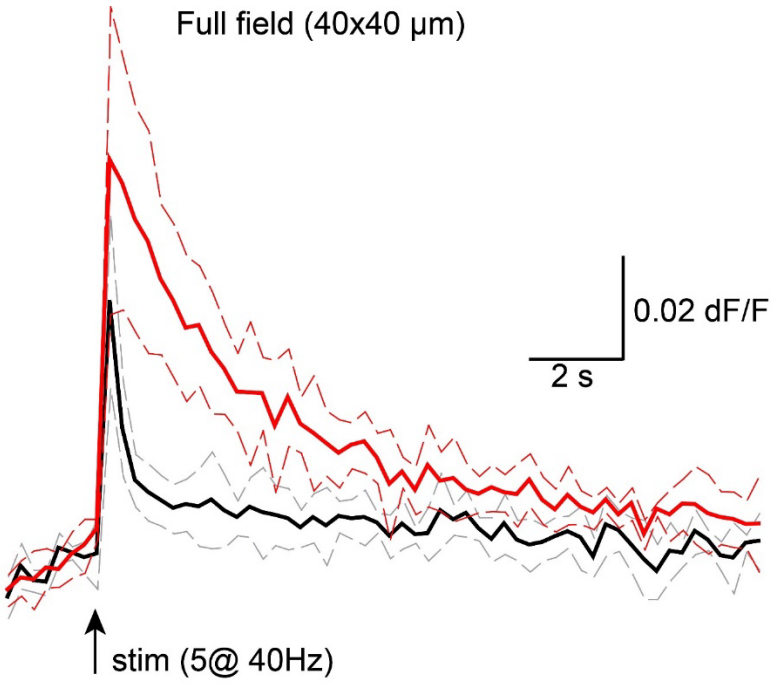

Supplemental Figure 6-1 Cocaine prolongs the presence of dopamine following electrical stimulation as detected with dLight1.3b (related to Figure 6.1).

Summarized results showing the rise and fall of fluorescence induced by electrical stimulation in control (black line) and in the presence of cocaine (10 µM, red line). Dotted lines indicate the 95% confidence limits (n=5 slices, 4 animals).

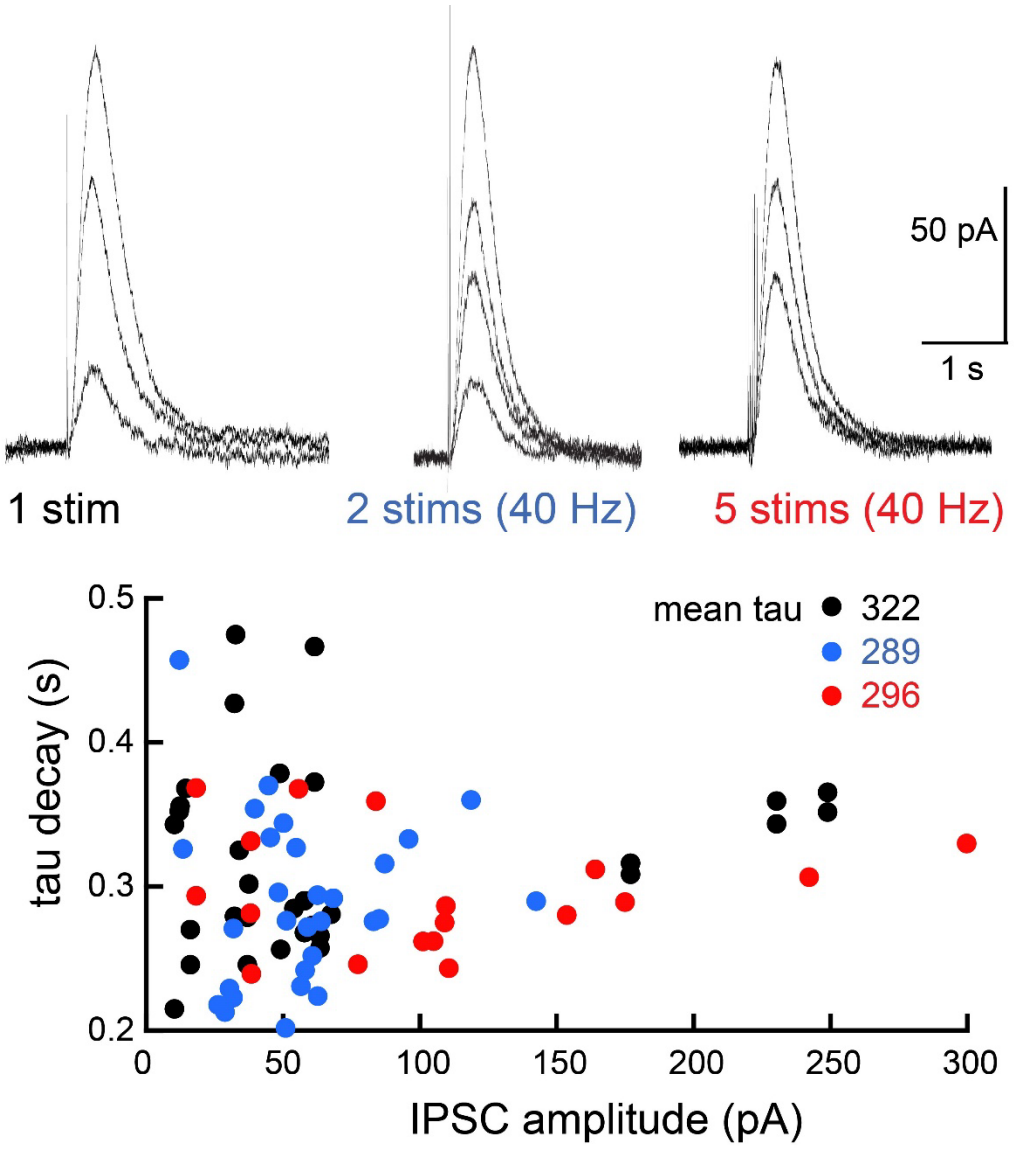

Supplemental Figure 6-2 The decay of the IPSC is independent of the stimulus strength and stimulus number (related to Figure 6-3).

Top – examples of IPSCs evoked with different stimulus intensities and stimulus numbers. Bottom – Summary of the time constant of IPSCs evoked with 1 (black), 2 (blue) and 5 (red) stimuli plotted against the amplitude of the IPSC.

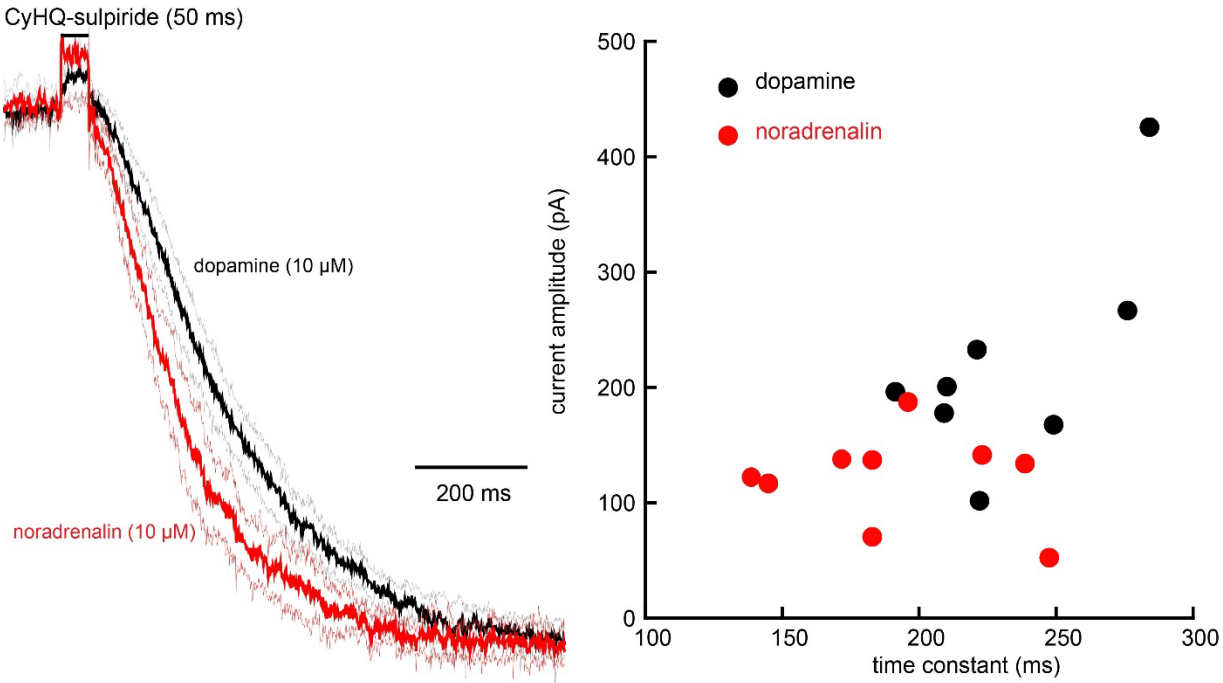

Supplemental Figure 6-3 The inhibition of current induced by noradrenalin by photoactivation of CyHQ-sulpiride is faster than dopamine (related to Figure 6-4).

Left – normalized average results showing the decline in dopamine (black) and noradrenalin (red) current induced by photoactivation of CyHQ-sulpiride. The faint lines are the 95% confidence results. Right is a plot of the currents induced by dopamine and noradrenalin plotted against the time constant of decay for each experiment. The time constant of decay for dopamine was 232.9 ±33.3 (mean ± SD, n=8) and noradrenalin was 191.6±38.5 (mean ± SD, n=9). The mean difference was 41.2 ms, p=0.033.

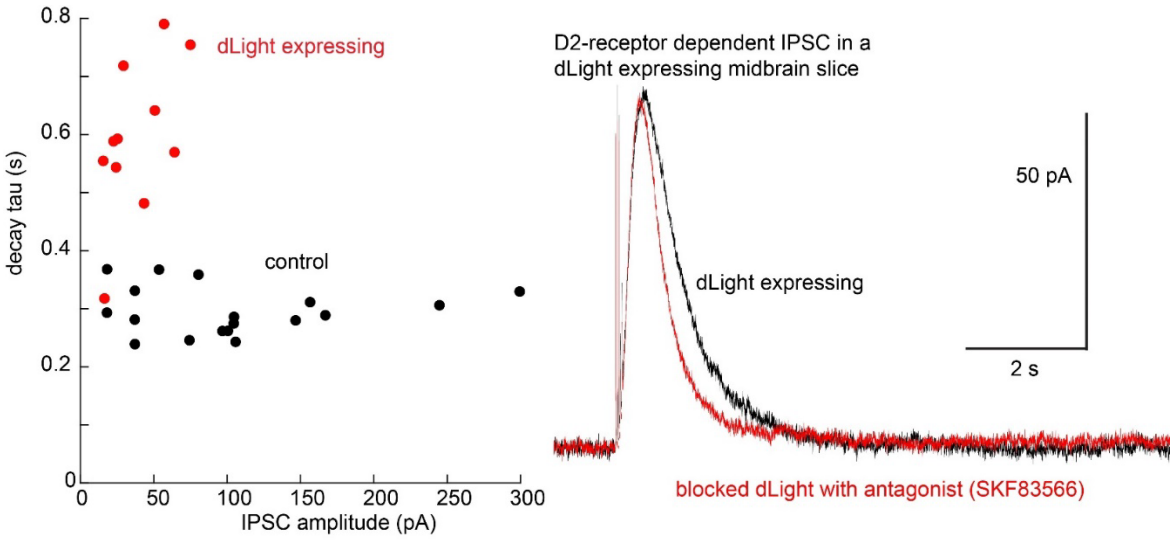

Supplemental Figure 6-4 Expression of dLight decreases the rate of decline of the IPSC (related to Figure 6-4).

Left is a plot of the time constant of decline of the IPSC against the amplitude of the IPSC. The time constant of decline in slices taken from animals expressing dLight (red) are slow compared to control animals. Right shows an example where blockade of dLight with the D1 antagonist (SKF83566, 1 µM) resulted in an increase in the decay of the IPSC (dLight expressing tau = 715±273, +SKF83566 = 415±173, n=8, mean±SD, p= 0.0005).

Chapter 7 – Heterologous interactions

Preface

This final research section consists of work that I consider the core of my dissertation with its foundations dating back to my initial qualifying exam to become a PhD candidate in my second year of graduate school. It began by asking how D2 receptor signaling recovered following desensitization, but quickly led in some unexpected directions. The first feature I uncovered was that D2 receptors desensitized not just following D2 receptor activation but to other inhibitory GPCRs as well. In exploring this heterologous desensitization, I found that co-activation of two inhibitory GPCRs led to the facilitation of GIRK currents despite desensitization.

One of the major questions I had in learning about GPCR signaling was how regulation could be specific to an individual receptor type if both receptors couple entirely to the same output systems. This work contributes to a conclusion that by-in-large, systems cross talk a lot more than I initially thought. The following manuscript is a paired down for clarity, but I present additional experiments at the end of the chapter. This version is unpublished at the time of writing this dissertation, but it is the version to be submitted to the Journal of Physiology.

It should also be noted that while my description of methods has its own chapter, I decided to move one section to this chapter instead (after the discussion section). I decided the story of facilitation would greatly benefit from modeling the proposed mechanism, but descriptions of the model and complete results were too complicated to put in a results section. Therefore, this method section also contains modeling results and a supplemental figure so I felt it should still be grouped into this chapter.

Co-activation of GPCRs facilitate GIRK-dependent current

Alec F Condon[1], Naeem Asad[2], Timothy M Dore[2], and John T Williams[1]

[1] The Vollum Institute, Oregon Health Sciences University, Portland, United States

[2] New York University Abu Dhabi, Saadiyat Island, PO Box 129188, Abu Dhabi, United Arab Emirates

Acknowledgments

This work was supported by the National Institutes of Health (RO1 DA04523 to JTW and F31 DA047007 to AFC), New York University Abu Dhabi (TMD), and the Core Technology Platform resources at New York University Abu Dhabi. We thank Drs Kim Neve, Brooks Robinson, Joseph Lebowitz, Christopher Ford, and Stephanie Gantz for insightful discussions. We also thank Julian Haft for assistance learning Mathematica and the Khaliq lab for gifting the CDNI-GABA.

[This manuscript is presented as submitted to the Journal of Physiology, Jan 2022]

Abstract

The activity of dopamine neurons is dependent on both intrinsic properties and afferent projections. One potent form of inhibition is mediated by the activation of two inhibitory G protein-coupled receptors, D2 and $GABA_B$ receptors. Each of these receptors activate G protein-coupled inwardly rectifying potassium (GIRK) channels. Recordings in brain slices have shown that co-activation using saturating concentrations of agonists results in occlusion of the GIRK current. The present study examined the interaction of agonists using transient applications of sub-saturating concentrations of agonists where the co-application of one agonist resulted in both facilitation and inhibition (desensitization) of the other. The heterologous facilitation was modeled based on the known cooperative interaction between the G protein βγ subunits and GIRK channels. The results indicate that a low tonic level of G βγ results in facilitation of GIRK current and a high level of G βγ results in occlusion. The kinetics of the current induced by transient receptor activation is prolonged in each case. The results suggest that the cooperative interaction between G βγ subunits and GIRK channels determines both the amplitude and kinetics of GPCR dependent current.

Introduction

Feedback inhibition of midbrain dopamine neurons is mediated by dendritic release of dopamine (DA) that activates D2 autoreceptors that increases a G protein-coupled inwardly rectifying potassium conductance (GIRK) (Pucak and Grace, 1995; Lacey et al, 1987; Beckstead et al., 2004). Thus, an increase in the activity of dopamine neurons results in autoinhibition that controls dopamine neuron firing (Beckstead et al., 2004). In addition to autoinhibition, local dopamine acts on presynaptic terminals to facilitate GABA release (Cameron and Williams, 1993) to activate $GABA_B$ receptors that induce inhibition through an increase in GIRK conductance (Lacey et al., 1988). The same GIRK channels are thought to mediate inhibition caused by both the D2 and $GABA_B$ receptors

based on the observation that the maximal activation of one receptor occludes the action of the second. Thus, two receptor-dependent forms of inhibition are mediated by a common mechanism: the activation of GIRK channels induced through the cooperative binding of 4 free G βγ produced by inhibitory G protein-coupled receptors (GPCRs) (Whorton and MacKinnon 2013; Wang et al., 2014; Wang et al., 2016). Despite the power of GIRK channel control of dopamine neuron activity, how D2 and $GABA_B$ receptor-dependent currents interact has not been examined. The common G βγ dependent pathway resulting in the activation of GIRK may well result in receptor interactions beyond occlusion.

The present study used whole cell recording in brain slices to examine how interactions between D2 and $GABA_B$ receptor signaling affect the D2 IPSC in the substantia nigra. The results using rapidly applied exogenous agonists show coactivation of these two receptors produces bidirectional actions, facilitation of GIRK conductance, and heterologous desensitization. Desensitization and the recovery from desensitization of the D2 receptor was similar whether it was induced by GABA or DA suggesting a shared pathway of desensitization. However, the activation of $GABA_B$ receptors also facilitated the D2 dependent current increasing the amplitude and prolonging the kinetics of current decline. Even when the combination of desensitization and occlusion suppressed the amplitude of D2 receptor-dependent current, there was a kinetic change that significantly increased total overall conductance. The properties of facilitation were consistent with predictions modeled based on the intrinsic properties of the G βγ/GIRK channel concentration response curve (Hartzell et al., 1975; Wang et al., 2014; Wang et al., 2016; Touhara and Mackinnon, 2018). The facilitation was further confirmed to include the currents induced by the synaptic release of GABA and DA. Together, results show robust interactions between D2 and $GABA_B$ signaling with contrasting facilitating and suppressing effects positioning these interactions to modulate the activity of dopamine neurons.

Results

$GABA_B$ receptor activation facilitates and suppresses D2 receptor activation of GIRK

The interactions between D2 and $GABA_B$ receptor signaling were first examined by the use of a photoactivatable dopamine (CyHQ-DA, 50 µM) (Asad et al., 2020). CyHQ-DA was recirculated and phasic D2-dependent currents (I-DA) were elicited by a flash of UV light (3.8 mW, 2.5 ms) through the objective every 60 s (Figure 7.1A). Baclofen (3 µM) was then added to the reperfusion solution to activate $GABA_B$ receptors followed by antagonism with CGP-55845 (1 µM). Several phases of interaction are observed (Figure 7.1B). First there was no consistent change in the amplitude of I-DA during the rising phase of $GABA_B$ receptor activation. The amplitude of I-DA decreased when the current induced by baclofen reached a peak. Finally, when the current induced by baclofen was blocked with that addition of CGP-55845, I-DA was significantly decreased. I-DA was normalized to the start of the experiment (1.014 ± 0.031, p= 0.4416), I-DA during the rising phase of baclofen was unchanged (1.073 ± 0.189, p=0.0001), after the peak of baclofen I-DA decreased (0.7032 ± 0.054, p= 0.0001, one-way ANOVA with Tukey's multiple comparison, n = 14) and following antagonism of the $GABA_B$ receptors I-DA declined to 40.6 ± 16.9% of baseline (n=14). Following the inhibition of the current induced by baclofen, I-DA recovered to pre-treatment amplitude over the course of about five minutes (time constant of recovery = 170 s).

The results were consistent with the presence of two competing forms of interaction between D2 and $GABA_B$ receptor activation of GIRK conductance: heterologous facilitation during simultaneous activation and a longer lasting desensitization. To confirm this interpretation of facilitation, DA was applied via iontophoretic pipette (Figure 7.1B, 1 mM in pipette, 8-15 ms, 20-50 nA, positioned 1-10 µm from soma) and evoked transient outward currents. Low concentrations of baclofen (300-600 nM) were then perfused. The result was a 34.5% increase in current response to DA (Figure 7.1, baseline mean = 76.9 ± 27.3, in baclofen mean = 103.4 ± 26.72 pA, p= 0.0003 by

paired two-tailed t-test, n=5) confirming a facilitating interaction between D2 and $GABA_B$ receptor signaling.

Heterologous desensitization regulates D2 receptor signaling

The depression and recovery of phasic D2 receptor activation of GIRK following treatment with baclofen was suggestive of heterologous desensitization. D2 receptor recovery from desensitization has not been described. To confirm heterologous desensitization, the time course of recovery from desensitization was measured using DA iontophoresis. After establishing a stable baseline response, the backing current holding dopamine in the pipette was turned off for one minute to induce a tonic level of dopamine (Figure 7.2A). The resulting outward current peaked and declined with a time constant of 38 s. Upon resumption of the backing current, the outward current returned to baseline. Following the tonic one min application of DA, the phasic current induced by pulses of DA were substantially smaller (first pulse = 55.7% ± 12.6% of pre-desensitization, n=17, Figure 7.2B). The current induced by pulses of DA recovered to pre-desensitized conditions with a time constant of 115 s. Similar results were obtained when the iontophoretic pulses of DA were paired with 60 s of GABA applied through a second iontophoretic pipette (Figure 7.2C). The first pulse of dopamine following the termination of GABA was 35.5 ± 14.5% of control (n = 8). The decrease in dopamine current induced by baclofen had a significantly greater effect than that induced by dopamine (p= 0.0017 by unpaired t-test). Despite a greater degree of desensitization, the time course of recovery of the D2 receptor dependent current following GABA was not significantly different from recovery following desensitization with DA ($GABA_B$ τ= 195 s, Figure 7.2C,D, DA τ= 115 s, Figure 7.2B,D, p=0.3329 by non-extra sum-of-squares F test). The results suggest D2 receptor activation of GIRK channels is regulated by a form of heterologous desensitization induced by either $GABA_B$ or D2 receptor activation.

A model of D2-$GABA_B$ receptor facilitation

Recent analysis of GIRK channel structure and function may provide explanation for the observed heterologous facilitation of GIRK activation (Whorton and MacKinnon 2013; Wang et al., 2014; Wang et al., 2016; Touhara and Mackinnon, 2018). Cooperative association of four G βγ molecules are necessary for activation of GIRKs. The result is an S-shaped concentration-response curve where an increase in βγ concentration at the foot of the curve produces less change in GIRK activation than the same net increase in concentration in the presence of a tonic level of βγ subunits (Figure 7.3A) (Hartzell et al., 1975). The increase in G βγ level produced by $GABA_B$ receptor activation therefore would be predicted to facilitate the response to DA by seeding or priming GIRK channels to βγ produced by D2 receptor activation. A similar facilitating interaction for is not predicted for ligand-GPCR interaction because receptors with a single ligand binding site have a different shaped concentration response curve (Figure 7.3A, green).

The predictions of the GIRK channel concentration response curve were modeled by calculating GIRK responses to phasic increases in βγ and comparing predicted currents at baseline and in high and low tonic βγ. The modeling results show that the presence of tonic GPCR activity producing standing βγ concentrations will facilitate the response to phasic pulses of βγ (Figure 7.3B "low tone" example). Furthermore, the shape of the GIRK channel response curve predicts that tonic βγ will slow the kinetics of decline of the phasic responses with larger effects at higher tonic concentrations (Figure 7.3B inset). Even when tonic concentrations are high enough that the model predicts partial occlusion of the phasic response by GIRK channel saturation (Figure 7.3B "high tone" example), the model predicts the phasic currents will be prolonged. While this model used βγ concentrations based on findings in dopamine neurons, results were replicated using a range of assumption concentrations with similar conclusions (see materials and methods for details on modeling).

These predictions of facilitation and kinetic augmentation was observed experimentally. In experiments pairing I-DA induced by photolysis and baclofen perfusion (Figure 7.1AB), the duration of D2-dependent GIRK current was significantly prolonged in the presence of baclofen (Figure 7.3C, width at 25% of peak at baseline = 1.029 ± 0.197 s, $p<0.0001$, in baclofen 1.345 ± 0.318 s, $p = 0.0037$, in CGP 1.075 ± 0.242 s, $p = 0.6356$, one-way ANOVA Tukey's multiple comparison). Kinetic shifts were observed even when the amplitude of the current was reduced due to desensitization and/or occlusion but lasted only as long as the $GABA_B$ dependent current remained.

The effects of facilitation were further confirmed by using pairs of short and long UV flashes for DA photolysis to examine different amplitude currents (Figure 7.4). With the perfusion of a low concentration of baclofen (1 μM), there was a consistent facilitation of the amplitude of the current induced by the short duration flash (short pulse baseline amplitude = 169.7 ± 30.38 pA, in bac = 215.7 ± 55.61 pA, $p = 0.0233$, paired t test, $n = 5$), but had no significant effect on larger current induced by the longer flash (long pulse baseline amplitude = 403.2 ± 100.8 pA, in bac = 401.7 ± 118.6 pA, $p = 0.9505$, paired t test, $n = 5$) (Figure 7.4). However, the kinetics of responses to both short and long duration flash were prolonged (short pulse baseline 25% width = 1.134 ± 0.3207, in bac 1.339 ± 0.4606, $p = 0.0358$ by paired t test, $n = 5$, long pulse baseline 25% width = 2.325 ± 0.8571, in bac 2.734 ± 1.047, $p = 0.0296$ by paired t test, $n = 5$). These results were consistent with the model that predicted that the facilitation of amplitude can saturate while changes in kinetics remain.

Facilitation modulates endogenous release

The experimental and modeling results showed robust facilitation of GIRK currents in both amplitude and duration, but saturation of GIRK channels or G protein saturation might reduce the relevance of heterologous facilitation to endogenous signaling. To test if the D2 receptor IPSC can

participate in heterologous facilitation, electrical stimulation was used to induce an IPSC and was paired with photolysis of caged DA or caged GABA. Electrical stimulation in the substantia nigra elicits release of both GABA and dopamine and the D2 IPSC is normally isolated pharmacologically (Beckstead et al., 2004). To probe the interactions between receptor types, $GABA_B$ receptors were not blocked such that electrical stimulation evoked a hybrid D2/$GABA_B$ IPSC (Figure 7.5B). The two components have different kinetics with $GABA_B$ IPSC peaks first followed by the D2 IPSC ($GABA_B$ peak location 135 ± 30 ms vs D2 380 ± 50 ms, $p > 0.0001$, unpaired t test, n = 5 and 6 respectively) (Figure 7.5A). A train of three flashes (10 Hz, 0.2 mW, 5 ms, 125 ms after electrical stimulations) was used to photolyze CDNI-GABA (50 μM) and produce a prolonged sub-saturating concentration of GABA to look for interactions with endogenous release. In each experiment, the stimulus was sequentially rotated between electrical stimulation alone, photolysis alone, and combined stimulation + photolysis with the specific order varied between cells (Figure 7.5B). The resulting currents were averaged in each condition ($n \geq 3$) to produce a single experimental replicate. The current generated from photolysis alone was subtracted from the combined stimulation + photolysis response to test the degree of linearity in signaling (Figure 7.5CD). If the currents induced by photolysis and stimulation occlude, then the calculated current generated from subtracting the photolysis response from the combined stimulation + photolysis current would be smaller than the current induced by stimulation alone. If the currents have no interaction, the calculated current should match the current induced by stimulation alone. Facilitation would result in a subtracted current that is larger than that induced by the stimulation alone.

The results show a ~20% enhancement of the IPSC as measured by total charge transfer (integral of the current, Figure 7.5DE; raw charge transfers of 25.7 ± 7.9 and 31.1 ± 8.0 pA*S for baseline and calculated IPSCs respectively, $p = 0.0065$ by two-way ANOVA Sidak's multiple comparison, n=6). To test if synaptically released GABA acting on $GABA_B$ receptors can participate in facilitation, the parallel experiment of uncaging DA on the hybrid ISPC was performed (uncaging

shifted forward to overlap with the $GABA_B$ portion of the hybrid IPSC). This manipulation had a biphasic effect on the amplitude (Figure 7.5D right). The early $GABA_B$ dominated portion was facilitated and the later dopamine dominated current was occluded. Both results are consistent with the model. The combination of the $GABA_B$ IPSC facilitating exogenous dopamine yet occlusion between exogenous and synaptic dopamine meant total charge transfer of the hybrid IPSC vs calculated/subtracted IPSC was not significantly different from baseline (Figure 7.5E; raw charge transfers of 19.0 ± 5.3 and 20.1 ± 3.9 pA*S for baseline and calculated IPSCs respectively, p = 0.7219 by two-way ANOVA Sidak's multiple comparison, n=6). These experiments confirm that $GABA_B$ and D2 receptors activated by endogenous release can both participate in heterologous facilitation.

Discussion

The results of this study show a rich interplay between D2 and $GABA_B$ receptor signaling through the activation of GIRK conductance. D2 dependent GIRK currents desensitized with the activation of both D2 or $GABA_B$ receptors, yet coincident activation facilitated even desensitized responses (Figure 7.1). Cross regulation between these two receptor types is functionally relevant due to the powerful control that GIRK channels have over dopamine neuron activity (Lacey et al., 1987; Lacey et al., 1988; Beckstead et al., 2004; Gantz et al., 2013; Evens et al., 2017; Gantz et al., 2018; Evens et al., 2020). Neuron firing can be silenced by exogenous application of either $GABA_B$ or D2 receptor agonists and both evoked and spontaneous DA release pause the pacemaker activity of dopamine neurons. Though current amplitudes are relatively small compared to those passed by ligand-gated channels such as AMPA receptors, the long duration of signals means the total charge transfer from GIRK channels is large. Beyond simple inhibition, these large GIRK currents can hyperpolarize neurons to the point of rebound firing in neurons expressing T-type calcium channels (Evens et al., 2017; Evens et al., 2020). Yet results of the present study showed that control of the magnitude of D2-dependent GIRK responses is as much dependent on GABA as DA itself as GABA

alone was able to suppress the response to phasic DA by as much as 65% (Figure 7.2, phasic responses ~35% of pre-desensitized control). On the other hand, low concentrations of baclofen facilitated the response to phasic dopamine by as much as 35% meaning that the response to the same DA stimulus might vary as much as 4-fold depending on context in GABA. Thus, extracellular measures of DA concentration are only loosely correlated with strength of post-synaptic response.

Heterologous facilitation of GIRK currents not only affects peak amplitude and kinetics, but what concentrations of DA meaningfully contribute to cellular computation. The amplitude of the D2 receptor IPSC is defined by high concentrations of DA acting on receptors within a few µm of the release site (Condon et al., 2021) but lower concentrations of DA "spill over" in a larger volume and extends the duration of current decay. This suggests that while such spillover transmission may have minimal effect on neuronal excitability on its own, both proximal and spillover dopamine transmission can participate in heterologous facilitation, act as inhibitory coincidence detectors with $GABA_B$ transmission, and make neuronal behavior such as T-type calcium channel dependent rebound firing more likely by increased strength of hyperpolarization (Evens et al., 2020).

This facilitation by intrinsic shape of the G βγ/GIRK channel concentration response curve not only has implications for increasing amplitude of responses, but for how much regulation is needed to suppress responses during desensitization. As seen with facilitation, GIRK channels can be sensitized by relatively small changes in G βγ concentration, but the inverse relationship is also true. For example, the steep slope of the curve at low concentrations means that a phasic pulse producing a peak concentration of 110 µM will produce almost double the peak amplitude of a phasic pulse producing 80 µM. In this range, a 30% reduction in G protein production would lead to a 50% reduction in current. Thus, relatively little regulation is needed to desensitize responses. The exact G βγ concentrations involved in D2 receptor signaling are unknown, but measurements using Na^+

dependent shifts in G βγ-GIRK affinity have suggested maximal $GABA_B$ receptor activation produces several hundred μM G βγ (Wang et al., 2016).

The mechanisms for heterologous desensitization are unclear. Heterologous regulation of GPCRs is common, but this heterologous desensitization of D2 receptor signaling is surprising as $GABA_B$ and D2 receptor currents have been extensively studied using bath perfusion of agonists and this cross regulation has not previously been reported (Lacey et al., 1988; Beckstead and Williams, 2007; Perra et al., 2011; Gantz et al., 2016; Robinson et al., 2017a; Robinson et al., 2017b). It is likely that the rapid rate of recovery (Figure 7.1 and 7.2) masked these interactions. Desensitization of comparable μ-opioid receptors in locus coeruleus neurons recover over the course of ~30 minutes (Quillinan et al., 2011, Arttamangkul et al., 2012) versus the ~5 minutes observed here with D2 receptors. However, recovery rate appears to be consistent with the means of desensitization. μ-opioid receptors have been found to desensitize by canonical homologous desensitization involving phosphorylation by G protein receptor kinase (GRK) and receptor internalization (Reviewed in Williams et al., 2013). In contrast, D2 receptors are resistant to trafficking following desensitization (Robinson et al., 2017a) and results from this present study showed that desensitization was heterologous which may be a more easily reversable process than trafficking (Zhang and Kim, 2017). There are numerous possible mechanisms for heterologous desensitization. Beyond phosphorylation, GRKs can sterically block receptor coupling to G proteins (Kanaid et al., 2007) or it can sequester G βγ by binding with higher affinity than GIRK channels (Raveh et al., 2010). KCTD 12 has been found to associate with $GABA_B$ receptors and similarly desensitizes signaling by G βγ sequestration (Schwenk et al., 2010; Turecek et al., 2014; Zheng et al., 2019). RGS proteins in dopamine neurons have also been suggested to play a role in downregulating $GABA_B$-GIRK coupling (Labouèbe et al., 2007). Regardless of the specific mechanism, the functional results of this study show that acute desensitization and recovery are poised to play homeostatic roles in normal dopamine neuron transmission.

The translation of these findings to other neuronal systems will depend on factors such as spatial relationships between receptor types and the specific effector system involved. Heterologous interactions between GPCRs can be blocked by localization to protected membrane compartments such as lipid rafts (Cui et al 2010). However, given the degree of mobility of G proteins (Sungkaworn et al., 2017), unless some feature specifically separates GPCR systems, the resulting pools of activated G proteins are expected to overlap and interact. The level of heterologous facilitation will also be dependent on the concentration response curve of the effector involved based on the affinities and cooperativity. The multiple cooperative binding sites on a GIRK channel accentuates the facilitation effect (Whorton et al., 2013, Wang et al., 2016), but even changing the subunit composition would be expected to change facilitation. GIRK1 has a higher affinity for G βγ than channels composed entirely of GIRK2/3 subunits as found in dopamine neurons (Touhara et al., 2016; Beckstead et al., 2004). With higher affinities, channel saturation becomes more likely and overlapping pools of G βγ may become less important for maximal response. Effector systems with a single binding site will likely not demonstrate this facilitating effect intrinsic to their concentration response curve, but non-linear heterologous effects when using more physiological-like modes of agonist application are still possible.

The findings of this study highlight that a rational modeling approach can be used to probe mechanisms of GPCR activation. With the current trend of considering biased agonists as potential solutions to the opioid epidemic (Herenbrink et al., 2016), more quantitative understandings of GPCR-effector coupling may be critical in translating theory to therapy. Despite the development of powerful fluorescent optical sensors which enable fine-detail measurements of extracellular DA concentrations (Patriarchi et al., 2018, Sun et al., 2018), the complexity of GPCR signaling means that quantitative translations between DA concentration to effector response is still difficult. By refining models of signaling to mimic those that exist for ionotropic receptors and voltage-gated channels, this gap can be bridged.

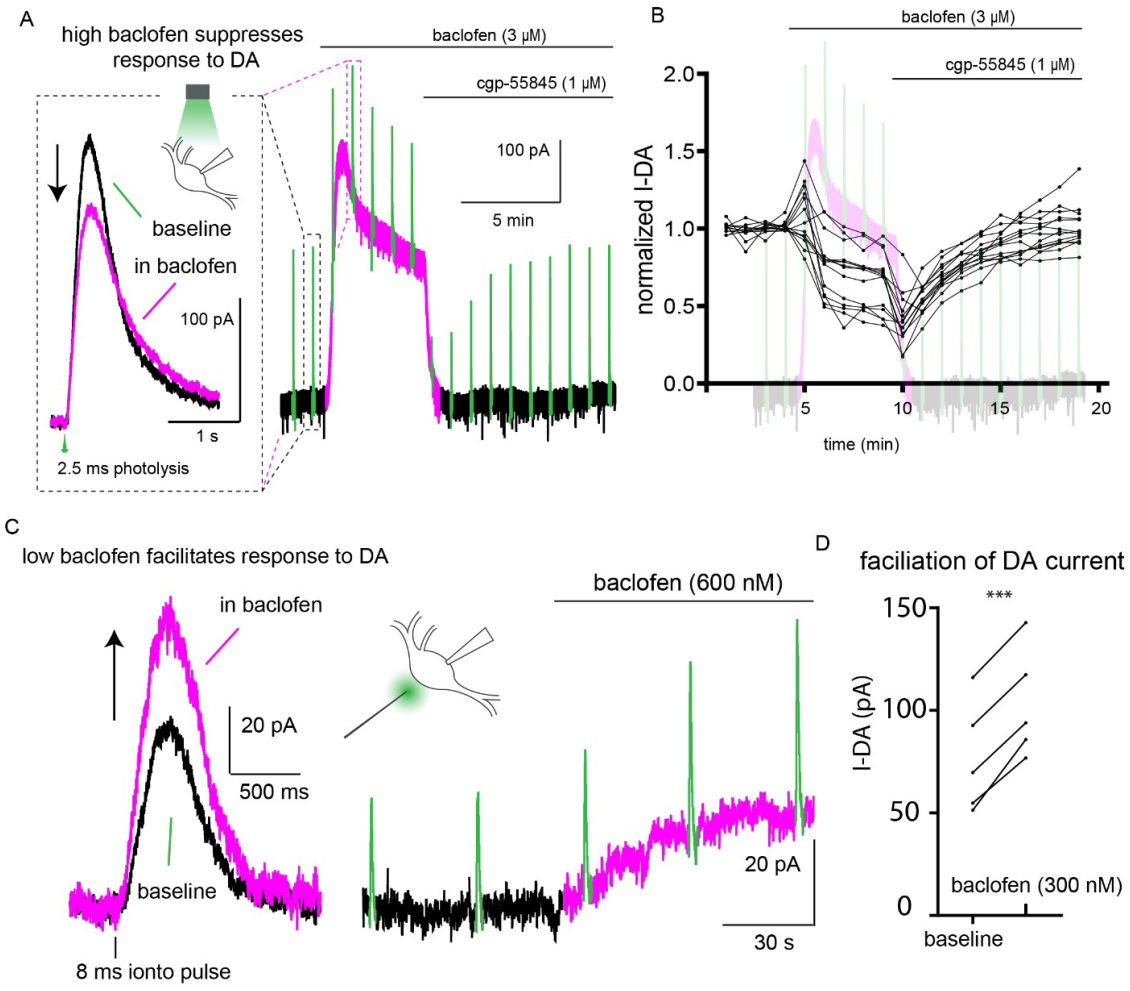

Figure 7-1 $GABA_B$ receptor activation contextually suppresses or facilitates D2 receptor activation of GIRK.

A) Example experiment using photoactivatable DA (CyHQ-DA) and baclofen perfusion. On zoomed traces, baseline D2 phasic currents are in black while D2 currents in the presence of baclofen are in magenta. For complete experiments, D2-dependent currents are pseudocolored green and $GABA_B$ dependent currents pseudocolored magenta. Left- Zoom of individual full-field UV flashes to elicit D2-receptor dependent phasic currents at baseline and in baclofen. Right- Example full experiment. B) Group data showing effects of high baclofen on the amplitude of phasic DA as normalized to pre-baclofen baseline (amplitudes of DA response for the pulse prior to baclofen, during the rising phase of baclofen, and after the peak of baclofen are 1.014 ± 0.031, 1.073 ± 0.189, and 0.7032 ± 0.054 respectively. Prior vs rising bac p = 0.4416, prior vs after peak bac p = 0.0001, and rising bac vs after peak bac p < 0001 by one-way ANOVA with Tukey's multiple comparison, n = 14) C) Example experiments showing the facilitating effects of combining low concentrations of baclofen and phasic

DA pulses. Left- Zoom on individual responses to iontophoretically applied DA at baseline and in low baclofen. Right- Example experiment showing the current produced by low baclofen and facilitation of D2-dependent GIRK current. D) Group data showing amplitudes of responses to iontophoretically applied DA at baseline and in low baclofen (baseline mean vs baclofen mean = 76.9 ± 27.3 vs 103.4 ± 26.72 pA respectively, p= 0.0003 by paired two-tailed t-test, n=5)

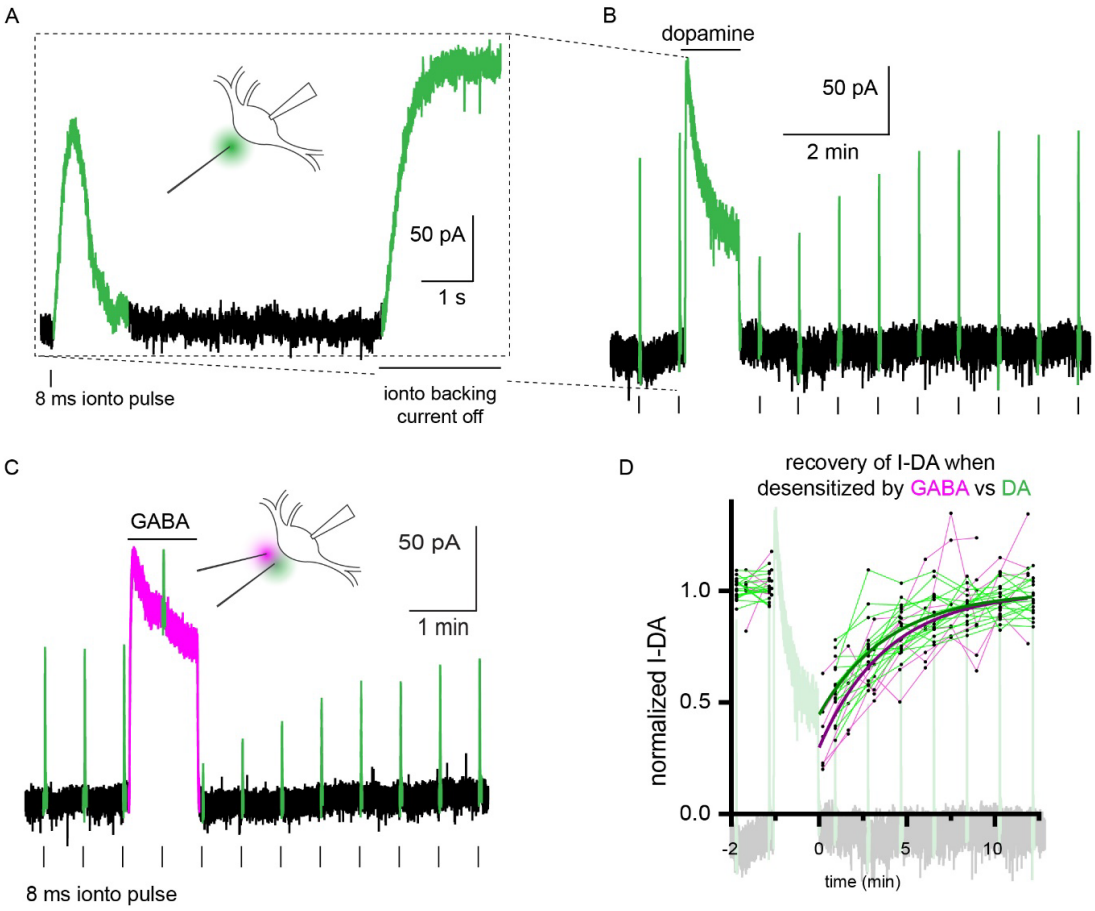

Figure 7-2 D2 receptors are sensitive to heterologous desensitization.

A) Diagram of experimental set up. Cartoon neuron and iontophoretic pipette showing standard positions for these experiments. The iontophoretic pipette is used to apply agonist in two different modes: phasic current ejections to monitor receptor sensitivity and prolonged desensitizing applications produced by allowing agonist to freely diffuse out of the pipette. D2-dependent currents are pseudocolored green. B) example experiment showing baseline dopamine pulses, desensitizing application, and recovery of phasic responses over time. C) Example experiment showing phasic D2 currents and desensitizing $GABA_B$ current (pseudocolored magenta). D) group data comparing recovery curves following desensitization with DA (green) versus GABA (magenta). Solid lines are single exponential fits of recovery. Recovery rates are not significantly different (Recovery rates= 195 and 115 s for recovery following desensitization with GABA or DA respectively. P= 0.3329, n=7 and 17).

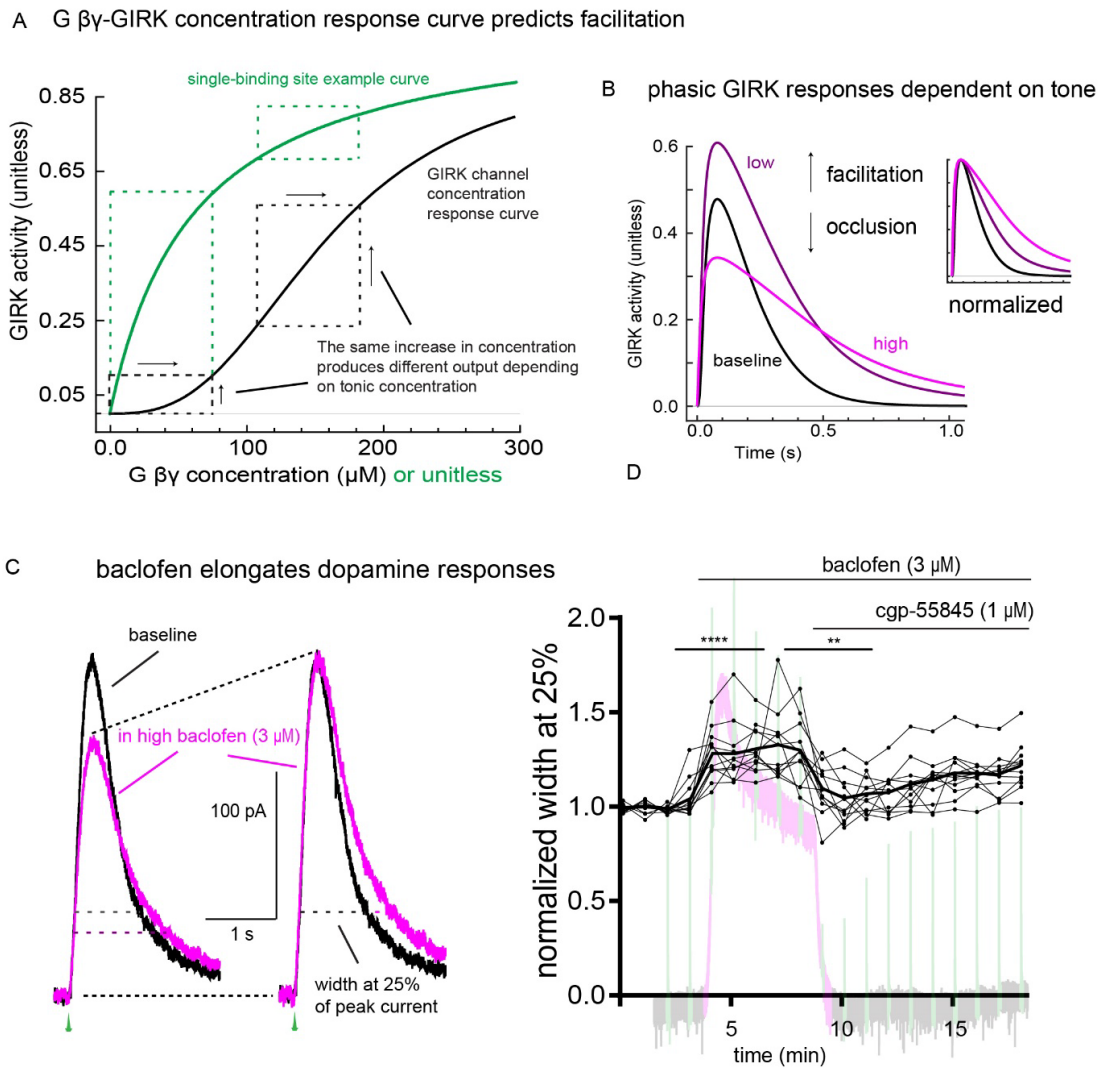

Figure 7-3 The G βγ-GIRK channel concentration response curve predicts facilitation of amplitude and kinetic shifts.

A) Diagram showing the effects of GIRK channel concentration curve (in 20 mM Na^+) compared to an example concentration response curve for a receptor-ligand interaction with a single binding site. GIRK channels require four bound βγ molecules to open it is insensitive to lower concentrations but each additional subunit binding increases affinity. Therefore, the same increase in βγ concentrations will produce smaller increases at baseline conditions versus when seeded with tonic concentrations of βγ. In contrast, ligand-receptor interactions for receptors with a single binding site (such as D2 receptors) quickly saturate and the relationship is inverse such that tonic concentrations reduce the sensitivity to the same increase in agonist concentration. B) Results of modeling a phasic rise and fall of βγ concentration passed through the GIRK channel concentration response curve. The same shape

of βγ concentration is then passed through the concentration response curve when simulated in high and low concentrations of tone. Responses are facilitated in low tone but saturation of the GIRK channel predicts occlusion in high tone. The inset depicted currents normalized to show predicted effects on kinetics where responses are slowed the higher the concentration of tone. C) Effects of tone on the kinetics of D2 receptor dependent currents. The experiments from Figure 1 are reanalyzed to measure kinetics of responses as measured by duration at 25% of peak amplitude at baseline and in high baclofen (3 μM). Left- Zoom on individual responses and same responses normalized to highlight kinetic change. High concentrations of baclofen produce predicted elongation of kinetics. Right- Group data showing the effect of baclofen on kinetics. Averaging response kinetics at baseline, during baclofen, and during recovery show significant augmentation of kinetics present only while the baclofen-dependent current remains (width at 25% of peak at baseline = 1.029 ± 0.197 s, in baclofen 1.345 ± 0.318 s, in CGP 1.075 ± 0.242 s, baseline vs baclofen $p<0.0001$, baclofen vs CGP $p = 0.0037$, baseline vs CGP $p = 0.6356$, one-way ANOVA Tukey's multiple comparison).

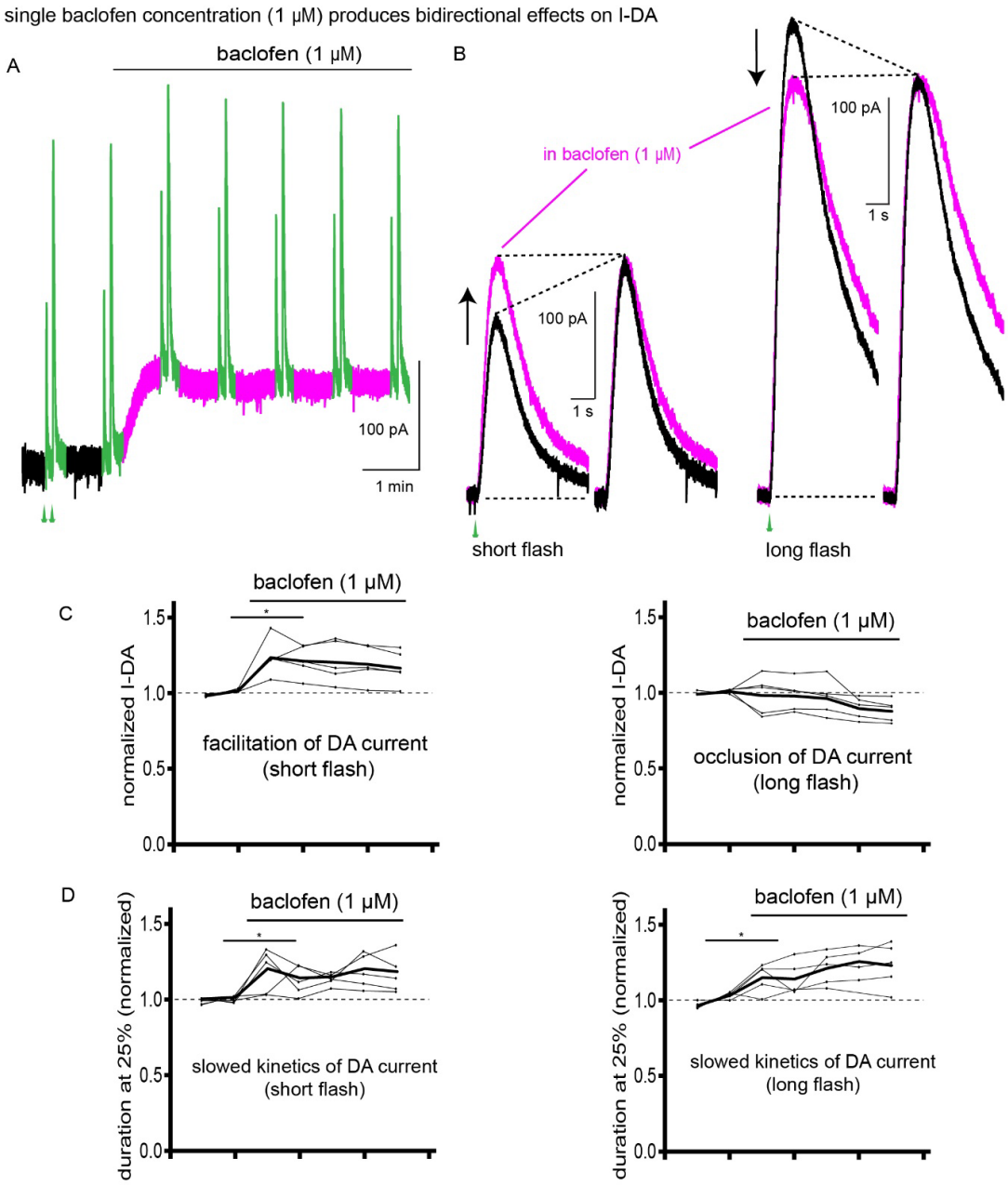

Figure 7-4 Facilitation can saturate, but kinetic shifts remain.

A) Example trace showing experimental setup. Short and long UV flashes were used to release DA and elicit small and large D2-dependent currents. A sub EC50 concentration of baclofen was then perfused on to the slice and the effects on small versus large DA currents were measured. D2-dependent currents are pseudocolored green and $GABA_B$ dependent currents pseudocolored magenta. B) Zoom on example phasic response at baseline and in baclofen. Left- Responses to short flashes of UV are facilitated in baclofen and kinetics are elongated. Right- Responses to long flashes

of UV show a mix of depression, facilitation, or no change in amplitude, but kinetics were augmented. Baseline D2 phasic currents are in black while D2 currents in the presence of baclofen are in magenta. C) Group data showing amplitude over time as baclofen is applied. Left- normalized amplitude of responses to short pulses (short pulse baseline amplitude = 169.7 ± 30.38 pA, in bac = 215.7 ± 55.61 pA, p = 0.0233, paired t test, n = 5). Right- normalized amplitude of responses to long pulses (long pulse baseline amplitude = 403.2 ± 100.8 pA, in bac = 401.7 ± 118.6 pA, p = 0.9505, paired t test, n = 5). D) Group data showing kinetic shift as baclofen is applied. Left- normalized width at 25% of peak current for responses to short pulses (short pulse baseline 25% width = 1.134 ± 0.3207 s, in bac 1.339 ± 0.4606 s, p = 0.0358 by paired t test, n = 5). Right- normalized width at 25% of peak current for responses to long pulses (long pulse baseline 25% width = 2.325 ± 0.8571 s, in bac 2.734 ± 1.047 s, p = 0.0296 by paired t test, n = 5).

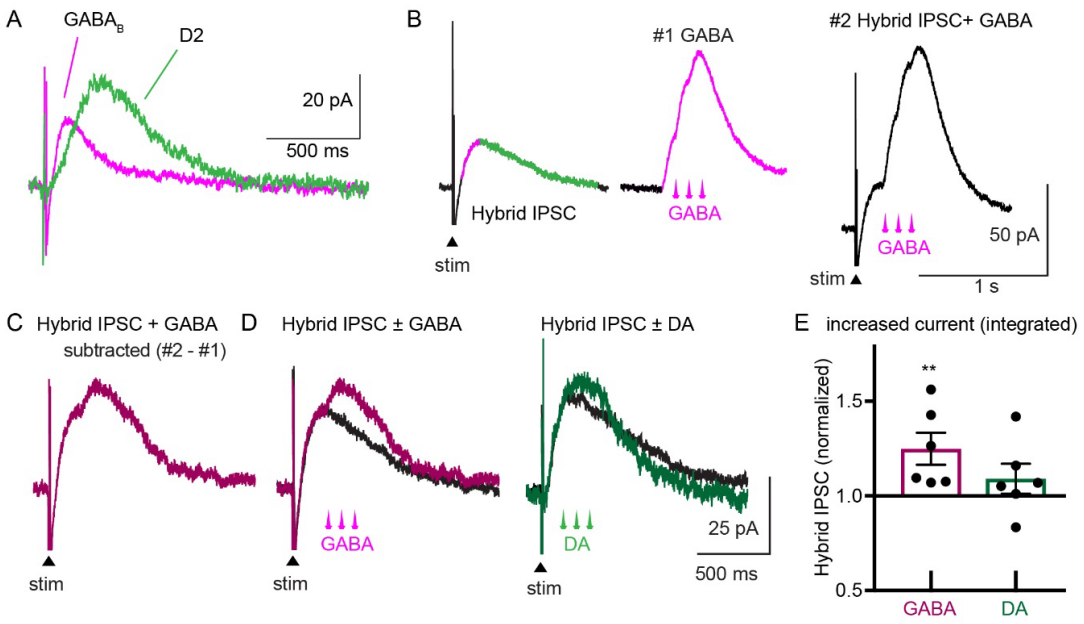

Figure 7-5 Currents generated from vesicular release can participate in heterologous facilitation.

A) Comparison of isolated D2 and $GABA_B$ IPSCs. B) Averaged traces from a single experiment showing a hybrid D2/$GABA_B$ receptor IPSC, a train of GABA photolysis, and photolysis coincident with a hybrid IPSC. Qualitative time course of $GABA_B$ and D2 receptor dominating currents respectively pseudocolored magenta and green. C) Example trace generated from subtracting the photolysis only response (trace #1 in B) from the combined IPSC + photolysis (trace #2 in B). D) Left- Example comparison of baseline IPSC (black) and calculated IPSC (dark magenta, shown in C) to measure facilitation induced by GABA photolysis on the IPSC. Right- Example comparison of baseline IPSC (black) and calculated IPSC (dark green) to measure facilitation induced by dopamine photolysis on the IPSC (note: photolysis time shifted forward to overlap with the $GABA_B$ dominated portion of the hybrid IPSC). The first part of this current ($GABA_B$ dominated region) was consistently facilitated whereas the latter (dopamine dominated) was consistently occluded. E) Group data for the experiments show in D with each cell representing a single N. The integral of each calculated current was quantified as a measure of total charge transfer and normalized to the same cell (GABA photolysis: raw charge transfers of 25.7 ± 7.9 and 31.1 ± 8.0 pA*S for baseline and calculated IPSCs respectively. p = 0.0065 by two-way ANOVA Sidak's multiple comparison, n=6; raw charge transfers of 19.0 ± 5.3 and 20.1 ± 3.9 pA*S for baseline and calculated IPSCs respectively, p = 0.7219 by two-way ANOVA Sidak's multiple comparison, n=6).

Kinetic simulations of G βγ concentrations and interaction with GIRK

The equations and starting conditions for kinetic simulations were reproduced from Tauhara and MacKinnon 2018 and the G βγ-GIRK concentration response curve was modified from Wang et al 2016.

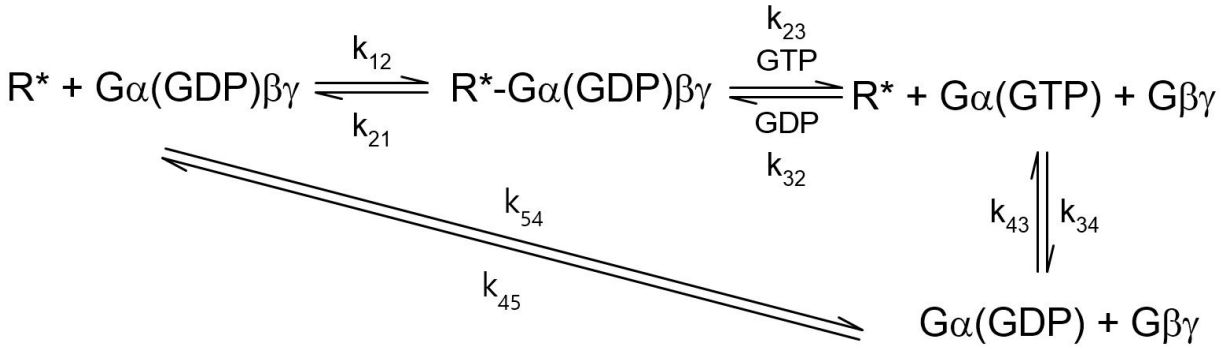

Supplemental Table 7-1 G protein cycle reactions and rates used to model GPRC-GIRK interactions

Reaction	Forward-rate	Backward-rate
R* + Gα(GDP)βγ ⇌ R*-Gα(GDP)βγ	k_{12}: 1 μM^{-1} sec^{-1}	k_{21}: 1 sec^{-1}
R*-Gα(GDP)βγ ⇌ R* + Gα(GTP) + Gβγ	k_{23}: 1 sec^{-1}	k_{23}: assumed irreversible
R* + Gα(GTP) + Gβγ ⇌ Gα(GDP) + Gβγ	k_{34}: 2 sec^{-1}	k_{43}: assumed irreversible
Gα(GDP) + Gβγ ⇌ Gα(GDP)βγ	k_{45}: 0.7x10^6 M^{-1} sec^{-1}	k_{54}: 0.002 sec^{-1}

The equations for change over time as a function of reactant concentration and rates were schematized in Mathematica and NDSolve was used to solve for reactant concentrations over time. The initial concentrations used for analysis in Tauhara and MacKinnon 2018 used receptor and heterotrimeric G proteins were concentrations of 10 and 20 μM, respectively. For the purposes of simulating phasic GPCR activation, receptor concentration was changed from static to a falling concentration with a time constant equal to dopamine concentration decay follow dendrodendritic release in the nigra (τ=223 ms, Supplemental Figure 7.1) as measured by dLight (Condon et al, 2021).

As the G βγ-GIRK binding reaction is thought to be diffusion limited, this interaction was simplified and predicted GIRK activity was simulated merely by passing the G βγ concentrations through the GIRK concentration response curve (Wang et al, 2016). It should be noted that the affinity of G βγ for GIRK2/3 channels is not static. To gate the channel requires the coordinated actions of Na^+ ions, phosphatidylinositol 4,5-bisphosphate (PIP2), and G βγ with each additional molecule increasing the affinity of others by stabilizing the open conformation and thermodynamic linkage (Wang et al, 2016). This affect also increases the maximal conductance of the GIRK channels. For the purposes of simulating G βγ-GIRK interactions in this context, PIP2 concentrations are assumed to be static, matching the conditions of Wang et al 2016, and sodium concentration set to be that used in the internal solution of the recording pipette, 20 mM. Note, it is also worth mentioning that both works discussed here from the MacKinnon lab, Wang et al 2016 and Taurara et al 2018, convert 2D protein density in the membrane to 3D concentration close to the membrane by multiplying by a linear distance into the cytoplasm equal to the length of G βγ. These two papers use slightly different assumptions of this multiplier, so calculations from Wang et al 2016 are here converted into the distances used by Tauhara and MacKinnon 2018 (70 vs 80 Å). As described in the results sections, the concentrations of G βγ produced using a phasic pulse under these initial assumptions are relatively low, so if these concentrations were accurate to a dopamine neuron, tonic G βγ concentrations produced by low-level $GABA_B$ receptor activation would also be low. To simulate tone in a normalized fashion, low tonic G βγ was set to be equal to 30% and high tone equal to 100% of the peak concentration and from the associated phasic pulse in each condition (Supplemental Figure 7.1A-D). As can be seen, this addition passed through the GIRK concentration-response curve does indeed show facilitation, however the level of facilitation is much greater than observed in dopamine neurons so already this first set of assumptions does not seem accurate to dopamine neurons.

To move beyond the set of assumptions from Tauhara et al 2018, which was attempting to model GPCR activation in CHO cells, conditions may be quite different in a dopamine neuron, that

natively uses GPCR-GIRK signaling. Whereas their set of assumptions produces a standing concentration of G βγ maxing out at ~5 μM, previous work from the MacKinnon lab gave estimates of G βγ concentrations in dopamine neurons produced by maximal $GABA_B$ activation equal to 245 μM (280 μM as published but converted from 70 to 80 Å assumption of linear distance into the cytoplasm). Clearly, this concentration is much higher than would be possible with the base assumptions of receptor concentrations of 10 μM and G protein concentrations of 20 μM.

For the next set of assumptions attempting to match conditions in dopamine neurons, both receptor and G protein concentration must be increased. Only increasing one reactant makes the other rate limiting such that the system cannot approach the 245 μM G βγ measured in dopamine neurons. Precise measurements of surface D2 or $GABA_B$ receptor density are not available, but detailed measurements of $GABA_B$ receptor density have been made with freeze-fracture EM for Purkinje neurons, another neuronal subtype where $GABA_B$ activation is coupled to GIRK channels (Luján et al, 2018). Here, authors give two density measurements, one for overall compartment-specific densities, and one for compartment-specific cluster densities. Tauhara and MacKinnon (2018) used the assumption that overall receptor density is concentrated into 10% of the membrane based on the previous observation that single-particle GPCR-G protein interaction happens in membrane hotspots equal to about 10% of the membrane, even in non-specialized cells (Sungkaworn et al 2017). It is notable that the density estimates given by freeze fracture gold-particle labeling of $GABA_B$ receptor clusters vs total membrane are in reasonable agreement with this 10% hypothesis, though there is an effect of cluster size on density. $GABA_B$ receptor density in spines was found to be 227.62 μM^{-1} or 2276.2 μM^{-1} cluster density by the 10% membrane hypothesis or 455.2 μM based on the Tauhara and MacKinnon (2018) conversions of membrane density to concentration at the membrane. Therefore, for the next model, initial receptor concentration was simplified to 500 μM and G protein concentration was set at 600 μM (Supplemental Figure 7.1E-H). With these conditions, G protein concentration peaks at ~55 μM. The same interactions with tonic G

βγ can be seen here with facilitation of the amplitude and duration of GIRK response. This model of receptor activation starts with full receptor occupancy that decays, which nicely mimics what would be expected with a strong pulse of dopamine photorelease. Given comparison to real data, this set of assumptions still does not produce a high enough concentration of G βγ if max $GABA_B$ response produces 245 μM G βγ. The high tone condition also results in more facilitation than low tone, which is a potential contrast to experimental data which shows the facilitation effect on amplitude can saturate.

For the final model (Figure 7.3 and Supplemental Figure 7.1 I-L), initial receptor and G protein concentrations are kept at 500 and 600 μM, but reaction rates are increased. Critical rates complied and used by Tauhara and MacKinnon (2018) were measured at room rather than physiological temperatures. Rather than attempting to accurately guess the temperature sensitivity of each reaction, the forward reaction rate of G protein-receptor binding (k_{12}), GDP-GTP exchange (k_{23}), and G protein GTPase activity (k_{34}) were all multiplied by 10. This results in similar equilibrium concentrations, but equilibrium is reached much faster and the simulated response to the phasic receptor activation is much higher (peak of ~160 μM). The specific numbers and assumptions for each of these models are certainly wrong, but in every case, the models predict facilitation of GIRK current amplitude and prolongation of decay times, and this final model additionally predicts saturation of facilitation of amplitude.

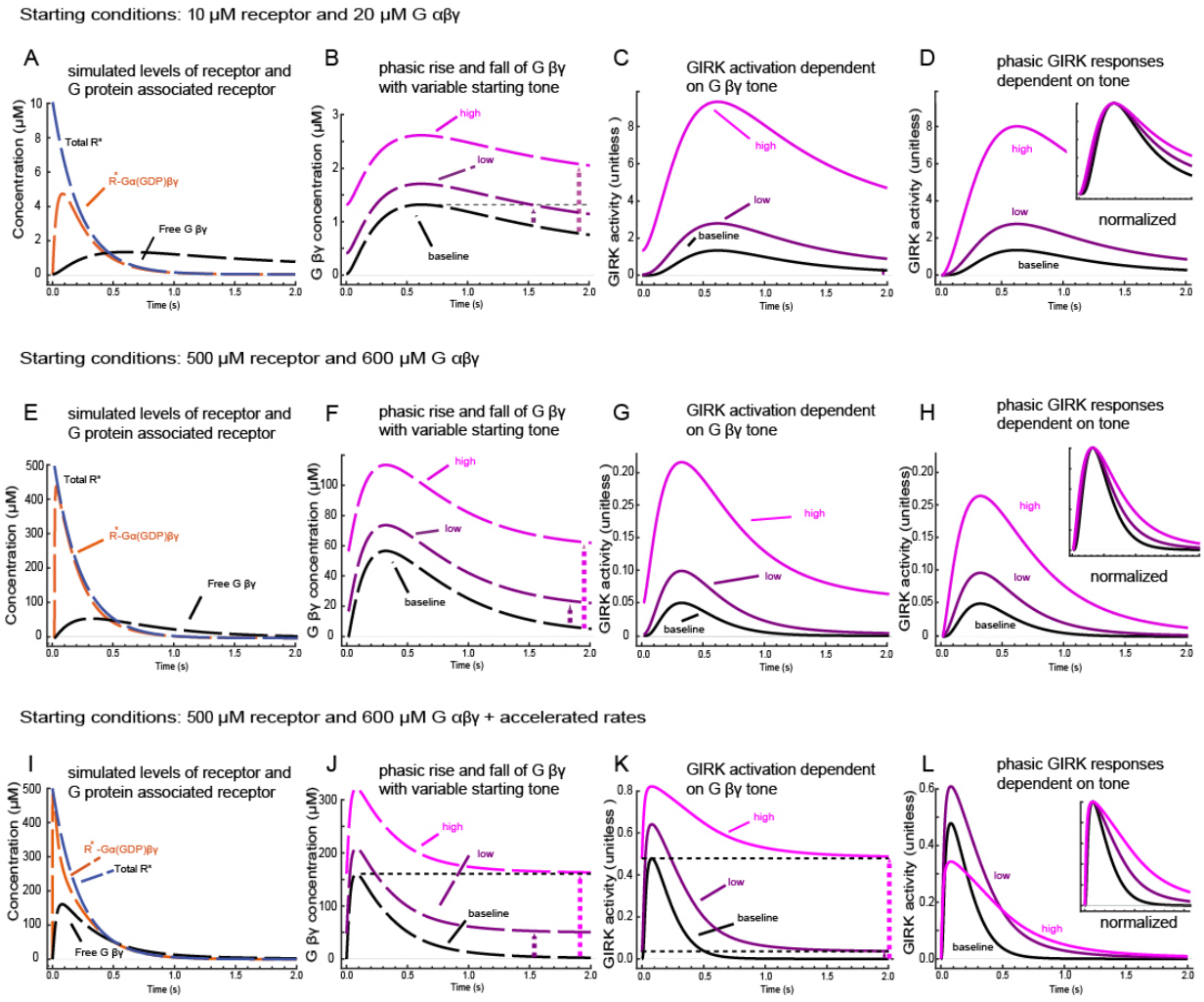

Supplemental Figure 7-1 Models of tonic and phasic G protein-GIRK interactions

A-D) Conservative model of G protein-GIRK interactions with starting assumption conditions of 10 µM receptor and 20 µM G protein. A) Solution to kinetic equations (Table 1) for a falling concentration of active receptor from a peak of 10 µM. All reaction components were solved, but only the input total active receptor (Total R*), active receptor in complex with G αβγ, and free G βγ are shown for clarity. B) Conditions of high and low tonic G βγ were simulated by adding a static concentration of tonic G βγ to phasic G βγ concentrations generated in A. The amount of simulated βγ added in low and high tone conditions were 30% and 100% of peak phasic concentrations respectively. C) Phasic concentrations in B are passed through the βγ-GIRK concentration response curve (Fig 3A) to show predicted responses. D) The current generated from tonic G βγ was subtracted out to isolate the phasic currents and demonstrate predictions of facilitation. Inset shows

simulated currents normalized to the peak to show kinetic shifts. E-F) Second model of G protein-GIRK interactions with starting assumption conditions of 500 μM receptor and 600 μM G protein. Individual panel descriptions the same as for A-D. I-L) Final model of G protein-GIRK interactions with starting assumption conditions of 500 μM receptor and 600 μM G protein and accelerated reaction rates. Individual panel descriptions the same as for A-D. The results from panel L are shown in Fig 3B.

Additional experiments

There are a several experiments regarding heterologous facilitation and desensitization that didn't make it into this manuscript essentially for being too complicated to discuss. The first experiment that led to my exploration of heterologous interactions came directly from Katz and Thesleff (1957), the paper that was essentially the first to describe the general principle of receptor desensitization. They showed that acetylcholine receptors not only desensitized to high concentrations, but to low concentrations as well. I was asked about this in one of my first meetings with my committee. This sort of behavior is not typical for GPCRs, so I thought I would see negative data, but tried it none-the-less. Initial experiments with perfusing low concentrations of dopamine during dopamine iontophoresis were inconclusive due to slow kinetics of was on and potential occlusion effects. To provide a rapidly reversable source of low dopamine, I used a second iontophoretic pipette to apply dopamine from a much farther distance. Turning off the backing current on this secondary pipette allowed for application of an unknown, but qualitatively lower concentration of dopamine as compared to phasic test pulses (Figure 7-6). After an initial rising phase in this secondary current, dopamine concentration reached equilibrium and produced a small standing outward current that was about 20% of that induced by the phasic pulses (Average ratio of BC-off current over phasic pulse = 0.21 ± 0.02 SEM). This application of low dopamine concentration was sufficient to desensitize the D2 response to the phasic pulses (Figure 7-6B, phasic pulses measured without including the tonic current), if at a slower rate (τ of declining phasic pulses = 59 s vs τ of declining desensitizing pulse in Figure 1 = 38 s).

After these unexpected findings, I tested if other unexpected sources could desensitize D2 responses. These experiments led to the experiments included in the main portion of this chapter showing $GABA_B$ activation both facilitates and desensitizes D2 responses. However, the facilitation made it more difficult to confirm that low levels of $GABA_B$ receptor activation could desensitize D2

responses. To isolate the extent of desensitization despite facilitation, slices were perfused with baclofen (500 nM) ~10-15 minutes prior to starting the transient application dopamine by iontophoresis. After establishing a stable outward current induced by dopamine in the continued presence of baclofen, the $GABA_B$ receptors were antagonized using CGP-55845 (300 nM). The change in amplitude of the transient currents induced by dopamine was distinctly biphasic (Figure 7-6CD). As the $GABA_B$-dependent current returned to baseline, the current induced by dopamine became smaller. After the initial depression, the D2-dependent current increased over the course of several minutes. The results are consistent with an initial loss of facilitation followed by recovery from desensitization as seen in the previous experiments. The results suggest the heterologous desensitization of D2 receptors is induced by modest receptor activation of either $GABA_B$ or D2 receptors

Next, I included experiments where I uncage GABA or dopamine onto a hybrid IPSC, but the obvious follow up experiments would be to uncage on isolated D2 or $GABA_B$ IPSCs. Figure 7.7 depicts the full cross comparison of conditions which repeats those included in the above manuscript. When I uncaged dopamine on an isolated D2 IPSC, the results were expected sublinear addition (Figure 7.7 C,F). However, when I uncaged GABA on an isolated $GABA_B$ IPSC, I again saw enhancement of the synaptic response (Figure 7.7 A,F). This result does not necessarily detract from the results of uncaging GABA on a hybrid IPSC. The $GABA_B$ IPSC was so small (Figure 7.7G) that the result of $GABA_B$-$GABA_B$ facilitation a 25% enhancement of integrated current equaling less than 2 pA*s would not significantly enhance the much larger hybrid IPSC. Therefore, heterologous enhancement of the hybrid IPSC must still be due to cross D2 and $GABA_B$ interactions.

As for the reasons, my immediate hypothesis was that the relevant pools of activated receptors were responsible for this enhancement. With the D2 IPSC, Chapter 6 shows that dopamine release will activate receptors over a region of several microns. That means exogenous dopamine

will activate the same pool of receptors as the IPSC. In contrast, it has been suggested that $GABA_B$ inputs to dopamine neurons are more point-to-point (Edwards et al., 2017) in addition to evidence in other neurons as to the specific nature of GABA transmission (Isaacson et al., 1993). This observation suggests that exogenous GABA versus vesicular release could activate a largely separate pool of receptors— exogenous application would still hit synaptic receptors, but they would hit an additional pool of receptors proximal to the synapse which would largely be inactive yet still close enough for overlapping pools of G proteins. Therefore, these overlapping pools of G proteins could participate in facilitation at the level of the GIRK channels for synaptic $GABA_B$ receptor activation that would be unavailable to D2 receptor signaling.

To test this hypothesis, I performed parallel experiments this time instead combining iontophoretic application and photolysis rather than photolysis + synaptic release. Though a similar level of current, the hypothesis was that these two diffuse means of application would again hit the same pool of receptors and facilitation would not be observed. As figure 7.8 depicts, no facilitation was observed via this method for GABA nor dopamine, supporting the hypothesis that separate pools of receptors underlies the GABA-GABA enhancement of the $GABA_B$ IPSC (Figure 7.7 A,F). However, ultimately this added additional complexity to an already complex story and the effect of adding an additional pA*s or two of current density to the $GABA_B$ IPSC was small anyway. In conversations with Dr. Williams, it was decided it would be best to leave these data out of the initial submission, with the ability to bring it back in if requested by reviewers.

Another set of experiments were left out because I felt they were insufficiently conclusive for inclusion. Though my experiments probing enhancement of synaptic currents were using exogenous agonist, overlapping activation from the hybrid D2/$GABA_B$ IPSC should already undergo heterologous facilitation. To measure this, I wanted to compare the component of the hybid IPSC blocked by antagonizing $GABA_B$ receptors to the basal $GABA_B$ IPSC. If the hybrid IPSC has components

of heterologous facilitation, the CGP-sensitive component should consist of both the basal $GABA_B$ IPSC and the component of facilitation and so should be larger than the basal $GABA_B$ IPSC. Run down and seal up are a constant factor to consider, and if access drops, so too would the measured currents. I didn't want to simply antagonize $GABA_B$ receptors as any rundown would be included in the portion blocked by CGP therefore biasing my assay towards seeing larger currents and confirming my hypothesis. To bypass this issue, I was able to use some free data with dopamine uncaging as a control. In the course of my experiments comparing dopamine uncaging on the hybrid and isolated D2 ISPC, in some experiments I was able to get both conditions from a single cell. I could record currents for the hybrid IPSC, then antagonize $GABA_B$ to record experiments uncaging dopamine on the D2 IPSC. This meant I also got the isolated CGP current with dopamine uncaging throughout as a control to confirm the lack of rundown/seal up. The results of this comparison were that the CGP-sensitive component of the hybrid IPSC was significantly larger than the baseline $GABA_B$ receptor IPSC (Figure 7.9; 20.1±1.0 vs 27.5±2.7, n=5, p=0.0331) which supports a hypothesis that heterologous facilitation is observable in the hybrid IPSC. Despite this positive result, sample size was small as was the baseline $GABA_B$ IPSC I felt I needed significantly more data to be sure of this observation and I was conducting these experiments in the winter of 2019 so future plans for this relatively difficult experiment got dropped a bit.

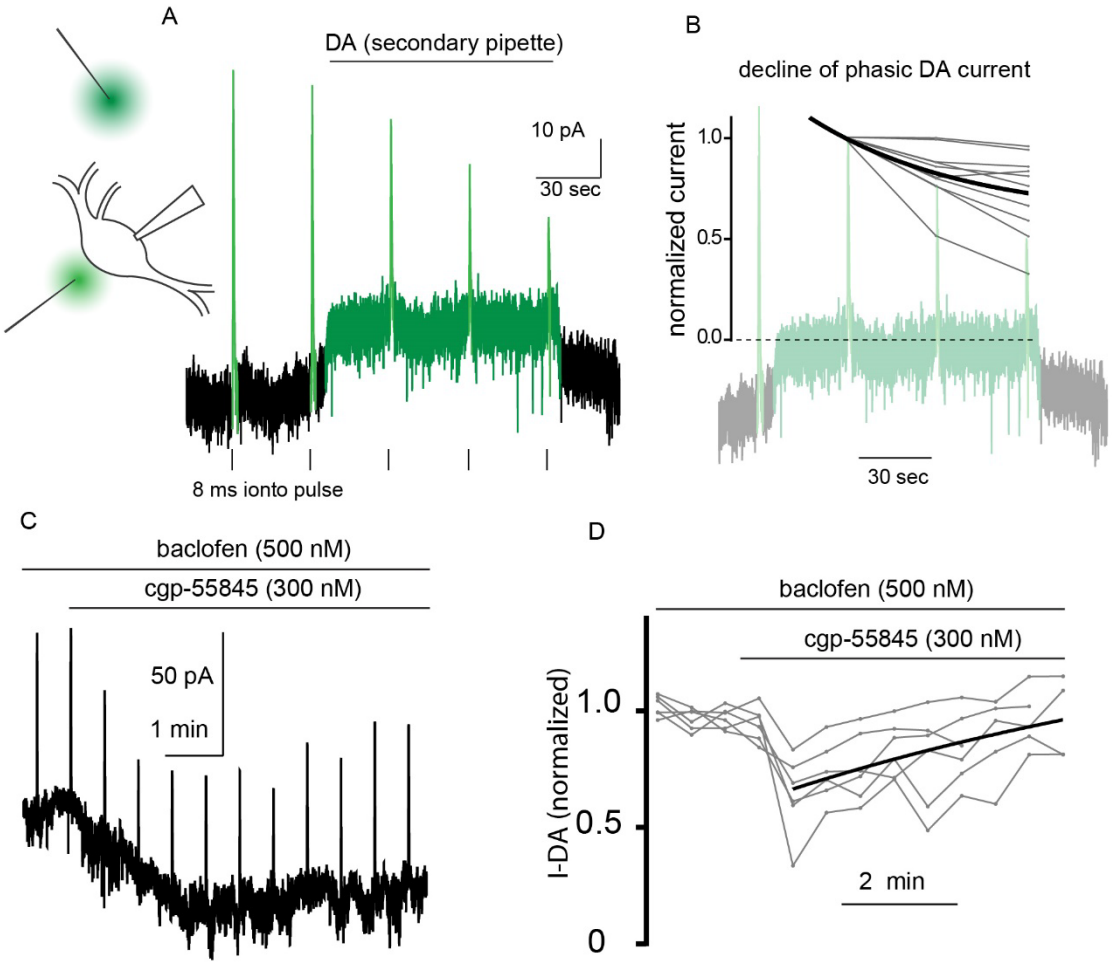

Figure 7-6 D2 receptor signaling is desensitized by low levels of GPCR activation.

A) Left- Experimental setup showing relative position of the iontophoretic delivering phasic pulse proximal to the neuron soma, and secondary pipette positioned far away from the cell. Right- example trace of showing desensitization of the phasic iontophoretic response by low concentrations of dopamine delivered by a secondary pipette. Dopamine-dependent currents are pseudocolored green. B) Group data for the experimental setup shown in A. Due to occlusion effects, desensitization is only measured during the period that the secondary pipette is supplying dopamine (subtracting out the tonic current). Dark black line is an exponential decay fit with a rate constant of 59s (n=10). C) Example experiment using DA iontophoresis with low baclofen included in the ACSF. $GABA_B$ receptors were then antagonized (300 nM cgp-55845) leading to a transient reduction in amplitude to the response to DA. D) Group data for experiments shown in C.

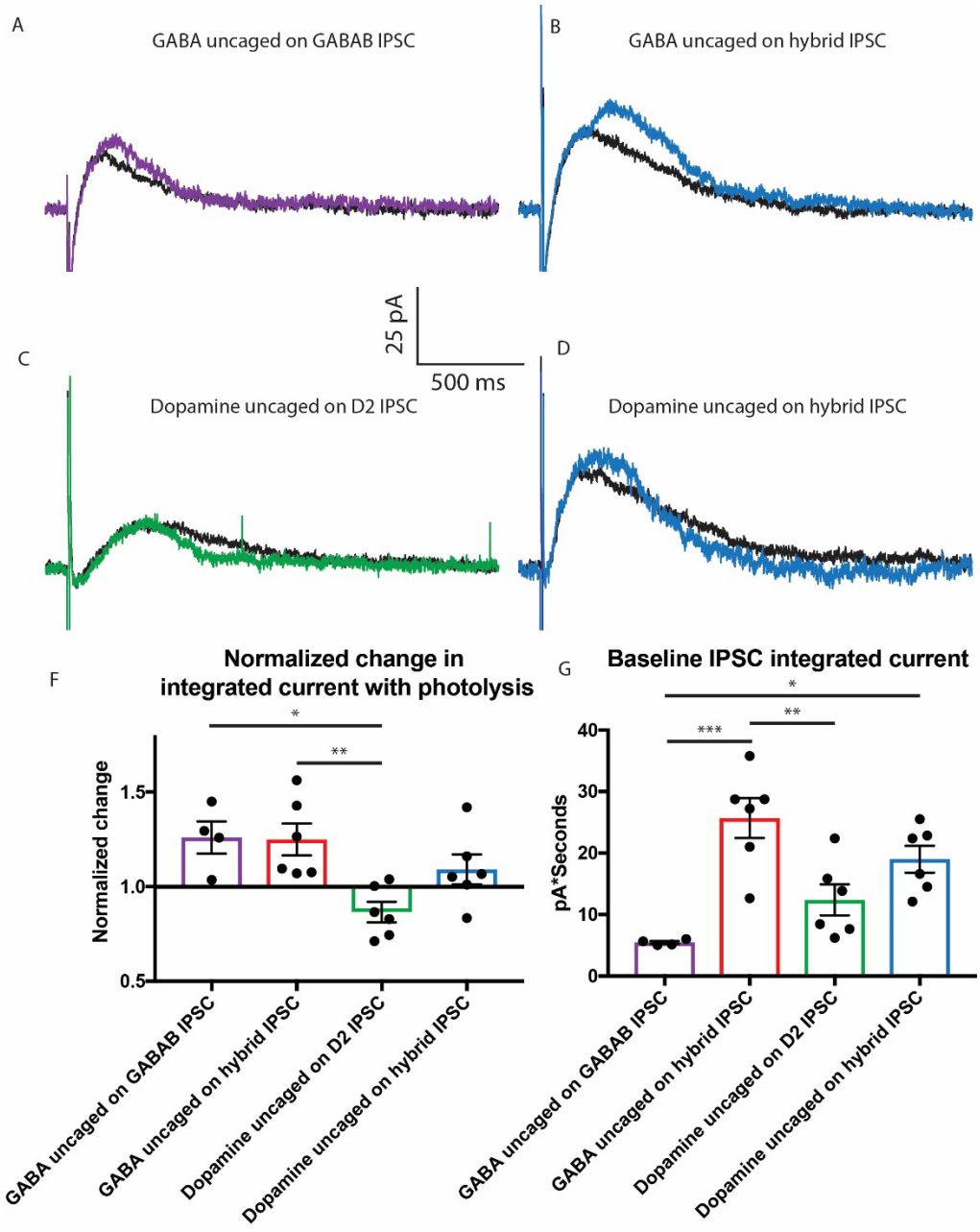

Figure 7-7 Full comparison of IPSC enhancement (extension to Figure 7.5)

A) example trace of $GABA_B$ IPSC vs the subtraction of GABA photolysis from photolysis + IPSC. B) Results of a similar calculation in A, but with GABA photolysis on a hybrid IPSC (repeated from Figure 7.5). C) Result of a similar calculation in A, but with dopamine photolysis on the D2 IPSC. D) Results of a similar calculation in A, but with dopamine photolysis on a hybrid IPSC (repeated from Figure 7.5). E) Group data for change in integrated current normalized to baseline IPSC. Quantified baseline integrated current for $GABA_B$ IPSC alone, D2 IPSC alone, and the two data sets of hybrid IPSCs.

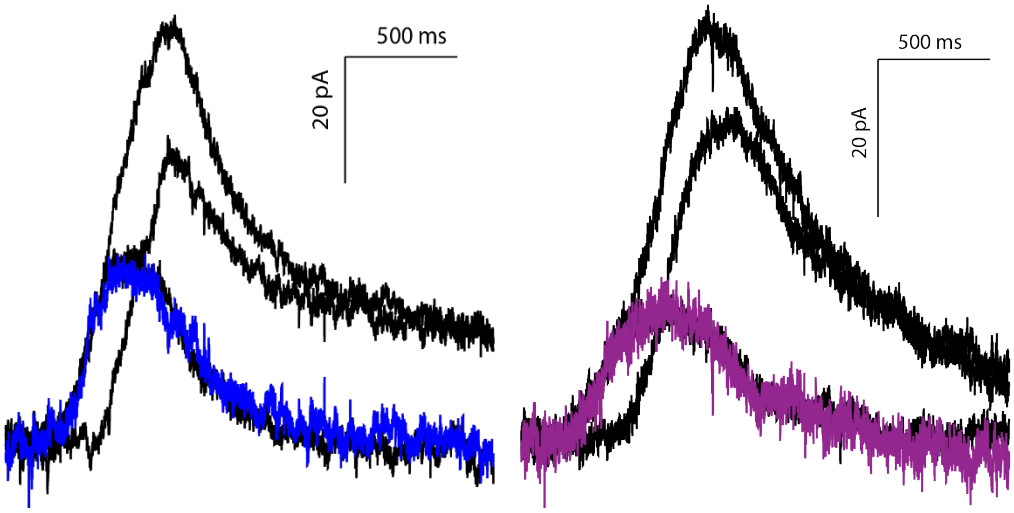

Figure 7-8 Comparison of combined or isolated photolysis and iontophoresis

Left—Comparison of currents generated from a train of GABA photolysis (medium current), GABA iontophoresis (small black current), iontophoresis + photolysis (largest current), and the subtraction of photolysis current from combined photolysis + iontophoresis (small blue current). As can be seen, the data showed no enhancement between the two application methods. Right— Same as left except using dopamine iontophoresis and photolysis. The purple current is the subtraction of combined minus isolated photolysis.

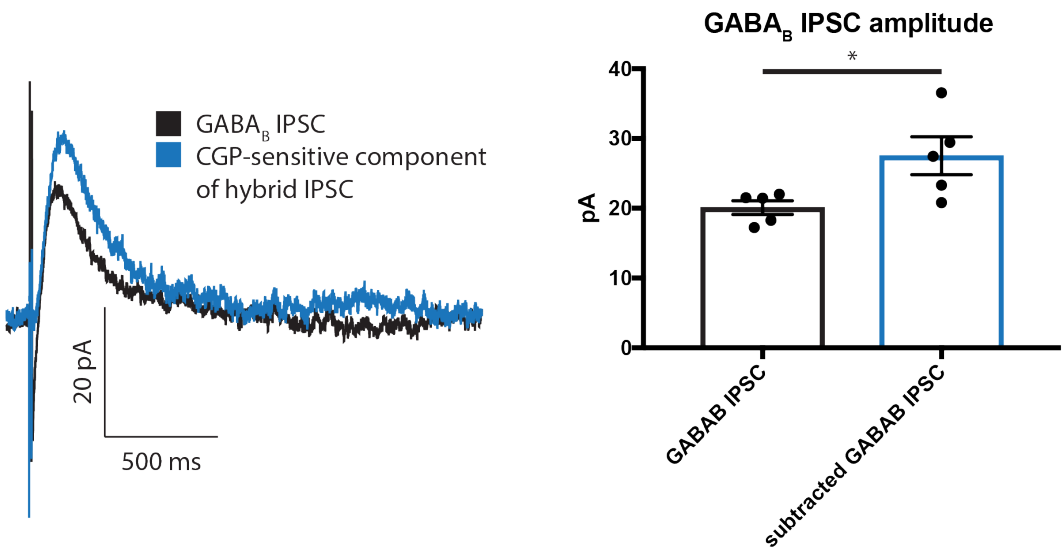

Figure 7-9 Comparison of the CGP-sensitive component of the hybrid ISPC with the baseline GABA$_B$ receptor IPSC

Left— Average of the GABA$_B$ IPSC generated from experiments in Figure 7.7 compared with the averaged CGP-sensitive current generated from antagonizing GABA$_B$ receptors after recording the hybrid IPSC. Right— group data of amplitudes from baseline GABAB IPSC vs CGP-sensitive component the hybrid IPSC which should include a component of facilitation. CGP-sensitive component is significantly larger by t-test.

Chapter 8 – Discussion and future directions

There remains an almost staggering amount of molecular biology and biochemistry work that needs to be done to fully understand the various mechanisms described in this dissertation. The benefits of working with WT animals and slice physiology can be enormous, but so, too, can the downsides where any genetic manipulation is time consuming and costly. This downside of working with *ex vivo* tissue samples has been a common barrier in pursuing questions of molecular biology. From just my experiences during my dissertation work, we had made attempts to run mass spectrometry on midbrain dopamine neurons to assess content, but the region is so small that there was insufficient extracted protein to collect clean samples. Pharmacology can also be more difficult in slice work. The time it takes drugs to penetrate deep into tissue makes rapid application difficult—the difficulties of which I spend a not small percentage of this manuscript discussing—but some drugs that seem easy to apply in cell culture have trouble penetrating the dense architecture of brain slices.

Were I to continue studying these same questions in my postgraduate work, a high priority would be to learn or develop a system more amenable to experimental manipulation. Neuronal cell culture is an experimental set up that takes its own level of equipment and expertise, but the manipulability and accessibility of such systems make them more suitable for some of the questions that I would wish to pursue.

Calcium dependent and independent desensitization of G protein signaling

Chapter 4 discusses a calcium dependent component of desensitization which is a pathway that has not entirely been clarified. A multitude of calcium binding proteins interact with the D2 receptor including calmodulin (Bofill-Cardona et al., 2000; Liu et al., 2007), NCS-1 (Kabbani et al.,

2002; Dragicevic et al., 2014; Pandalaneni et al., 2015), and S100B (Liu et al., 2008; Dempsey and Shaw, 2011) yet even some basic observations remain contradictory. For instance, NCS-1 and its interactions with calcium was found to in fact inhibit D2 receptor desensitization in dopamine neurons (Dragicevic et al., 2014) rather than the opposite effect in preparations from older animals (Beckstead and Williams, 2007). There have been suggestions that CAMKII regulates calcium dependent desensitization of D2 receptors (Perra et al., 2011), but again the prep and experimental paradigm make direct comparisons difficult.

Unpublished data done by Dr. Robinson showed that calcium dependent desensitization can be significantly modulated by shifting holding potential. By holding at negative potentials to remove inactivation from calcium channels, then stepping to either -65 (calcium channels largely still inactive) or -55 mV (at the foot of the L-type calcium channel activation curve) just prior to quinpirole superfusion to measure desensitization, he showed significantly more desensitization for the -55 mV condition. This means facilitation of desensitization by calcium is easily poised to regulate D2 autoreceptor function by weakening D2 receptor inhibition when the neuron rapidly fires, but where desensitization is less pronounced if a neuron is quiescent. The combination of effects essentially produce a feedback loop where the current neuronal state is reinforced. High on a list of follow up experiments to understand both calcium dependent desensitization and the seemingly related question of D2L versus D2S splice variants (though certainly the link between splice variant and calcium desensitization is less clear following the results of Chapter 3).

Beyond repetition of pharmacology and use of inhibitory peptides, proximity-based labeling (Qin et al., 2021) would be useful in studying the calcium-sensitive component of desensitization, but a time-resolved system like APEX (Lobingier et al., 2017) would be the gold standard. Such experiments would not be cheap both from the price of mass spectroscopy but also in a theoretical

world of APEX in neuronal culture, simply producing enough cells for such experiments might be herculean. Still, with sufficient effort, it could make for an interesting study.

The calcium dependent desensitization appears to be at least somewhat independent of the heterologous desensitization described in Chapter 7. The heterologous desensitization was present both in experiments with BAPTA and EGTA included in internal recording solutions and so were grouped, but further dissection of the interactions would be warranted. In unpublished experiments, $GABA_B$ receptor signaling is also sensitive to heterologous desensitization, though in agreement with previous reports showing $GABA_B$ receptor signaling desensitizes less than D2 receptors (Beckstead and Williams, 2007; Perra et al., 2011; Gantz et al., 2015; Robinson et al., 2017), the degree of desensitization for $GABA_B$ induced by dopamine was less than was achievable for D2 receptor signaling (evidence of this is also seen in the additional experiments section of Chapter 5). As those same previous reports also show that $GABA_B$ receptors are insensitive to calcium dependent desensitization, it suggests calcium dependent and heterologous desensitization are separate pathways and that the locus for calcium dependent desensitization is at the D2 receptor or in associated proteins.

The locus for heterologous desensitization is less clear. As discussed in Chapter 7 and elsewhere, the mechanism for turning off GIRK signaling is by sequestration of G βγ by G α (Wang et al., 2016) and essentially any effector that binds G βγ will inhibit its ability to couple to GIRK channels. GRK has been shown to have a phosphorylation-independent ability to sequester G βγ and inhibit its coupling to GIRKs (Raveh et al., 2010). KCTD12 is an auxiliary protein for $GABA_B$ receptors that translocates to the membrane by binding and sequestering G βγ to desensitize local $GABA_B$ signaling (Turecek et al., 2014; Zheng et al., 2019). Even proteins that have no affinity for GRK but translocate to the membrane based on G protein activity or cytoskeletal remodeling could reduce coupling to GIRK channels by restricting the mobility of G βγ.

Regulation at the level of the GIRK channel is also possible. Direct modification of the channel is possible as is regulation by controlling PI(4,5)P2 levels which are needed for efficient channel gating (Mathiharan et al., 2021). PLC beta is activated by G βγ (Park et al., 1993) which provides a link between $G_{i/o}$ signaling to potential control of the channel by cleaving PI(4,5)P2.

Still, use of knockout studies should be able to help clarify some repertoire of relevant proteins. Despite the complexity of G protein signaling and despite the not inconsiderable cost for doing so in brain slice, viral transduction of neurons with Cas9 constructs to knockout proteins of interest from specific neurons would be a good starting point for such investigations.

Regardless of specific mechanism, other unpublished experiments I performed suggest desensitization is also inducible by the nociception/OFQ receptor (in addition to $GABA_B$ receptor desensitization of D2 signaling). A future direction to pursue would be to test if exogenously expressed DREADDs could also induce D2 receptor desensitization. Designer Receptors Exclusively Activated by Designer Drugs (DREADDs) have been used for cellular control with the promise of a system that provides inducible control of neuronal function. Even moving beyond the finding that the supposedly pharmacologically inert agonist for DREADDs, clozapine-N-oxide, metabolizes into the distinctly non-inert clozapine (Manvich et al., 2018), an exogenously overexpressed receptor hooking into endogenous systems of GPCR control seems anything but non-impactful. I hoped to test if inhibitory DREADD activation desensitized D2 receptor signaling. If yes, not only would DREADDs have the desired acute effect of inhibiting neuronal activity, they would change synaptic weights both by potentially desensitizing inhibitory G protein signaling and potentially also participating in heterologous facilitation. These planned experiments and potential pitfalls highlight the need for additional controls when using a tool like DREADDs.

Signal transduction from agonist to effector

There has yet to be a quantitative description of the signaling pathway from extracellular agonist concentrations to receptor occupancy to G protein catalysis diffusion, interactions with effectors, and kinetics of cessation of signaling. Touhara et al. (2018) makes estimates and I made some of my own by changing the variables in their equations (Chapter 7), but these estimates are not based on direct measurements of neuron. This means many aspects of D2 receptors signaling are mysterious. If approximately half of this dissertation has focused on desensitization of receptor-channel coupling, the other half has worked to understand the underpinnings of the D2 receptor IPSC and the kinetics of signaling.

Chapter 6 and its description of the time course of dopamine-D2 receptor interactions in the IPSC highlights the slow nature of signaling. There is about a 50 ms delay between the stimulation and onset of current. The relevant contributions of agonist binding, build-up of G protein concentration, and diffusion to effectors is unclear. There is some reasoning to suggest D2 receptors are somewhat uncoupled from GIRK channels. Part of the function of the family of KCTD accessory proteins is to physically link $GABA_B$ receptors to GIRK channels (Schwenk et al., 2010). If the mechanism of heterologous desensitization in dopamine neurons is by sequestration of G βγ, that $GABA_B$ receptors commonly form tight associations with GIRK channels would make them more resistant to interference of signaling and could explain why $GABA_B$ receptors do not desensitize as much as D2 receptors (Beckstead et al., 2007). $GABA_B$ receptors also have a shorter time-to-peak for their IPSC (Figure 7.5) which could certainly be due to differences in the kinetics of agonist removal but may represent tighter coupling. $GABA_B$ receptors also have a higher current density—potentially due to close associate with channels—though again this has other potential explanations.

I hoped to answer these questions of receptor-channel distance by immunofluorescent labeling of $GABA_B$, D2, and GIRK channels. I began these experiments in the first couple months of 2020 so they took an abrupt pause. Later in the year, I continued my efforts in these experiments but quickly concluded that there were going to be enough problems to troubleshoot that it would be a difficult task to complete, particularly as I have only minimal microscopy experience. Available antibodies for GIRK and $GABA_B$ targeted intracellular epitopes meaning I would have to fix and permeabilize samples. Our transgenic lines of labeled D2 receptors all have extracellular epitope tags that lose immunoreactivity with fixation. This meant I had to do double labeling steps, one before and after fixation, then be able to take sufficiently high quality images to be able to parse surface from intracellular labeling of GIRK and $GABA_B$. Though the distribution of channels and receptors is critical for understanding the D2 IPSC, I dropped this line of research at the time, but very much would wish to know more what imaging could tell us about receptor-channel interactions.

Also highlighted in Chapter 6 is the delay between photolysis of sulpiride and decline in current response (Figure 6.2 and in text). There was a 50 ms delay between CyHQ-sulpiride photolysis and visible current decline when perfusing dopamine (10 µM) and a delay of 100 ms before current declined 5%. The blockade of D2 receptors is a competition reaction between sulpiride and dopamine so the full effect of sulpiride would not be expected to be instant, but sulpiride should immediately begin to have some antagonistic effects. The stable current response for a perfused drug means the rate of G βγ reaching GIRK channels is the same as G βγ is removed from the system. This means that G βγ concentrations will instantly drop the moment receptors stop producing additional free G βγ. However, the farther GIRK channels are from the receptor, the more of a delay between blockade of D2 receptors and any reduction in GIRK channel activity. A future direction for this line of investigation will be use of a new caged CGP-55845 (produced by the Dore lab, waiting to be used) to run similar experiments with $GABA_B$ receptors. If the onset to visible

current deflection is more rapid for $GABA_B$ receptors, this may be additional evidence for tighter channel-receptor coupling.

The unknowns and effects of agonist affinity certainly still can cloud interpretation. In comparing latency to decline between GABA and dopamine receptors, it is remarkably difficult to find accurate measurements for the dwell time of dopamine. Part of the problem comes from the state dependence of receptor affinities where G protein interaction with receptors can change agonist affinity (De Lean et al., 1980). It is possible 50 ms is a reasonable minimal dwell time for dopamine to reside on a receptor, but the correlation with the latency to rise following stimulation lends credence to the delay being based on intracellular dynamics.

The effects of agonist affinity have been highlighted several times in this dissertation. Figure 3.5 shows faster current declines for dopamine vs quinpirole following sulpiride photolysis and Supplementary Figure 6.3 shows even faster declines for noradrenaline activated D2 currents. This means that much of the current decline is dependent on agonist unbinding rate, but it is unclear how much faster the system can get.

Chapter 5 shows the results of increasing receptor affinity and slowing intrinsic suppression mechanisms. The mutation in the D2-I212F receptor is in the intracellular face suggesting that a conformation that stabilizes the active open state increases agonist affinity by thermodynamic linkage. But it is again unclear how much each component contributes to the slowing of D2 responses. With the linkage of agonist binding and opening of intracellular face, I would assume the actions are thermodynamically linked such that it is a simultaneous unbinding and receptor inactivation, but I am not sure these details have been sufficiently finely parsed even in the context of WT receptors. Photolysis of sulpiride in a reserpine treated and theoretically agonist-free slice still resulted in a slow relaxation of GIRK response suggesting it is the intrinsic slowness of GPCR relaxation rather than slow rate of GTPase activity and sequestration of G βγ. This raises the inverse

possibility— though the rates certainly would be linked, it may be that the relaxation of D2 currents is dependent on the rebinding of the intracellular ionic lock following agonist release as an additional rate on top of agonist unbinding.

Parsing such details of signal transduction will be a difficult task, but certain of those rate constants are nearly in reach. The molecular toolkit is expanding with every passing week, and I would be surprised if there isn't a lab out there working on a sensor for G βγ that would be suitable for studying the dynamics of G βγ concentrations in fine detail. Ultimately such experiments are necessary to prove the mechanisms of things like heterologous facilitation and at last give the full quantitative description of GPCR signaling that has existed for ionotropic receptors for decades.

Regarding heterologous facilitation there are a number of potential future directions. I showed that synaptically released agonist can participate in this facilitation, but I still only used exogenous agonist to show the interaction. The ideal experiment would be to use two different variants of channelrhodopsin to be able to specifically excited dopamine neurons vs GABA inputs. A similar paradigm of sequential inducement of dopamine release, then GABA, then both together should cleanly demonstrate interactions between purely synaptically released agonists.

References

Aghajanian GK, Marek GJ. Serotonin and hallucinogens. Neuropsychopharmacology. 1999 Aug;21(2 Suppl):16S-23S. doi: 10.1016/S0893-133X(98)00135-3. PMID: 10432484.

Alewijnse, A. E., Timmerman, H., Jacobs, E. H., Smit, M. J., Roovers, E., Cotecchia, S., and Leurs, R. (2000) The effect of mutations in the DRY motif on the constitutive activity and structural instability of the histamine H(2) receptor. Mol. Pharmacol. 57 (5), 890– 8

Arttamangkul S, Lau EK, Lu HW, Williams JT. Desensitization and trafficking of μ-opioid receptors in locus ceruleus neurons: modulation by kinases. Mol Pharmacol. 2012 Mar;81(3):348-55. doi: 10.1124/mol.111.076208. Epub 2011 Nov 23. PMID: 22113080; PMCID: PMC3286302.

Asad, N., McLain, D. E., Condon, A. F., Gore, S., Hampton, S. E., Vijay, S., Williams, J. T., and Dore, T. M. (2020) Photoactivatable dopamine and sulpiride to explore the function of dopaminergic neurons and circuits. ACS Chem. Neurosci. 11 (6), 939– 951, DOI: 10.1021/acschemneuro.9b00675

Backman, C. M., Malik, N., Zhang, Y., Shan, L., Grinberg, A., Hoffer, B. J., Westphal, H., and Tomac, A. C. (2006) Characterization of a mouse strain expressing Cre recombinase from the 3′ untranslated region of the dopamine transporter locus. Genesis 44 (8), 383– 390, DOI: 10.1002/dvg.20228

Ballesteros, J. A., Jensen, A. D., Liapakis, G., Rasmussen, S. G., Shi, L., Gether, U., and Javitch, J. A. (2001) Activation of the β2 adrenergic receptor involves disruption of an ionic lock between the cytoplasmic ends of transmembrane segments 3 and 6. J. Biol. Chem. 276, 29171– 29177, DOI: 10.1074/jbc.M103747200

Ballesteros, J. and Weinstein, H. (1995) Integrated methods for modeling G-protein coupled receptors. Methods Neurosci. 25, 366– 428, DOI: 10.1016/S1043-9471(05)80049-7

Bateup, H. S., Santini, E., Shen, W., Birnbaum, S., Valjent, E., Surmeier, D. J., Fisone, G., Nestler, E. J., and Greengard, P. (2010) Distinct subclasses of medium spiny neurons differentially regulate striatal motor behaviors. Proc. Natl. Acad. Sci. U. S. A. 107 (33), 14845– 14850, DOI: 10.1073/pnas.1009874107

Beaulieu, J. M., Sotnikova, T. D., Marion, S., Lefkowitz, R. J., Gainetdinov, R. R., and Caron, M. G. (2005) An Akt/β-arrestin 2/PP2A signaling complex mediates dopaminergic neurotransmission and behavior. Cell 122 (2), 261– 273, DOI: 10.1016/j.cell.2005.05.012

Beckstead MJ, Ford CP, Phillips PE, Williams JT. Presynaptic regulation of dendrodendritic dopamine transmission. Eur J Neurosci. 2007 Sep;26(6):1479-88. doi: 10.1111/j.1460-9568.2007.05775.x. Epub 2007 Sep 6. PMID: 17822435; PMCID: PMC3633601.

Beckstead MJ, Grandy DK, Wickman K, Williams JT. Vesicular dopamine release elicits an inhibitory postsynaptic current in midbrain dopamine neurons. Neuron. 2004 Jun 24;42(6):939-46. doi: 10.1016/j.neuron.2004.05.019. PMID: 15207238.

Beckstead MJ, Williams JT. Long-term depression of a dopamine IPSC. J Neurosci. 2007 Feb 21;27(8):2074-80. doi: 10.1523/JNEUROSCI.3251-06.2007. PMID: 17314302; PMCID: PMC6673562.

Bello, E. P., Mateo, Y., Gelman, D. M., Noain, D., Shin, J. H., Low, M. J., Alvarez, V. A., Lovinger, D. M., and Rubinstein, M. (2011) Cocaine supersensitivity and enhanced motivation for reward in mice lacking dopamine D2 autoreceptors. Nat. Neurosci. 14 (8), 1033– 1038, DOI: 10.1038/nn.2862

Birnbaumer L. G proteins in signal transduction. Annu Rev Pharmacol Toxicol. 1990;30:675-705. doi: 10.1146/annurev.pa.30.040190.003331. PMID: 2111655.

Björklund A, Lindvall O. 1975. Dopamine in dendrites of substantia nigra neurons: suggestions for a role in dendritic terminals. Brain Res. 83, 531–537. (10.1016/0006-8993(75)90849-5)

Bliss TV, Lomo T. Long-lasting potentiation of synaptic transmission in the dentate area of the anaesthetized rabbit following stimulation of the perforant path. J Physiol. 1973 Jul;232(2):331-56. doi: 10.1113/jphysiol.1973.sp010273. PMID: 4727084; PMCID: PMC1350458.

Bofill-Cardona E, Kudlacek O, Yang Q, Ahorn H, Freissmuth M, Nanoff C (2000) Binding of calmodulin to the D2-dopamine receptor reduces receptor signaling by arresting the G protein activation switch Journal of Biological Chemistry 275:32672–32680. https://doi.org/10.1074/jbc.M002780200

Bridi MCD, de Pasquale R, Lantz CL, Gu Y, Borrell A, Choi SY, He K, Tran T, Hong SZ, Dykman A, Lee HK, Quinlan EM, Kirkwood A. Two distinct mechanisms for experience-dependent homeostasis. Nat Neurosci. 2018 Jun;21(6):843-850. doi: 10.1038/s41593-018-0150-0. Epub 2018 May 14. PMID: 29760525; PMCID: PMC6019646.

Brownstein MJ. A brief history of opiates, opioid peptides, and opioid receptors. Proc Natl Acad Sci U S A. 1993 Jun 15;90(12):5391-3. doi: 10.1073/pnas.90.12.5391. PMID: 8390660; PMCID: PMC46725.

Cameron DL, Williams JT. Dopamine D1 receptors facilitate transmitter release. Nature. 1993 Nov 25;366(6453):344-7. doi: 10.1038/366344a0. PMID: 8247128.

Cepeda, C., Murphy, K. P., Parent, M., and Levine, M. S. (2014) The role of dopamine in Huntington's disease. Prog. Brain Res. 211, 235– 254, DOI: 10.1016/B978-0-444-63425-2.00010-6

Citri A, Malenka RC. Synaptic plasticity: multiple forms, functions, and mechanisms. Neuropsychopharmacology. 2008 Jan;33(1):18-41. doi: 10.1038/sj.npp.1301559. Epub 2007 Aug 29. PMID: 17728696.

Clarke TK, Weiss AR, Ferarro TN, Kampman KM, Dackis CA, Pettinati HM, O'brien CP, Oslin DW, Lohoff FW, Berrettini WH (2014) The dopamine receptor D2 (DRD2) SNP rs1076560 is associated with opioid addiction Annals of Human Genetics 78:33–39. https://doi.org/10.1111/ahg.12046

Clayton, C. C., Donthamsetti, P., Lambert, N. A., Javitch, J. A., and Neve, K. A. (2014) Mutation of three residues in the third intracellular loop of the dopamine D2 receptor creates an internalization-defective receptor. J. Biol. Chem. 289 (48), 33663– 33675, DOI: 10.1074/jbc.M114.605378

Coffeen U, Pellicer F. *Salvia divinorum*: from recreational hallucinogenic use to analgesic and anti-inflammatory action. J Pain Res. 2019 Mar 22;12:1069-1076. doi: 10.2147/JPR.S188619. PMID: 30962708; PMCID: PMC6434906.

Condon AF, Robinson BG, Asad N, Dore TM, Tian L, Williams JT. The residence of synaptically released dopamine on D2 autoreceptors. Cell Rep. 2021 Aug 3;36(5):109465. doi:

10.1016/j.celrep.2021.109465. PMID: 34348146.

Corrêa SA, Munton R, Nishimune A, Fitzjohn S, Henley JM. Development of GABAB subunits and functional GABAB receptors in rat cultured hippocampal neurons. Neuropharmacology. 2004 Sep;47(4):475-84. doi: 10.1016/j.neuropharm.2004.04.021. PMID: 15380367; PMCID: PMC3310902.

Courtney, N.A., and Ford, C.P. (2014). The timing of dopamine- and noradrenaline-mediated transmission reflects underlying differences in the extent of spillover and pooling. J. Neurosci. 34, 7645–7656.

Cragg, S.J., and Rice, M.E. (2004). DAncing past the DAT at a DA synapse. Trends Neurosci. 27, 270–277.

Cui S, Ho WK, Kim ST, Cho H. Agonist-induced localization of Gq-coupled receptors and G protein-gated inwardly rectifying K+ (GIRK) channels to caveolae determines receptor specificity of phosphatidylinositol 4,5-bisphosphate signaling. J Biol Chem. 2010 Dec 31;285(53):41732-9. doi: 10.1074/jbc.M110.153312. Epub 2010 Nov 1. PMID: 21041306; PMCID: PMC3009900.

DALE H.H. The action of certain esters and ethers of choline, and their relation to muscarine. J. Pharmacol. Exp. Ther. 1914;6:147–190.

De Lean A, Stadel JM, Lefkowitz RJ. A ternary complex model explains the agonist-specific binding properties of the adenylate cyclase-coupled beta-adrenergic receptor. J Biol Chem. 1980 Aug 10;255(15):7108-17. PMID: 6248546.

de Witte W. E. A.; Versfelt J. W.; Kuzikov M.; Rolland S.; Georgi V.; Gribbon P.; Gul S.; Huntjens D.; van der Graaf P. H.; Danhof M.; Fernandez-Montalvan A.; Witt G.; de Lange E. C. M. (2018) In vitro and in silico analysis of the effects of D2 receptor antagonist target binding kinetics on the cellular response to fluctuating dopamine concentrations. *Br. J. Pharmacol.* 175, 4121–4136. 10.1111/bph.14456.

Dempsey BR, Shaw GS (2011) Identification of calcium-independent and calcium-enhanced binding between S100B and the dopamine D2 receptor Biochemistry 50:9056–9065. https://doi.org/10.1021/bi201054x

Deupi X. Relevance of rhodopsin studies for GPCR activation. Biochim Biophys Acta. 2014 May;1837(5):674-82. doi: 10.1016/j.bbabio.2013.09.002. Epub 2013 Sep 13. PMID: 24041646.

Donthamsetti, P., Gallo, E. F., Buck, D. C., Stahl, E. L., Zhu, Y., Lane, J. R., Bohn, L. M., Neve, K. A., Kellendonk, C., and Javitch, J. A. (2020) Arrestin recruitment to dopamine D2 receptor mediates locomotion but not incentive motivation. Mol. Psychiatry 25, 2086– 2100, DOI: 10.1038/s41380-018-0212-4

Dragicevic E, Poetschke C, Duda J, Schlaudraff F, Lammel S, Schiemann J, Fauler M, Hetzel A, Watanabe M, Lujan R, Malenka RC, Striessnig J, Liss B (2014) Cav1.3 channels control D2-autoreceptor responses via NCS-1 in substantia nigra dopamine neurons Brain 137:2287–2302. https://doi.org/10.1093/brain/awu131

Dunham TD, Farrens DL. Conformational changes in rhodopsin. Movement of helix f detected by site-specific chemical labeling and fluorescence spectroscopy. J Biol Chem. 1999 Jan 15;274(3):1683-90. doi: 10.1074/jbc.274.3.1683. PMID: 9880548.

Edwards NJ, Tejeda HA, Pignatelli M, Zhang S, McDevitt RA, Wu J, Bass CE, Bettler B, Morales M, Bonci A. Circuit specificity in the inhibitory architecture of the VTA regulates cocaine-induced

behavior. Nat Neurosci. 2017 Mar;20(3):438-448. doi: 10.1038/nn.4482. Epub 2017 Jan 23. Erratum in: Nat Neurosci. 2017 Jul 26;20(8):1189. PMID: 28114294.

Eisenberg, D., Lüthy, R., and Bowie, J. U. (1997) VERIFY3D: assessment of protein models with three-dimensional profiles. Methods Enzymol. 277, 396– 404, DOI: 10.1016/S0076-6879(97)77022-8

Evans RC, Twedell EL, Zhu M, Ascencio J, Zhang R, Khaliq ZM. Functional Dissection of Basal Ganglia Inhibitory Inputs onto Substantia Nigra Dopaminergic Neurons. Cell Rep. 2020 Sep 15;32(11):108156. doi: 10.1016/j.celrep.2020.108156. PMID: 32937133.

Evans RC, Zhu M, Khaliq ZM. Dopamine Inhibition Differentially Controls Excitability of Substantia Nigra Dopamine Neuron Subpopulations through T-Type Calcium Channels. J Neurosci. 2017 Mar 29;37(13):3704-3720. doi: 10.1523/JNEUROSCI.0117-17.2017. Epub 2017 Mar 6. PMID: 28264982; PMCID: PMC5373143.

Farrens, D. L., Altenbach, C., Yang, K., Hubbell, W. L., and Khorana, H. G. (1996) Requirement of rigid-body motion of transmembrane helices for light activation of rhodopsin. Science 274 (5288), 768– 770, DOI: 10.1126/science.274.5288.768

Fonnum F. Glutamate: a neurotransmitter in mammalian brain. J Neurochem. 1984 Jan;42(1):1-11. doi: 10.1111/j.1471-4159.1984.tb09689.x. PMID: 6139418.

Ford CP, Beckstead MJ, Williams JT. Kappa opioid inhibition of somatodendritic dopamine inhibitory postsynaptic currents. J Neurophysiol. 2007 Jan;97(1):883-91. doi: 10.1152/jn.00963.2006. Epub 2006 Nov 22. PMID: 17122312; PMCID: PMC3633483.

Ford, C.P., Gantz, S.C., Phillips, P.E.M., and Williams, J.T. (2010). Control of extracellular dopamine at dendrite and axon terminals. J. Neurosci. 30, 6975–6983.

Ford, C.P., Phillips, P.E.M., and Williams, J.T. (2009). The time course of dopamine transmission in the ventral tegmental area. J. Neurosci. 29, 13344–13352.

Fortin GD, Desrosiers CC, Yamaguchi N, Trudeau LE. Basal somatodendritic dopamine release requires snare proteins. J Neurochem. 2006 Mar;96(6):1740-9. doi: 10.1111/j.1471-4159.2006.03699.x. PMID: 16539689.

Gantz SC, Bunzow JR, Williams JT. Spontaneous inhibitory synaptic currents mediated by a G protein-coupled receptor. Neuron. 2013 Jun 5;78(5):807-12. doi: 10.1016/j.neuron.2013.04.013. PMID: 23764286; PMCID: PMC3697754.

Gantz SC, Ford CP, Morikawa H, Williams JT. The Evolving Understanding of Dopamine Neurons in the Substantia Nigra and Ventral Tegmental Area. Annu Rev Physiol. 2018 Feb 10;80:219-241. doi: 10.1146/annurev-physiol-021317-121615. Epub 2017 Sep 22. PMID: 28938084.

Gantz SC, Robinson BG, Buck DC, Bunzow JR, Neve RL, Williams JT, Neve KA (2015) Distinct regulation of dopamine D2S and D2L autoreceptor signaling by calcium eLife 4:e09358. https://doi.org/10.7554/eLife.09358

Gazi, L., Nickolls, S. A., and Strange, P. G. (2003) Functional coupling of the human dopamine D2 receptor with Gαi1, Gαi2, Gαi3 and Gαo G proteins: evidence for agonist regulation of G protein selectivity. Br. J. Pharmacol. 138 (5), 775– 786, DOI: 10.1038/sj.bjp.0705116

Gether, U., Ballesteros, J. A., Seifert, R., Sanders-Bush, E., Weinstein, H., and Kobilka, B. K. (1997) Structural instability of a constitutively active G protein-coupled receptor. Agonist-independent

activation due to conformational flexibility. J. Biol. Chem. 272 (5), 2587– 90, DOI: 10.1074/jbc.272.5.2587

Gierschik P, Codina J, Simons C, Birnbaumer L, Spiegel A. Antisera against a guanine nucleotide binding protein from retina cross-react with the beta subunit of the adenylyl cyclase-associated guanine nucleotide binding proteins, Ns and Ni. Proc Natl Acad Sci U S A. 1985 Feb;82(3):727-31. doi: 10.1073/pnas.82.3.727. PMID: 3919382; PMCID: PMC397119.

Gillespie PG, Walker RG. Molecular basis of mechanosensory transduction. Nature. 2001 Sep 13;413(6852):194-202. doi: 10.1038/35093011. PMID: 11557988.

Gilman AG. G proteins and dual control of adenylate cyclase. Cell. 1984 Mar;36(3):577-9. doi: 10.1016/0092-8674(84)90336-2. PMID: 6321035.

Gondin, A. B., Halls, M. L., Canals, M., and Briddon, S. J. (2019) GRK mediates μ-opioid receptor plasma membrane reorganization. Front. Mol. Neurosci. 12, 104, DOI: 10.3389/fnmol.2019.00104

Groves, P.M., and Linder, J.C. (1983). Dendro-dendritic synapses in substantia nigra: descriptions based on analysis of serial sections. Exp. Brain Res. 49, 209–217.

Gurevich, E. V., Gainetdinov, R. R., and Gurevich, V. V. (2016) G protein-coupled receptor kinases as regulators of dopamine receptor functions. Pharmacol. Res. 111, 1– 16, DOI: 10.1016/j.phrs.2016.05.010

Gurevich, V. V. and Gurevich, E. V. (2006) The structural basis of arrestin-mediated regulation of G-protein-coupled receptors. Pharmacol. Ther. 110 (3), 465– 502, DOI: 10.1016/j.pharmthera.2005.09.008

Hajdu, F., Hassler, R., and Bak, I.J. (1973). Electron microscopic study of the substantia nigra and the strio-nigral projection in the rat. Z. Zellforsch. Mikrosk. Anat. 146, 207–221.

Handler A, Ginty DD. The mechanosensory neurons of touch and their mechanisms of activation. Nat Rev Neurosci. 2021 Sep;22(9):521-537. doi: 10.1038/s41583-021-00489-x. Epub 2021 Jul 26. PMID: 34312536.

Hartzell HC, Kuffler SW, Yoshikami D. Post-synaptic potentiation: interaction between quanta of acetylcholine at the skeletal neuromuscular synapse. J Physiol. 1975 Oct;251(2):427-63. doi: 10.1113/jphysiol.1975.sp011102. PMID: 171379; PMCID: PMC1348437.

Hauser AS, Attwood MM, Rask-Andersen M, Schiöth HB, Gloriam DE. Trends in GPCR drug discovery: new agents, targets and indications. Nat Rev Drug Discov. 2017 Dec;16(12):829-842. doi: 10.1038/nrd.2017.178. Epub 2017 Oct 27. PMID: 29075003; PMCID: PMC6882681.

Hawkins RD, Abrams TW, Carew TJ, Kandel ER. A cellular mechanism of classical conditioning in Aplysia: activity-dependent amplification of presynaptic facilitation. Science. 1983 Jan 28;219(4583):400-5. doi: 10.1126/science.6294833. PMID: 6294833.

Hebb DO. The Organization of Behavior. New York: Wiley; 1949.

Henry DJ, Greene MA, White FJ. Electrophysiological effects of cocaine in the mesoaccumbens dopamine system: repeated administration. J Pharmacol Exp Ther. 1989 Dec;251(3):833-9. PMID: 2557418.

Hilger, D., Masureel, M., and Kobilka, B. K. (2018) Structure and dynamics of GPCR signaling complexes. Nat. Struct. Mol. Biol. 25 (1), 4– 12, DOI: 10.1038/s41594-017-0011-7

Hille B. Ion channels of excitable membranes. 3rd edition. Sunderland (MA): Sinauer and Associates, Inc.; 2001

HODGKIN AL, HUXLEY AF. A quantitative description of membrane current and its application to conduction and excitation in nerve. J Physiol. 1952 Aug;117(4):500-44. doi: 10.1113/jphysiol.1952.sp004764. PMID: 12991237; PMCID: PMC1392413.

Howlett AC, Blume LC, Dalton GD. CB(1) cannabinoid receptors and their associated proteins. Curr Med Chem. 2010;17(14):1382-93. doi: 10.2174/092986710790980023. PMID: 20166926; PMCID: PMC3179980.

Huang, W., Masureel, M., Qu, Q., Janetzko, J., Inoue, A., Kato, H. E., Robertson, M. J., Nguyen, K. C., Glenn, J. S., Skiniotis, G.(2020) Structure of the neurotensin receptor 1 in complex with β-arrestin 1. Nature 579 (7798), 303– 308, DOI: 10.1038/s41586-020-1953-1

Hyman SE, Malenka RC, Nestler EJ. Neural mechanisms of addiction: the role of reward-related learning and memory. Annu Rev Neurosci. 2006;29:565-98. doi: 10.1146/annurev.neuro.29.051605.113009. PMID: 16776597.

Isaacson JS, Solís JM, Nicoll RA. Local and diffuse synaptic actions of GABA in the hippocampus. Neuron. 1993 Feb;10(2):165-75. doi: 10.1016/0896-6273(93)90308-e. PMID: 7679913.

Ito K, Haga T, Lameh J, Sadée W (1999) Sequestration of dopamine D2 receptors depends on coexpression of G-protein-coupled receptor kinases 2 or 5 European Journal of Biochemistry 260:112–119. https://doi.org/10.1046/j.1432-1327.1999.00125.x

Itokawa M, Toru M, Ito K, Tsuga H, Kameyama K, Haga T, Arinami T, Hamaguchi H (1996) Sequestration of the short and long isoforms of dopamine D2 receptors expressed in Chinese hamster ovary cells Molecular Pharmacology 49:560–566.

Jang JY, Jang M, Kim SH, Um KB, Kang YK, Kim HJ, Chung S, Park MK (2011) Regulation of dopaminergic neuron firing by heterogeneous dopamine autoreceptors in the substantia nigra pars compacta Journal of Neurochemistry 116:966–974. https://doi.org/10.1111/j.1471-4159.2010.07107.x

Jiang, L. I., Collins, J., Davis, R., Lin, K. M., DeCamp, D., Roach, T., Hsueh, R., Rebres, R. A., Ross, E. M., Taussig, R.(2007) Use of a cAMP BRET sensor to characterize a novel regulation of cAMP by the sphingosine 1-phosphate/G13 pathway. J. Biol. Chem. 282 (14), 10576– 10584, DOI: 10.1074/jbc.M609695200

Jiang, M. and Bajpayee, N. S. (2009) Molecular mechanisms of Go signaling. Neurosignals 17 (1), 23– 41, DOI: 10.1159/000186688

Jiang, M. S., Spicher, K., Boulay, G., Wang, Y., and Birnbaumer, L. (2001) Most central nervous system D2 dopamine receptors are coupled to their effecters by Go. Proc. Natl. Acad. Sci. U. S. A. 98 (6), 3577– 3582, DOI: 10.1073/pnas.051632598

Jiménez-Baranda S, Gómez-Moutón C, Rojas A, Martínez-Prats L, Mira E, Ana Lacalle R, Valencia A, Dimitrov DS, Viola A, Delgado R, Martínez-A C, Mañes S. Filamin-A regulates actin-dependent clustering of HIV receptors. Nat Cell Biol. 2007 Jul;9(7):838-46. doi: 10.1038/ncb1610. Epub 2007 Jun 17. PMID: 17572668.

Jomphe C, Tiberi M, Trudeau LE (2006) Expression of D2 receptor isoforms in cultured neurons reveals equipotent autoreceptor function Neuropharmacology 50:595–605. https://doi.org/10.1016/j.neuropharm.2005.11.010

Jones MV, Westbrook GL. Desensitized states prolong GABAA channel responses to brief agonist pulses. Neuron. 1995 Jul;15(1):181-91. doi: 10.1016/0896-6273(95)90075-6. PMID: 7542462.

Jones, E. M., Lubock, N. B., Venkatakrishnan, A. J., Wang, J., Tseng, A. M., Paggi, J. M., Latorraca, N. R., Cancilla, D., Satyadi, M., and Davis, J. E. (2020) Structural and functional characterization of G protein-coupled receptors with deep mutational scanning. eLife 9, 1, DOI: 10.7554/eLife.54895

Kabbani N, Negyessy L, Lin R, Goldman-Rakic P, Levenson R (2002) Interaction with neuronal calcium sensor NCS-1 mediates desensitization of the D2 dopamine receptor Journal of Neuroscience 22:8476–8486.

Kalant H. The pharmacology and toxicology of "ecstasy" (MDMA) and related drugs. CMAJ. 2001 Oct 2;165(7):917-28. PMID: 11599334; PMCID: PMC81503.

Kanaide M, Uezono Y, Matsumoto M, Hojo M, Ando Y, Sudo Y, Sumikawa K, Taniyama K. Desensitization of GABA(B) receptor signaling by formation of protein complexes of GABA(B2) subunit with GRK4 or GRK5. J Cell Physiol. 2007 Jan;210(1):237-45. doi: 10.1002/jcp.20863. PMID: 17013811.

Katz B, Miledi R. Ionic requirements of synaptic transmitter release. Nature. 1967 Aug 5;215(5101):651. doi: 10.1038/215651a0. PMID: 4292912.

Katz B, Thesleff S. A study of the desensitization produced by acetylcholine at the motor end-plate. J Physiol. 1957 Aug 29;138(1):63-80. doi: 10.1113/jphysiol.1957.sp005838. PMID: 13463799; PMCID: PMC1363030.

Kebabian JW. Multiple classes of dopamine receptors in mammalian central nervous system: the involvement of dopamine-sensitive adenylyl cyclase. Life Sci. 1978 Aug 7;23(5):479-83. doi: 10.1016/0024-3205(78)90157-1. PMID: 357876.

Kelly E, Bailey CP, Henderson G. Agonist-selective mechanisms of GPCR desensitization. Br J Pharmacol. 2008 Mar;153 Suppl 1(Suppl 1):S379-88. doi: 10.1038/sj.bjp.0707604. Epub 2007 Dec 3. PMID: 18059321; PMCID: PMC2268061.

Khan ZU, Mrzljak L, Gutierrez A, de la Calle A, Goldman-Rakic PS (1998) Prominence of the dopamine D2 short isoform in dopaminergic pathways PNAS 95:7731–7736. https://doi.org/10.1073/pnas.95.13.7731

Kim JH, Cho EY, Min C, Park JH, Kim KM. Characterization of functional roles of DRY motif in the 2nd intracellular loop of dopamine D2 and D3 receptors. Arch Pharm Res. 2008 Apr;31(4):474-81. doi: 10.1007/s12272-001-1181-x. Epub 2008 May 1. PMID: 18449505.

Kim KM, Nakajima Y, Nakajima S. G protein-coupled inward rectifier modulated by dopamine agonists in cultured substantia nigra neurons. Neuroscience. 1995 Dec;69(4):1145-58. doi: 10.1016/0306-4522(95)00326-e. PMID: 8848103.

Kim, K. M., Valenzano, K. J., Robinson, S. R., Yao, W. D., Barak, L. S., and Caron, M. G. (2001) Differential regulation of the dopamine D2 and D3 receptors by G protein-coupled receptor kinases and β-arrestins. J. Biol. Chem. 276 (40), 37409– 37414, DOI: 10.1074/jbc.M106728200

Kjelsberg, M. A., Cotecchia, S., Ostrowski, J., Caron, M. G., and Lefkowitz, R. J. (1992) Constitutive activation of the α1B-adrenergic receptor by all amino acid substitutions at a single site: evidence for a region which constrains receptor activation. J. Biol. Chem. 267 (3), 1430–1433, DOI: 10.1016/S0021-9258(18)45962-5

Klein Herenbrink C, Sykes DA, Donthamsetti P, Canals M, Coudrat T, Shonberg J, Scammells PJ, Capuano B, Sexton PM, Charlton SJ, Javitch JA, Christopoulos A, Lane JR. The role of kinetic context in apparent biased agonism at GPCRs. Nat Commun. 2016 Feb 24;7:10842. doi: 10.1038/ncomms10842. PMID: 26905976; PMCID: PMC4770093.

Kling, R. C., Clark, T., and Gmeiner, P. (2016) Comparative MD simulations indicate a dual role for Arg1323.50 in dopamine-dependent D2R activation. PLoS One 11 (1), e0146612, DOI: 10.1371/journal.pone.0146612

Krieger, E., Darden, T., Nabuurs, S. B., Finkelstein, A., and Vriend, G. (2004) Making optimal use of empirical energy functions: force-field parameterization in crystal space. Proteins: Struct., Funct., Genet. 57 (4), 678– 83, DOI: 10.1002/prot.20251

Krieger, E., Joo, K., Lee, J., Lee, J., Raman, S., Thompson, J., Tyka, M., Baker, D., and Karplus, K. (2009) Improving physical realism, stereochemistry, and side-chain accuracy in homology modeling: Four approaches that performed well in CASP8. Proteins: Struct., Funct., Genet. 77 (Suppl 9), 114– 22, DOI: 10.1002/prot.22570

Krieger, E., Koraimann, G., and Vriend, G. (2002) Increasing the precision of comparative models with YASARA NOVA–a self-parameterizing force field. Proteins: Struct., Funct., Genet. 47 (3), 393– 402, DOI: 10.1002/prot.10104

Kulik A, Vida I, Fukazawa Y, Guetg N, Kasugai Y, Marker CL, Rigato F, Bettler B, Wickman K, Frotscher M, Shigemoto R. Compartment-dependent colocalization of Kir3.2-containing K+ channels and GABAB receptors in hippocampal pyramidal cells. J Neurosci. 2006 Apr 19;26(16):4289-97. doi: 10.1523/JNEUROSCI.4178-05.2006. PMID: 16624949; PMCID: PMC6673994.

Labouèbe G, Lomazzi M, Cruz HG, Creton C, Luján R, Li M, Yanagawa Y, Obata K, Watanabe M, Wickman K, Boyer SB, Slesinger PA, Lüscher C. RGS2 modulates coupling between GABAB receptors and GIRK channels in dopamine neurons of the ventral tegmental area. Nat Neurosci. 2007 Dec;10(12):1559-68. doi: 10.1038/nn2006. Epub 2007 Oct 28. PMID: 17965710.

Lacey MG, Mercuri NB, North RA. (1987) Dopamine acts on D2 receptors to increase potassium conductance in neurones of the rat substantia nigra zona compacta. J. Physiol. 1987; 392: 397-416

Lacey MG, Mercuri NB, North RA. (1990) Actions of cocaine on rat dopaminergic neurons in vitro. Br. J. Pharmacol. 99, 731–735. 10.1111/j.1476-5381.1990.tb12998.x.

Lacey MG, Mercuri NB, North RA. On the potassium conductance increase activated by GABAB and dopamine D2 receptors in rat substantia nigra neurones. J Physiol. 1988 Jul;401:437-53. doi: 10.1113/jphysiol.1988.sp017171. PMID: 2459376; PMCID: PMC1191858.

Lan, H., Liu, Y., Bell, M. I., Gurevich, V. V., and Neve, K. A. (2009) A dopamine D2 receptor mutant capable of G protein-mediated signaling but deficient in arrestin binding. Mol. Pharmacol. 75, 113– 123, DOI: 10.1124/mol.108.050534

Laskowski, R. A., MacArthur, M. W., Moss, D. S., and Thornton, J. M. (1993) PROCHECK - a program to check the stereochemical quality of protein structures. J. Appl. Crystallogr. 26, 283–291, DOI: 10.1107/S0021889892009944

Lee, H.-J., Rodriguez-Contreras, D., and Neve, K. A. (2021) Commentary on “Novel interaction of the dopamine D2 receptor and the CA2+ binding protein S100B: role in D2 receptor function”.

Mol. Pharmacol. DOI: 10.1124/molpharm.121.000284

Lefkowitz RJ. A brief history of G-protein coupled receptors (Nobel Lecture). Angew Chem Int Ed Engl. 2013 Jun 17;52(25):6366-78. doi: 10.1002/anie.201301924. Epub 2013 May 6. PMID: 23650015.

Lepiku M, Rinken A, Jarv J, Fuxe K. (1997) Modulation of [3H]quinpirole binding to dopaminergic receptors by adenosine A2A receptors. Neurosci. Lett. 239, 61–64. 10.1016/S0304-3940(97)00874-4.

Lester, R.A., Clements, J.D., Westbrook, G.L., and Jahr, C.E. (1990). Channel kinetics determine the time course of NMDA receptor-mediated synaptic cur-rents. Nature 346, 565–567.

Levran O, Randesi M, da Rosa JC, Ott J, Rotrosen J, Adelson M, Kreek MJ (2015) Overlapping dopaminergic pathway genetic susceptibility to heroin and cocaine addictions in African Americans Annals of Human Genetics 79:188–198. https://doi.org/10.1111/ahg.12104

Liechti ME. Modern Clinical Research on LSD. Neuropsychopharmacology. 2017 Oct;42(11):2114-2127. doi: 10.1038/npp.2017.86. Epub 2017 Apr 27. PMID: 28447622; PMCID: PMC5603820.

Liu Y, Buck DC, Macey TA, Lan H, Neve KA (2007) Evidence that calmodulin binding to the dopamine D2 receptor enhances receptor signaling Journal of Receptors and Signal Transduction 27:47–65. https://doi.org/10.1080/10799890601094152

Liu Y, Buck DC, Neve KA (2008) Novel interaction of the dopamine D2 receptor and the Ca2+ binding protein S100B: role in D2 receptor function Molecular Pharmacology 74:371–378. https://doi.org/10.1124/mol.108.044925

Liu YF, Civelli O, Grandy DK, Albert PR (1992) Differential sensitivity of the short and long human dopamine D2 receptor subtypes to protein kinase C Journal of Neurochemistry 59:2311–2317. https://doi.org/10.1111/j.1471-4159.1992.tb10125.x

Liu, Y., Buck, D. C., Macey, T. A., Lan, H., and Neve, K. A. (2007) Evidence that calmodulin binding to the dopamine D2 receptor enhances receptor signaling. J. Recept. Signal Transduction Res. 27 (1), 47– 65, DOI: 10.1080/10799890601094152

Lobingier BT, Hüttenhain R, Eichel K, Miller KB, Ting AY, von Zastrow M, Krogan NJ. An Approach to Spatiotemporally Resolve Protein Interaction Networks in Living Cells. Cell. 2017 Apr 6;169(2):350-360.e12. doi: 10.1016/j.cell.2017.03.022. PMID: 28388416; PMCID: PMC5616215.

Loewi O: Über humorale Übertragbarkeit der Herznervenwirkung. I. Mittei-lung. Pflügers Arch Ges Physiol 1921; 189: 239–242

Luján R, Aguado C, Ciruela F, Cózar J, Kleindienst D, de la Ossa L, Bettler B, Wickman K, Watanabe M, Shigemoto R, Fukazawa Y. Differential association of GABAB receptors with their effector ion channels in Purkinje cells. Brain Struct Funct. 2018 Apr;223(3):1565-1587. doi: 10.1007/s00429-017-1568-y. Epub 2017 Nov 25. PMID: 29177691; PMCID: PMC5869904.

Madhavan A, Argilli E, Bonci A, Whistler JL. Loss of D2 dopamine receptor function modulates cocaine-induced glutamatergic synaptic potentiation in the ventral tegmental area. J Neurosci. 2013 Jul 24;33(30):12329-36. doi: 10.1523/JNEUROSCI.0809-13.2013. PMID: 23884939; PMCID: PMC3721842.

Mafi, A., Kim, S. K., and Goddard, W. A., 3rd (2020) Mechanism of β-arrestin recruitment by the

μ-opioid G protein-coupled receptor. Proc. Natl. Acad. Sci. U. S. A. 117 (28), 16346– 16355, DOI: 10.1073/pnas.1918264117

Manvich DF, Webster KA, Foster SL, Farrell MS, Ritchie JC, Porter JH, Weinshenker D. The DREADD agonist clozapine N-oxide (CNO) is reverse-metabolized to clozapine and produces clozapine-like interoceptive stimulus effects in rats and mice. Sci Rep. 2018 Mar 1;8(1):3840. doi: 10.1038/s41598-018-22116-z. PMID: 29497149; PMCID: PMC5832819.

Marcott, P. F., Gong, S., Donthamsetti, P., Grinnell, S. G., Nelson, M. N., Newman, A. H., Birnbaumer, L., Martemyanov, K. A., Javitch, J. A., and Ford, C. P. (2018) Regional heterogeneity of D2-receptor signaling in the dorsal striatum and nucleus accumbens. Neuron 98 (3), 575– 587, DOI: 10.1016/j.neuron.2018.03.038

Marinelli M, Cooper DC, Baker LK, White FJ. Impulse activity of midbrain dopamine neurons modulates drug-seeking behavior. Psychopharmacology (Berl). 2003 Jul;168(1-2):84-98. doi: 10.1007/s00213-003-1491-1. Epub 2003 Apr 30. Erratum in: Psychopharmacology (Berl). 2003 Nov;170(3):334. Erratum in: Psychopharmacology (Berl). 2003 Nov;170(3):334. PMID: 12721782.

Mathiharan YK, Glaaser IW, Zhao Y, Robertson MJ, Skiniotis G, Slesinger PA. Structural insights into GIRK2 channel modulation by cholesterol and PIP2. Cell Rep. 2021 Aug 24;36(8):109619. doi: 10.1016/j.celrep.2021.109619. PMID: 34433062.

Matsuda W, Furuta T, Nakamura KC, Hioki H, Fujiyama F, Arai R, Kaneko T. Single nigrostriatal dopaminergic neurons form widely spread and highly dense axonal arborizations in the neostriatum. J Neurosci. 2009 Jan 14;29(2):444-53. doi: 10.1523/JNEUROSCI.4029-08.2009. PMID: 19144844; PMCID: PMC6664950.

Mendez JA, Bourque MJ, Fasano C, Kortleven C, Trudeau LE. Somatodendritic dopamine release requires synaptotagmin 4 and 7 and the participation of voltage-gated calcium channels. J Biol Chem. 2011 Jul 8;286(27):23928-37. doi: 10.1074/jbc.M111.218032. Epub 2011 May 16. PMID: 21576241; PMCID: PMC3129174.

Miess, E., Gondin, A. B., Yousuf, A., Steinborn, R., Mösslein, N., Yang, Y., Göldner, M., Ruland, J. G., Bünemann, M., and Krasel, C. (2018) Multisite phosphorylation is required for sustained interaction with GRKs and arrestins during rapid μ-opioid receptor desensitization. Sci. Signal 11 (539), 1, DOI: 10.1126/scisignal.aas9609

Moore, C. A., Milano, S. K., and Benovic, J. L. (2007) Regulation of receptor trafficking by GRKs and arrestins. Annu. Rev. Physiol. 69, 451– 82, DOI: 10.1146/annurev.physiol.69.022405.154712

Moritz, A. E., Free, R. B., and Sibley, D. R. (2018) Advances and challenges in the search for D2 and D3 dopamine receptor-selective compounds. Cell. Signalling 41, 75– 81, DOI: 10.1016/j.cellsig.2017.07.003

Morris SJ, Van-Ham II, Daigle M, Robillard L, Sajedi N, Albert PR (2007) Differential desensitization of dopamine D2 receptor isoforms by protein kinase C: the importance of receptor phosphorylation and pseudosubstrate sites European Journal of Pharmacology 577:44–53. https://doi.org/10.1016/j.ejphar.2007.08.027

Moyer RA, Wang D, Papp AC, Smith RM, Duque L, Mash DC, Sadee W (2011) Intronic polymorphisms affecting alternative splicing of human dopamine D2 receptor are associated with cocaine abuse Neuropsychopharmacology 36:753–762. https://doi.org/10.1038/npp.2010.208

Namkung, Y., Dipace, C., Javitch, J. A., and Sibley, D. R. (2009a) G protein-coupled receptor kinase-mediated phosphorylation regulates post-endocytic trafficking of the D2 dopamine receptor. J. Biol. Chem. 284 (22), 15038– 15051, DOI: 10.1074/jbc.M900388200

Namkung, Y., Dipace, C., Urizar, E., Javitch, J. A., and Sibley, D. R. (2009b) G protein-coupled receptor kinase-2 constitutively regulates D2 dopamine receptor expression and signaling independently of receptor phosphorylation. J. Biol. Chem. 284 (49), 34103– 34115, DOI: 10.1074/jbc.M109.055707

Neve KA, Ford CP, Buck DC, Grandy DK, Neve RL, Phillips TJ (2013) Normalizing dopamine D2 receptor-mediated responses in D2 null mutant mice by virus-mediated receptor restoration: comparing D2L and D2S Neuroscience 248:479–487. https://doi.org/10.1016/j.neuroscience.2013.06.035

Neve, K. A., Seamans, J. K., and Trantham-Davidson, H. (2004) Dopamine receptor signaling. J. Recept. Signal Transduction Res. 24 (3), 165– 205, DOI: 10.1081/RRS-200029981

Otis T, Zhang S, Trussell LO. Direct measurement of AMPA receptor desensitization induced by glutamatergic synaptic transmission. J Neurosci. 1996 Dec 1;16(23):7496-504. doi: 10.1523/JNEUROSCI.16-23-07496.1996. PMID: 8922405; PMCID: PMC6579098.

Pandalaneni S, Karuppiah V, Saleem M, Haynes LP, Burgoyne RD, Mayans O, Derrick JP, Lian LY (2015) Neuronal calcium sensor-1 binds the D2 dopamine receptor and G-protein-coupled receptor kinase 1 (GRK1) peptides using different modes of interactions Journal of Biological Chemistry 290:18744–18756. https://doi.org/10.1074/jbc.M114.627059

Park D, Jhon DY, Lee CW, Lee KH, Rhee SG. Activation of phospholipase C isozymes by G protein beta gamma subunits. J Biol Chem. 1993 Mar 5;268(7):4573-6. PMID: 8383116.

Parker, E. M. and Ross, E. M. (1991) Truncation of the extended carboxyl-terminal domain increases the expression and regulatory activity of the avian β-adrenergic receptor. J. Biol. Chem. 266 (15), 9987– 9996, DOI: 10.1016/S0021-9258(18)92917-0

Patriarchi T, Cho JR, Merten K, Howe MW, Marley A, Xiong WH, Folk RW, Broussard GJ, Liang R, Jang MJ, Zhong H, Dombeck D, von Zastrow M, Nimmerjahn A, Gradinaru V, Williams JT, Tian L. Ultrafast neuronal imaging of dopamine dynamics with designed genetically encoded sensors. Science. 2018 Jun 29;360(6396):eaat4422. doi: 10.1126/science.aat4422. Epub 2018 May 31. PMID: 29853555; PMCID: PMC6287765.

Perra S, Clements MA, Bernier BE, Morikawa H. In vivo ethanol experience increases D(2) autoinhibition in the ventral tegmental area. Neuropsychopharmacology. 2011 Apr;36(5):993-1002. doi: 10.1038/npp.2010.237. Epub 2011 Jan 19. PMID: 21248720; PMCID: PMC3077268.

Pfleger, K. D., Seeber, R. M., and Eidne, K. A. (2006) Bioluminescence resonance energy transfer (BRET) for the real-time detection of protein-protein interactions. Nat. Protoc. 1 (1), 337– 345, DOI: 10.1038/nprot.2006.52

Pitcher JA, Inglese J, Higgins JB, Arriza JL, Casey PJ, Kim C, Benovic JL, Kwatra MM, Caron MG, Lefkowitz RJ. Role of beta gamma subunits of G proteins in targeting the beta-adrenergic receptor kinase to membrane-bound receptors. Science. 1992 Aug 28;257(5074):1264-7. doi: 10.1126/science.1325672. PMID: 1325672.

Pologruto, T.A., Sabatini, B.L., and Svoboda, K. (2003). ScanImage: flexible software for operating laser scanning microscopes. Biomed. Eng. Online 2,13.

Ponder, J. W. and Case, D. A. (2003) Force fields for protein simulations. Adv. Protein Chem. 66, 27– 85, DOI: 10.1016/S0065-3233(03)66002-X

Pucak ML, Grace AA. Evidence that systemically administered dopamine antagonists activate dopamine neuron firing primarily by blockade of somatodendritic autoreceptors. J Pharmacol Exp Ther. 1994 Dec;271(3):1181-92. PMID: 7996424.

Qin W, Cho KF, Cavanagh PE, Ting AY. Deciphering molecular interactions by proximity labeling. Nat Methods. 2021 Feb;18(2):133-143. doi: 10.1038/s41592-020-01010-5. Epub 2021 Jan 11. PMID: 33432242.

Quillinan N, Lau EK, Virk M, von Zastrow M, Williams JT. Recovery from mu-opioid receptor desensitization after chronic treatment with morphine and methadone. J Neurosci. 2011 Mar 23;31(12):4434-43. doi: 10.1523/JNEUROSCI.4874-10.2011. PMID: 21430144; PMCID: PMC3092436.

Radl D, De Mei C, Chen E, Lee H, Borrelli E (2013) Each individual isoform of the dopamine D2 receptor protects from lactotroph hyperplasia Molecular Endocrinology 27:953–965. https://doi.org/10.1210/me.2013-1008

Radl, D., Chiacchiaretta, M., Lewis, R. G., Brami-Cherrier, K., Arcuri, L., and Borrelli, E. (2018) Differential regulation of striatal motor behavior and related cellular responses by dopamine D2L and D2S isoforms. Proc. Natl. Acad. Sci. U. S. A. 115 (1), 198– 203, DOI: 10.1073/pnas.1717194115

Rasmussen SG, DeVree BT, Zou Y, Kruse AC, Chung KY, Kobilka TS, Thian FS, Chae PS, Pardon E, Calinski D, Mathiesen JM, Shah ST, Lyons JA, Caffrey M, Gellman SH, Steyaert J, Skiniotis G, Weis WI, Sunahara RK, Kobilka BK. Crystal structure of the β2 adrenergic receptor-Gs protein complex. Nature. 2011 Jul 19;477(7366):549-55. doi: 10.1038/nature10361. PMID: 21772288; PMCID: PMC3184188.

Rasmussen, S. G. F., Jensen, A. D., Liapakis, G., Ghanouni, P., Javitch, J. A., and Gether, U. (1999) Mutation of a highly conserved aspartic acid in the β2 adrenergic receptor: Constitutive activation, structural instability, and conformational rearrangement of transmembrane segment 6. Mol. Pharmacol. 56 (1), 175– 184, DOI: 10.1124/mol.56.1.175

Rasmussen, S. G., Choi, H. J., Rosenbaum, D. M., Kobilka, T. S., Thian, F. S., Edwards, P. C., Burghammer, M., Ratnala, V. R., Sanishvili, R., Fischetti, R. F.(2007) Crystal structure of the human β2 adrenergic G-protein-coupled receptor. Nature 450 (7168), 383– 387, DOI: 10.1038/nature06325

Raveh A, Cooper A, Guy-David L, Reuveny E. Nonenzymatic rapid control of GIRK channel function by a G protein-coupled receptor kinase. Cell. 2010 Nov 24;143(5):750-60. doi: 10.1016/j.cell.2010.10.018. PMID: 21111235.

Robinson BG, Bunzow JR, Grimm JB, Lavis LD, Dudman JT, Brown J, Neve KA, Williams JT (2017) Desensitized D2 autoreceptors are resistant to trafficking Scientific Reports 7:4379. https://doi.org/10.1038/s41598-017-04728-z

Robinson BG, Cai X, Wang J, Bunzow JR, Williams JT, Kaeser PS. RIM is essential for stimulated but not spontaneous somatodendritic dopamine release in the midbrain. Elife. 2019 Sep 5;8:e47972. doi: 10.7554/eLife.47972. PMID: 31486769; PMCID: PMC6754207.

Robinson BG, Condon AF, Radl D, Borrelli E, Williams JT, Neve KA. Cocaine-induced adaptation of

dopamine D2S, but not D2L autoreceptors. Elife. 2017 Nov 20;6:e31924. doi: 10.7554/eLife.31924. PMID: 29154756; PMCID: PMC5695907.

Rodriguez-Contreras, D., Condon, A.F., Buck, D.C., Asad, N., Dore, T.M., Ver-beek, D.S., Tijssen, M.A.J., Shinde, U., Williams, J.T., and Neve, K.A. (2021). A signaling-biased and constitutively active dopamine D2 receptor variant. ACS Chem. Neurosci. 12, 1873–1884.

Rose, S. J., Pack, T. F., Peterson, S. M., Payne, K., Borrelli, E., and Caron, M. G. (2018) Engineered D2R variants reveal the balanced and biased contributions of G-protein and β-arrestin to dopamine-dependent functions. Neuropsychopharmacology 43 (5), 1164– 1173, DOI: 10.1038/npp.2017.254

Sasabe T, Furukawa A, Matsusita S, Higuchi S, Ishiura S (2007) Association analysis of the dopamine receptor D2 (DRD2) SNP rs1076560 in alcoholic patients Neuroscience Letters 412:139–142. https://doi.org/10.1016/j.neulet.2006.10.064

Saulière, A., Bellot, M., Paris, H., Denis, C., Finana, F., Hansen, J. T., Altié, M. F., Seguelas, M. H., Pathak, A., Hansen, J. L.(2012) Deciphering biased-agonism complexity reveals a new active AT1 receptor entity. Nat. Chem. Biol. 8 (7), 622– 30, DOI: 10.1038/nchembio.961

Schindelin, J., Arganda-Carreras, I., Frise, E., Kaynig, V., Longair, M., Pietzsch, T., Preibisch, S., Rueden, C., Saalfeld, S., Schmid, B., et al. (2012). Fiji: an open-source platform for biological-image analysis. Nat. Methods 9, 676–682.

Schöneberg T, Schulz A, Biebermann H, Hermsdorf T, Römpler H, Sangkuhl K. Mutant G-protein-coupled receptors as a cause of human diseases. Pharmacol Ther. 2004 Dec;104(3):173-206. doi: 10.1016/j.pharmthera.2004.08.008. PMID: 15556674.

Schultz W. Multiple dopamine functions at different time courses. Annu Rev Neurosci. 2007;30:259-88. doi: 10.1146/annurev.neuro.28.061604.135722. PMID: 17600522.

Schwenk J, Metz M, Zolles G, Turecek R, Fritzius T, Bildl W, Tarusawa E, Kulik A, Unger A, Ivankova K, Seddik R, Tiao JY, Rajalu M, Trojanova J, Rohde V, Gassmann M, Schulte U, Fakler B, Bettler B. Native GABA(B) receptors are heteromultimers with a family of auxiliary subunits. Nature. 2010 May 13;465(7295):231-5. doi: 10.1038/nature08964. Epub 2010 Apr 18. PMID: 20400944.

Schwenk J, Metz M, Zolles G, Turecek R, Fritzius T, Bildl W, Tarusawa E, Kulik A, Unger A, Ivankova K, Seddik R, Tiao JY, Rajalu M, Trojanova J, Rohde V, Gassmann M, Schulte U, Fakler B, Bettler B. Native GABA(B) receptors are heteromultimers with a family of auxiliary subunits. Nature. 2010 May 13;465(7295):231-5. doi: 10.1038/nature08964. Epub 2010 Apr 18. PMID: 20400944.

Seeman P, Lee T, Chau-Wong M, Wong K. Antipsychotic drug doses and neuroleptic/dopamine receptors. Nature. 1976 Jun 24;261(5562):717-9. doi: 10.1038/261717a0. PMID: 945467.

Seeman P. Atypical antipsychotics: mechanism of action. Can J Psychiatry. 2002 Feb;47(1):27-38. PMID: 11873706.

Sodickson, D.L., and Bean, B.P. (1996). GABAB receptor-activated inwardly rectifying potassium current in dissociated hippocampal CA3 neurons. J. Neurosci. 16, 6374–6385.

Staus, D. P., Hu, H., Robertson, M. J., Kleinhenz, A. L. W., Wingler, L. M., Capel, W. D., Latorraca, N. R., Lefkowitz, R. J., and Skiniotis, G. (2020) Structure of the M2 muscarinic receptor-β-arrestin complex in a lipid nanodisc. Nature 579 (7798), 297– 302, DOI: 10.1038/s41586-020-1954-0

Sternweis PC, Northup JK, Smigel MD, Gilman AG. The regulatory component of adenylate cyclase. Purification and properties. J Biol Chem. 1981 Nov 25;256(22):11517-26. PMID: 6271754.

Sun F, Zeng J, Jing M, Zhou J, Feng J, Owen SF, Luo Y, Li F, Wang H, Yamaguchi T, Yong Z, Gao Y, Peng W, Wang L, Zhang S, Du J, Lin D, Xu M, Kreitzer AC, Cui G, Li Y. A Genetically Encoded Fluorescent Sensor Enables Rapid and Specific Detection of Dopamine in Flies, Fish, and Mice. Cell. 2018 Jul 12;174(2):481-496.e19. doi: 10.1016/j.cell.2018.06.042. PMID: 30007419; PMCID: PMC6092020.

Sungkaworn T, Jobin ML, Burnecki K, Weron A, Lohse MJ, Calebiro D. Single-molecule imaging reveals receptor-G protein interactions at cell surface hot spots. Nature. 2017 Oct 26;550(7677):543-547. doi: 10.1038/nature24264. Epub 2017 Oct 18. PMID: 29045395.

Thal, D. M., Yeow, R. Y., Schoenau, C., Huber, J., and Tesmer, J. J. (2011) Molecular mechanism of selectivity among G protein-coupled receptor kinase 2 inhibitors. Mol. Pharmacol. 80 (2), 294– 303, DOI: 10.1124/mol.111.071522

Thibault D, Albert PR, Pineyro G, Trudeau LÉ (2011) Neurotensin triggers dopamine D2 receptor desensitization through a protein kinase C and beta-arrestin1-dependent mechanism Journal of Biological Chemistry 286:9174–9184. https://doi.org/10.1074/jbc.M110.166454

Touhara KK and MacKinnon R. Molecular basis of signaling specificity between GIRK channels and GPCRs. Elife. 2018 Dec 10;7:e42908. doi: 10.7554/eLife.42908. PMID: 30526853; PMCID: PMC6335053.

Touhara KK, Wang W, MacKinnon R. The GIRK1 subunit potentiates G protein activation of cardiac GIRK1/4 hetero-tetramers. Elife. 2016 Apr 13;5:e15750. doi: 10.7554/eLife.15750. PMID: 27074664; PMCID: PMC4866825.

Turecek R, Schwenk J, Fritzius T, Ivankova K, Zolles G, Adelfinger L, Jacquier V, Besseyrias V, Gassmann M, Schulte U, Fakler B, Bettler B. Auxiliary GABAB receptor subunits uncouple G protein βγ subunits from effector channels to induce desensitization. Neuron. 2014 Jun 4;82(5):1032-44. doi: 10.1016/j.neuron.2014.04.015. Epub 2014 May 15. PMID: 24836506.

Urs, N. M., Bido, S., Peterson, S. M., Daigle, T. L., Bass, C. E., Gainetdinov, R. R., Bezard, E., and Caron, M. G. (2015) Targeting β-arrestin2 in the treatment of L-DOPA-induced dyskinesia in Parkinson's disease. Proc. Natl. Acad. Sci. U. S. A. 112 (19), E2517– E2526, DOI: 10.1073/pnas.1502740112

Usiello A, Baik JH, Rougé-Pont F, Picetti R, Dierich A, LeMeur M, Piazza PV, Borrelli E (2000) Distinct functions of the two isoforms of dopamine D2 receptors Nature 408:199–203. https://doi.org/10.1038/35041572

van der Weijden, M. C. M., Rodriguez-Contreras, D., Delnooz, C. C.S., Robinson, B. G., Condon, A. F., Kielhold, M. L., Stormezand, G. N., Ma, K. Y., Dufke, C., Williams, J. T., Neve, K. A., Tijssen, M. A.J., and Verbeek, D. S. (2021) A Gain-of-Function Variant in Dopamine D2 Receptor and Progressive Chorea and Dystonia Phenotype. Mov. Disord. 36 (3), 729– 739, DOI: 10.1002/mds.28385

Wacker D, Stevens RC, Roth BL. How Ligands Illuminate GPCR Molecular Pharmacology. Cell. 2017 Jul 27;170(3):414-427. doi: 10.1016/j.cell.2017.07.009. PMID: 28753422; PMCID: PMC5560499.

Wang S, Che T, Levit A, Shoichet BK, Wacker D, Roth BL. Structure of the D2 dopamine receptor bound to the atypical antipsychotic drug risperidone. Nature. 2018 Mar 8;555(7695):269-273. doi: 10.1038/nature25758. Epub 2018 Jan 24. PMID: 29466326; PMCID: PMC5843546.

Wang W, Touhara KK, Weir K, Bean BP, MacKinnon R. Cooperative regulation by G proteins and Na(+) of neuronal GIRK2 K(+) channels. Elife. 2016 Apr 13;5:e15751. doi: 10.7554/eLife.15751. PMID: 27074662; PMCID: PMC4866826.

Wang W, Whorton MR, MacKinnon R. Quantitative analysis of mammalian GIRK2 channel regulation by G proteins, the signaling lipid PIP2 and Na+ in a reconstituted system. Elife. 2014 Jul 20;3:e03671. doi: 10.7554/eLife.03671. PMID: 25049222; PMCID: PMC4135351.

Watts, V. J. and Neve, K. A. (1996) Sensitization of endogenous and recombinant adenylate cyclase by activation of D2 dopamine receptors. Mol. Pharmacol. 50 (4), 966– 976

Watts, V. J. and Neve, K. A. (2005) Sensitization of adenylate cyclase by Gαi/o-coupled receptors. Pharmacol. Ther. 106 (3), 405– 421, DOI: 10.1016/j.pharmthera.2004.12.005

Whorton MR, MacKinnon R. X-ray structure of the mammalian GIRK2-βγ G-protein complex. Nature. 2013 Jun 13;498(7453):190-7. doi: 10.1038/nature12241. Epub 2013 Jun 5. PMID: 23739333; PMCID: PMC4654628.

Wiencke, K., Horstmann, A., Mathar, D., Villringer, A., and Neumann, J. (2020). Dopamine release, diffusion and uptake: A computational model for synaptic and volume transmission. PLoS Comput. Biol. 16, e1008410.

Williams JT, Ingram SL, Henderson G, Chavkin C, von Zastrow M, Schulz S, Koch T, Evans CJ, Christie MJ. Regulation of μ-opioid receptors: desensitization, phosphorylation, internalization, and tolerance. Pharmacol Rev. 2013 Jan 15;65(1):223-54. doi: 10.1124/pr.112.005942. PMID: 23321159; PMCID: PMC3565916.

Wilson CJ, Groves PM, Fifková E. Monoaminergic synapses, including dendro-dendritic synapses in the rat substantia nigra. Exp Brain Res. 1977 Nov 24;30(2-3):161-74. doi: 10.1007/BF00237248. PMID: 598426.

Wilson, C.J., Groves, P.M., and Fifková, E. (1977). Monoaminergic synapses, including dendro-dendritic synapses in the rat substantia nigra. Exp. Brain Res. 30, 161–174.

Wilson, J., Lin, H., Fu, D., Javitch, J. A., and Strange, P. G. (2001) Mechanisms of inverse agonism of antipsychotic drugs at the D2 dopamine receptor: use of a mutant D2 dopamine receptor that adopts the activated conformation. J. Neurochem. 77 (2), 493– 504, DOI: 10.1046/j.1471-4159.2001.00233.x

Wolf ME, White FJ, Nassar R, Brooderson RJ, Khansa MR. Differential development of autoreceptor subsensitivity and enhanced dopamine release during amphetamine sensitization. J Pharmacol Exp Ther. 1993 Jan;264(1):249-55. PMID: 8093727.

Wong AH, Buckle CE, Van Tol HH. Polymorphisms in dopamine receptors: what do they tell us? Eur J Pharmacol. 2000 Dec 27;410(2-3):183-203. doi: 10.1016/s0014-2999(00)00815-3. PMID: 11134669.

Wu YN, Mercuri NB, Johnson SW. Presynaptic inhibition of gamma-aminobutyric acidB-mediated synaptic current by adenosine recorded in vitro in midbrain dopamine neurons. J Pharmacol Exp Ther. 1995 May;273(2):576-81. PMID: 7752058.

Yin, J., Chen, K. M., Clark, M. J., Hijazi, M., Kumari, P., Bai, X. C., Sunahara, R. K., Barth, P., and Rosenbaum, D. M. (2020) Structure of a D2 dopamine receptor-G-protein complex in a lipid membrane. Nature 584 (7819), 125– 129, DOI: 10.1038/s41586-020-2379-5

Yung-Chi, C. and Prusoff, W. H. (1973) Relationship between the inhibition constant (KI) and the concentration of inhibitor which causes 50% inhibition (I50) of an enzymatic reaction. Biochem. Pharmacol. 22, 3099– 3108, DOI: 10.1016/0006-2952(73)90196-2

Zhang X, Kim KM. Multifactorial Regulation of G Protein-Coupled Receptor Endocytosis. Biomol Ther (Seoul). 2017 Jan 1;25(1):26-43. doi: 10.4062/biomolther.2016.186. PMID: 28035080; PMCID: PMC5207461.

Zheng S, Abreu N, Levitz J, Kruse AC. Structural basis for KCTD-mediated rapid desensitization of GABAB signaling. Nature. 2019 Mar;567(7746):127-131. doi: 10.1038/s41586-019-0990-0. Epub 2019 Feb 27. PMID: 30814734; PMCID: PMC6405316.

Zhuang, T., Chen, Q., Cho, M. K., Vishnivetskiy, S. A., Iverson, T. M., Gurevich, V. V., and Sanders, C. R. (2013) Involvement of distinct arrestin-1 elements in binding to different functional forms of rhodopsin. Proc. Natl. Acad. Sci. U. S. A. 110 (3), 942– 7, DOI: 10.1073/pnas.1215176110